UNIVERSITAT POLITÈCNICA DE CATALUNYA
Deparment of Construction Engineering

A model for the non linear dynamic analysis of reinforced concrete and masonry framed structures

Thesis submitted in the fulfillment of the requirements for the degree of Doctor Engineer

JOSÉ FERNANDO SIMA BRUM

Supervisors:
PERE ROCA FABREGAT
CLIMENT MOLINS BORRELL

To my Mother

Acknowledgements

This Thesis would not have been possible without the continuous support and encouragement of my family, my mother Gloria, my grandmother Angela who recently passed away, my sister Anna Rosa and, of course, my two loves: my wife Gaby and my little daughter Olivia. To them, I would like to express my love and infinite gratitude.

I would like to express my sincere gratitude to my supervisors, Prof. Pere Roca and Prof. Climent Molins for their support and for many good academical advises. This work has been benefited by their rigorous editorial reviews and comments. I would like to thank Prof. Pere Roca for proposing me the subject of this research, for trusting in my person and skills by providing me financial support during the first steps of the research, until I received the FPU scholarship. I would also like to acknowledge the financial support given by the Education and Science Ministry of the Spanish Government by means of a FPU scholarship, which supported two and a half years of this research.

I wish to thank all my colleagues in the Construction Engineering Department with whom I shared a wonderful time during the last years. In special to my friends Javier Charry, Miguel Lobato and Alvaro Viviescas, whose friendship, I'm sure, will remain during the years. I would also like to thank my colleagues and professors at the IET (Structures and Transport Institute) of the University of the Republic (Uruguay), which encouraged me to this PhD.

Finally, I would like to thank all my friends from Uruguay as well as my "new" family, my brother in law Gian Franco and the whole Abarno-Huguet family, for their support and friendship.

Abstract

The assessment of the dynamic or seismic performance of complex structures often requires the integration in the time domain of the structural equation of motion in the frame of a non-linear analysis. In the case of masonry and reinforced concrete structures, the use of these methods for the assessment of the structure become of great importance, due to its complex non linear behavior, even for low levels of loading. A great number of these structures may be idealized as spatial frames. A generalization of the conventional matrix methods for the analysis of spatial framed structures has been developed in the UPC during the last two decades, the so-called Generalized Matrix Formulation (GMF). The basic formulation for curved elements with variable cross section was presented by Carrascón et al. (1987). Carol and Murcia (1989) extended this flexibility based formulation to the non linear time dependant analysis. This formulation was later extended to the geometrical and material non linear analysis of masonry framed structures (Molins, 1996; Molins and Roca, 1998). An extension of the basic formulation to the linear dynamic analysis was later proposed by Molins et al. (1998) through the introduction of a consistent mass matrix. The formulation has proved for more than fifteen years of extensive use, to be an efficient tool for the analysis of 3D framed structures.

The aim of this research is to extend the GMF to the non linear dynamic analysis of reinforced concrete and masonry framed structures. Following this main goal, the basic formulation has been complemented with a series of new features:

- A uniaxial constitutive model for concrete and masonry subjected to cyclic loadings in both compression and tension has been proposed. Particular emphasis has been paid to the description of the strength and stiffness degradation produced by the load cycling in both, tension and compression, the shape of unloading and reloading curves and the transition between opening and closing of cracks. Two independent damage parameters in compression and in tension have been

introduced to model the concrete degradation due to increasing loads. In the case of cyclic compressive loading, the model has been derived from experimental results obtained by other authors by considering the dependency of the cyclic variables with the damage level attained by the concrete. In the case of cyclic tension a simple model is adopted based on experimental observations.

- A constitutive model for the cyclic behavior of reinforcing steel, the well known Menegotto-Pinto model, has been adopted.

- Finally, a time step procedure for the integration of the dynamic equilibrium equation of the structure has been adopted.

In order to show the capabilities of the proposed formulation, once implemented in a computer program, it has been applied in three examples of structures subjected to cyclic and dynamic loadings. The obtained results show that the model may adequately predict the cyclic/dynamic response of this type of structures.

Resumen

La evaluación de la respuesta dinámica o sísmica de estructuras complejas a menudo requiere de la integración en el dominio del tiempo de la ecuación de equilibro dinámico de la estructura, en el marco de un análisis no lineal. En el caso de estructuras de fábrica y hormigón armado, el uso de este tipo de métodos cobra especial importancia, debido al complejo comportamiento no lineal que presentan, incluso para niveles bajos de carga. Muchas de estas estructuras pueden idealizarse como entramados espaciales de barras. En las últimas dos décadas, se ha desarrollado en la UPC una generalización de los métodos matriciales convencionales para el análisis de entramados espaciales de barras, la llamada Formulación Matricial Generalizada (FMG). La formulación básica para elementos de directriz curva y sección variable fue presentada inicialmente por Carrascón et al. (1987). Posteriormente, Carol y Murcia (1989) aplicaron esta formulación al análisis non lineal de procesos variables en el tiempo. Esta formulación fue extendida luego al análisis no lineal geométrico y del material de estructuras de obra de fábrica (Molins, 1996; Molins y Roca, 1998). Una extensión de la formulación estática básica al análisis dinámico lineal fue presentada por Molins et al. (1998) a través de la propuesta de una matriz de masa consistente. Esta formulación ha probado ser una herramienta eficiente para el análisis no lineal de estructuras de pórticos espaciales, durante más de quince años de aplicación en el Departamento de Ingeniería de la Construcción de la UPC.

El objetivo fundamental de este trabajo es extender la FMG al análisis dinámico no lineal de estructuras espaciales de barras de hormigón armado y obra de fábrica. Para ello, la formulación básica ha sido complementada con varias nuevas características:

- Se ha desarrollado un modelo constitutivo cíclico uniaxial para el hormigón y la obra de fábrica sometida tanto a cargas cíclicas de compresión como de tracción. Se ha puesto especial énfasis en la descripción de la degradación de la rigidez producida durante los ciclos de carga en tracción y compresión, la forma de las

curvas de carga y descarga, y la transición entre abertura y cierre de fisuras. Se consideran dos parámetros independientes de daño, una para tracción y otro para compresión. En el caso de cargas cíclicas de compresión, el modelo se derivo de resultados experimentales obtenidos por otros autores, considerando la dependencia de las diferentes variables con el nivel de daño alcanzado, mientras que en el caso de cargas cíclicas de tracción, se propone un modelo simple basado en observaciones experimentales.

- Se adoptó un modelo constitutivo para el acero de refuerzo sometido a cargas cíclicas, el conocido modelo de Menegotto-Pinto.

- Finalmente, se adoptó un procedimiento para la integración de la ecuación de equilibrio dinámico de la estructura.

Una vez implementado en ordenador, el modelo propuesto a sido aplicado a varios casos de estructuras aporticadas de hormigón armado y obra de fábrica sometidas a cargas de tipo cíclico y dinámico. Los resultados obtenidos demuestran que el modelo propuesto permite predecir adecuadamente la respuesta cíclica/dinámica de este tipo estructuras.

Index

List of symbols

a_0, a_1, a_2	Parameters of the Menegotto-Pinto model
α_f, α_m	Parameters of the generalized-α integration method
β	Parameter of the Newmark's integration method
$\mathbf{C}$	Rotation matrix
$\boldsymbol{C}_D$	Damping matrix
ε_0	Strain at the elastic limit of concrete in compression
ε'_c	Strain at peak of the stress-strain curve of concrete in compression
ε_{ct}	Tensile strain corresponding to the tensile strength of concrete
ε_{un}	Unloading strain on envelope curve for concrete in compression
ε_{re}	Reloading strain on envelope curve after a complete cycle of concrete in compression
ε_{pl}	Residual plastic strain after the unloading curve of concrete in compression
ε_I	Strain at the intersection of the asymptotes in the Menegotto-Pinto model
ε_r	Strain at the point where load reversal occurs in the Menegotto-Pinto model
$\boldsymbol{\varepsilon}_s = (\boldsymbol{\Lambda}, \boldsymbol{\Omega})^T$	Vector of sectional strains and curvatures
$\boldsymbol{\varepsilon}_s^0$	Vector of initial strains of the section
$\boldsymbol{\varepsilon}_{XY}(s) = (\boldsymbol{\Lambda}, \boldsymbol{\Omega})^T$	Strain vector of the section with curvilinear coordinate s
$\boldsymbol{d}^0$	Vector of displacements in B due to the initial strains and stresses

$\boldsymbol{d}^*$	Vector of displacements in B produced by the deformation of the element in its basic isostatic configuration under the effect of distributed loads
δ^-	Concrete damage in compression
δ^+	Concrete damage in tension
δ_{un}	Damage at the unloading strain on envelope curve for concrete in compression
δ_{re}	Damage at the reloading strain on envelope curve for concrete in compression
E_0	Initial elastic modulus of concrete
E_{pl}	Stiffness at zero stress after unloading of concrete
E_{re}	Reloading stiffness of concrete in compression
E'	Unloading-reloading stiffness of concrete in tension
E_{s0}	Elastic modulus of reinforcing steel
E_{sh}	Hardening modulus of reinforcing steel
f_0	Stress at the elastic limit in compression
f'_c	Compressive strength of concrete
f_{ct}	Tensile strength of concrete
$\boldsymbol{F}$	Flexibility matrix of the element
γ	Parameters of the Newmark's integration method
G_f	Fracture energy of the concrete in tension
$\boldsymbol{\Gamma} = (X, Y, Z)$	Reference vector of points belonging to the axial curve
$\boldsymbol{K}_s$	Sectional stiffness matrix
$\boldsymbol{K}$	Stiffness matrix of the element
l^*	Characteristic length or crack band width
$\boldsymbol{\lambda}(s)$	Vector of displacements reference axial curve at the point with curvilinear coordinate s
$\boldsymbol{\Lambda}(\xi) = (\varepsilon_X, \varepsilon_Y, \varepsilon_Z)$	Vector of sectional strains in the curvilinear coordinate point ξ

$\boldsymbol{M}$	Mass matrix of the element
$\boldsymbol{N}(s, s_B)$	Interpolation matrix that describes the exact equilibrium forces between the transverse sections B and s
$\boldsymbol{\omega}(s)$	Vector of rotations of the reference axial curve at the point with curvilinear coordinate s
$\boldsymbol{\Omega}(\xi) = (\phi_X, \phi_Y, \phi_Z)$	Vector of sectional curvatures in the curvilinear coordinate point ξ
$\boldsymbol{p}(t)$	Vector of applied loads
$[\boldsymbol{p}, \boldsymbol{m}]^T$	Vector of distributed forces and moments
$\boldsymbol{P}$	Vector of forces at the extreme of the element
$\boldsymbol{P}^{*0}$	Vector of reactions corresponding to the perfect clamping at the ends of the element due to initial strains and stresses.
$\boldsymbol{P}_A$	Vector of forces at the end A
$\boldsymbol{P}_B$	Vector of forces at the end B
σ_f	Crack closure stress
σ_f^0	Initial crack closure stress
σ_I	Stress at the intersection of the asymptotes in the Menegotto-Pinto model
σ_r	Stress at the point where load reversal occurs in the Menegotto-Pinto model
$\boldsymbol{\sigma}_s = (N, V_y, V_z, M_x, M_y, M_z)^T$	Vector of sectional forces
$\boldsymbol{\sigma}_s^0$	Vector of forces due to initial stresses
$\boldsymbol{\sigma}_{XY}(s)$	Vector of sectional forces at a section of curvilinear coordinate s
$\boldsymbol{\sigma}_{XY}^*(s)$	Vector of forces produced by the distributed loads on a cantilever isostatic configuration
$\boldsymbol{u}$	Vector of displacements at the extremes of the element
$\boldsymbol{u}(t)$	Vector of displacements at instant t
$\boldsymbol{u}_i, \boldsymbol{u}_{i+1}$	Vectors of displacements at time t_i and t_{i+1}
$\dot{\boldsymbol{u}}_i$, $\dot{\boldsymbol{u}}_{i+1}$	Vectors of velocities at time t_i and t_{i+1}

$\ddot{\boldsymbol{u}}_i$, $\ddot{\boldsymbol{u}}_{i+1}$	Vectors of accelerations at time t_i and t_{i+1}
$\ddot{\boldsymbol{u}}(s)$	Vector of accelerations of a point on the axis with curvilinear coordinate s

List of figures

List of tables

Chapter 1

Introduction and Objectives

Nowadays, there are a great number of reinforced concrete and masonry structures around the world that, due to its geometrical characteristics, may be idealized as spatial frames. Reinforced concrete structures and masonry structures show an extremely complex behavior as a consequence of the properties of the constituent materials and due to the work in conjunction of these materials. The behavior of these structures differs, even for low levels of loading, from the classical linear elastic behavior. The effects of cyclic and dynamic loading, such as earthquake or wind loading, increase even more the level of complexity of the structural behavior of these structures. Therefore, the proposal of new tools allowing reproducing the complex behavior of these structures by means of mathematical models of non linear analysis became of great importance for the assessment of existing structures or the design of new ones, subjected to extraordinary loading conditions of this kind. In this chapter, a basic introduction and the problem statement are presented. Finally, a series of specific objectives to be reached at the end of this research are outlined.

1.1 Introduction

After recent major earthquakes (Northridge, 1994, Kobe 1995, Izmir 1999, Sichuan 2008) the necessity for using ever more accurate methods for evaluating seismic demand on structures, became evident. In the last decades, the continuous increase of computational capacity has permitted the use of mathematical models which explicitly account for geometrical and material nonlinearities. This has allowed starting the process of leaving behind the use of the widely extended equivalent elastic force approaches of old design codes, which proved to be inefficient in preventing earthquake destructive consequences. Two main analysis tools are currently proposed for the assessment of structures, with different levels of complexity and of required computational effort: the nonlinear static analysis (the so-called pushover analysis) and the non linear dynamic analysis (time history). The later constitutes the most powerful and accurate tool for seismic assessment. In the latest generation of seismic codes (Eurocode 8, 2004; AS/NZS 1170.4, 2004; ASCE/SEI 7-05, 2005; among others) non linear dynamic analysis of three dimensional structural models is indeed recommended for the assessment of critical structures in zones of elevated seismic risk or for the design of appropriate retrofitting strategies over existing structures.

Most of the structural design computer programs already include a module for the non linear time history analysis of structures. However, the use of those methods in common professional practice is not completely extended, due to the difficulty of the theoretical background for practical engineers or the complexity of the material models involved. Therefore, the proposal of new models simplifying and reducing the computational effort of the whole process of time history analysis is of great importance. However, the extensive use of these methods requires first a clear demonstration of its accuracy and reliability.

In the case of masonry and reinforced concrete structures, the use of these methods for the assessment of the structure become of great importance, due to the its complex non linear

behavior, even for low levels of loading. Most of these structures may be idealized as spatial frames. A generalization of the conventional matrix methods for the analysis of spatial framed structures has been developed during the last two decades in the UPC, the so-called Generalized Matrix Formulation. The basic formulation for curved elements with variable cross section was presented by Carrascón et al. (1987). Carol and Murcia (1989) extended the flexibility based formulation to non linear time dependent analysis. This formulation was later extended to the geometrical and material non linear analysis of masonry framed structures (Molins, 1996; Molins and Roca, 1998). An extension of the basic formulation to the linear dynamic analysis was later proposed by Molins et al. (1998) through the proposal of a consistent mass matrix. The formulation has proved for more than fifteen years of extensive use, to be an efficient tool for the analysis of 3D framed structures. The natural next step is to extend the formulation to the non linear dynamic analysis.

The facts described above motivated the development of this thesis with the goal of proposing a model for non linear dynamic analysis of reinforced concrete and masonry framed structures in the framework of the Generalized Matrix Formulation.

1.2 Objectives

1.2.1 General objective

The objective of this research is to develop a model for the non linear dynamic analysis of masonry and reinforced concrete spatial frame structures, by means of the direct integration of the dynamic equation of motion of the structure, on the frame of the Generalized Matrix Formulation, capable of reproducing the main characteristics of the non linear behavior of this type of structures.

1.2.2 Specific objectives

In order to achieve the general goal stated above, the following set of specific objectives is also considered:

- To make an update on the state of the art, by means of an extensive documentation study in the following two main subjects:

    1) Identification of the main behavioral features of the mechanics of reinforced concrete or masonry, when subjected to cyclic and dynamic loadings and identifying the most important constitutive models allowing reproducing the complex stress-strain behavior of these materials (concrete, reinforcing steel and masonry) in those load conditions.

    2) Identification of the different methods available in the literature for the resolution of the dynamic equilibrium equation of the structure, through time step integration schemes.

- Formulation and implementation of a cyclic constitutive model for concrete and masonry subjected to general load conditions as well as the implementation of a cyclic constitutive model for reinforced steel.

- Validation of the constitutive equations adopted for the materials by the reproduction and comparison with cyclic loading tests performed by other authors, available in the literature.

- Extension of the existing Generalized Matrix Formulation to the non linear dynamic analysis by means of the implementation of a time step integration procedure for the integration of the dynamic equation of equilibrium of the structure.

- Validation of the proposed formulation through the application and comparison to specific examples of structures, including reinforced concrete and masonry, subjected to cyclic and dynamic loadings available in the literature.

1.3 Content of this document

This document is divided in six chapters, being the current chapter the first of them.

In the chapter two, the main aspects of the state of the art in the non linear cyclic and dynamic analysis and modeling of reinforced concrete and masonry structures is presented, as well as the most important integration schemes of the equation of motion proposed to date.

In chapter three, a constitutive model for the description of the response of concrete and masonry under general cyclic loading is presented and validated by its application to experimental results available in the literature.

In chapter four, the main features of the generalized matrix formulation are presented, as well as the extension to the non linear dynamic analysis by means of the direct integration of the equation of motion of the structure. The implementations of a cyclic constitutive model for reinforcing steel as well as some particularities of the numerical implementation are also addressed in this chapter.

In chapter five, the capabilities of the proposed model are shown through its application in three different examples of reinforced concrete and masonry framed structures available in the literature. In the case of reinforced concrete, two examples are presented. The first of them refers to the analysis of a reinforced concrete column subjected to transversal cyclic loading at the center of the span (Atalay and Penzien, 1975) and aims to show the ability of the proposed model to reproduce energy dissipation mechanisms on reinforced concrete elements. In the second reinforced concrete case analysis presented, the proposed model is compared against existing results on a two-storey reinforced concrete frame subjected a

seismic base motion (Carydis, 1997). In the case of masonry structures, one of the three-story scaled plain masonry buildings subjected to a seismic excitation by Tomazevic and Weiss (1994) has been reproduced with the model proposed herein.

Finally, the conclusions obtained through out this research are summarized in chapter six, as well as a set of recommendations for future research.

Chapter 2

State of the Art

Detailed non linear cyclic and dynamic analysis of reinforced concrete and masonry framed structures is increasingly applied to the assessment of existing structures experiencing vibrational or dynamic effects. These methods become particularly important for the assessment and strengthening of structures located in high seismic risk regions. However, there is still significant need for efficient methods affording this type of analysis. In this chapter, the main aspects of the state of the art in the non linear cyclic and dynamic analysis and modeling of these type of structures is presented, as well as the most important integration schemes of the equation of motion proposed to date.

2.1 Non linear analysis of RC elements under cyclic loading

2.1.1 Numerical modeling strategies

Analysis of spatial reinforced concrete structures by means of solid elements is the most general and versatile approach. However, it becomes too expensive, in the computational sense, when it is applied to non linear analysis of complex structures involving multiple members. In this case, the most common and economical strategy is the use of linear elements.

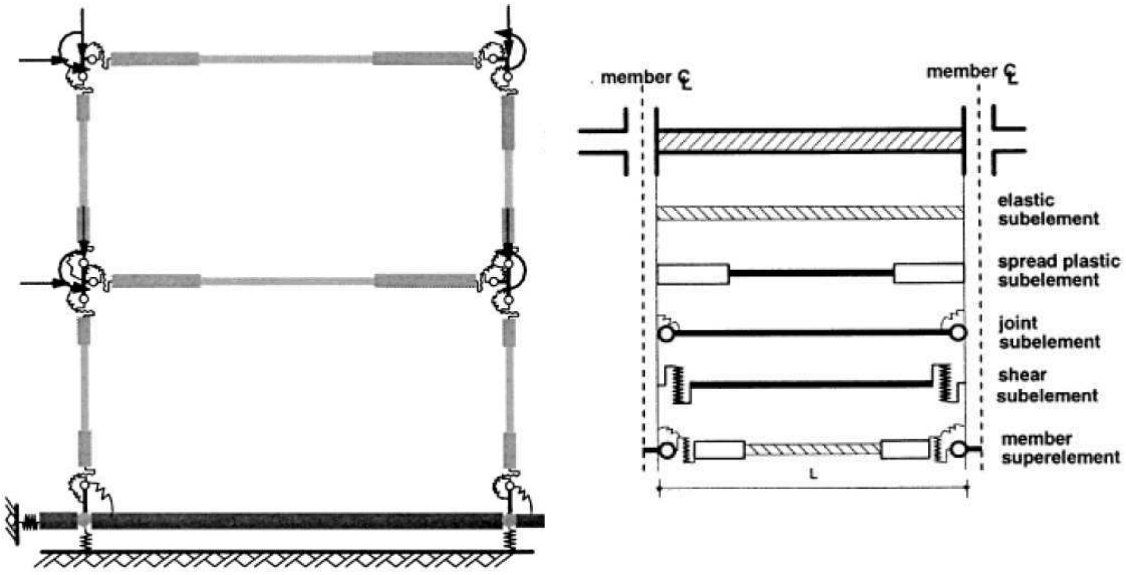

a) b)

Figure 2.1 – Typical concentrated plasticity model a) Two story frame model b) Typical frame element (D'ambrisi and Filippou, 1997)

Several beam element models suitable for the analysis of reinforced concrete structures have been proposed to date. A first set of methods (the so called concentrated plasticity methods) are based on the fact that the non linear behavior of reinforced concrete framed structures is generally concentrated at the end of columns and girders. These methods concentrate the inelastic behavior in non linear springs located at the ends of the elements (Fig. 2.1). Examples of these methods have been proposed by Clough and Jhonston (1966),

Giberson (1967), and Takizawa (1976), among others. Some of these methods include stiffness degradation in flexure and shear (Clough and Benuska 1967, Takeda et al. 1970, Brancaleoni et al. 1983), "pinching" under reversal load (Banon et al. 1981, Brancaleoni et al. 1983) and fixed end rotations at the beam-column joint interface to simulate the effect of bar "pull-out" (Otani 1974, Filippou and Issa 1988).

A practical advantage of the lumped inelasticity model is that practically all of the available experimental results are in the form of force-displacement relationships, or equivalently moment-curvature diagrams and hysteresis loops, allowing direct empirical fitting and facilitating the selection of model parameters (CEB 1996). On the other hand, the limitations of lumped models have been discussed in several correlation studies (Charney and Bertero 1982, Bertero et al. 1984).

A second and more accurate approach for the modelization of the inelastic behavior of reinforced concrete structures consists of distributing the nonlinearity along the length of the member. The constitutive behavior of the cross section is either formulated in terms of stress and strain resultants derived from the classical plasticity theory or is explicitly derived by the discretization of the cross section into fibers. In a fiber finite element model the member is discretized both longitudinally, into segments represented by discrete cross-sections or slices, and at the cross sectional level, into finite regions. In the more general case of biaxial bending, the cross-section is divided into a number of finite regions by a rectangular grid of lines. These formulations have been successfully employed in the non linear analysis of reinforced concrete framed structures, as in Kang and Scordelis (1980), Buckle and Jackson (1981), Mahasuverachai and Powell (1982), Kaba and Mahin (1984), Zeris and Mahin (1988), Chan (1981), Mari (1984), Ulm et al. (1994), Petrangeli and Ciampi (1997) or Spacone et al. (1996), among others.

Time and segmental construction effects were introduced following similar approaches by Ghali and Elbadry (1985), Kang and Scordelis (1980), Abbas and Scordelis (1993), Ketchum (1986), Murcia and Herkenhoff (1994), Cruz et al. (1998), Mari (2000), among others.

Saritas and Filippou (2006) and Petrangeli et al. (1999) proposed fiber element models for cyclic bending and shear of reinforced concrete structures. More recently, Bairán and Mari (2007) developed a non linear sectional formulation to account for full 3D stress-strain states on frame elements. This approach is applied to the non linear coupled behavior of reinforced concrete sections and may be implemented on any 3D frame element without introducing additional degrees of freedom on the frame element. In the same way, Navarro et al. (2007) also presented a general 3D model for the analysis of reinforced and prestressed concrete frame elements with arbitrary cross section geometries and combined loading conditions, including axial force, biaxial bending moment, torsion and biaxial shear forces. To the author knowledge, none of these two models are capable to deal with the complex behavior of reinforced concrete frames subjected to cyclic combined loading conditions and both are intended to obtain the ultimate load capacity of the structure.

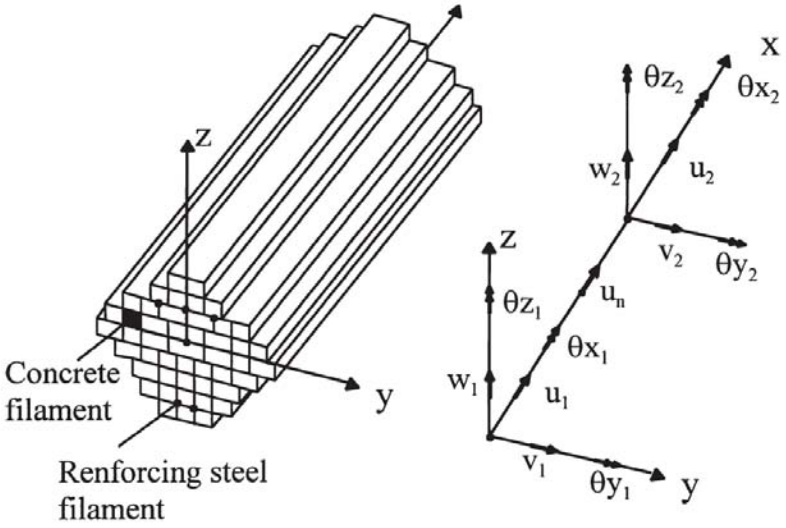

Figure 2.2 – Typical filament beam element model (Mari, 2000)

Two different approaches have been used in the derivation of the member stiffness: the stiffness approach where the nodal displacements of the structure are derived from the element forces, and the flexibility approach, which considers the member forces as the

primary unknowns. The second one permits a more accurate description of the force and stress distribution inside the member.

An alternative for the non linear analysis of frame structures, which provides a virtually "exact" solution, is the so-called Generalized Matrix Formulation (GMF). It consists of a generalization of the flexibility based conventional matrix methods, in which the frame deformation shape is a result of the exact integration of the equilibrium and compatibility equations of an element. A first precedent of this approach is found in Baron (1961). More recently, flexibility formulations for the non linear analysis of framed structures have been developed by Backlund (1976) and Grelat (1978). Carol and Murcia (1989) extended the flexibility based formulation to non linear time dependent analysis. Carrascón et al. (1987) generalized this formulation to curved elements with variable cross section. This basic formulation has been extended to the geometrical and material non linear analysis of masonry framed structures by Molins and Roca (1998), and a consistent mass-matrix for the linear dynamic analysis of spatial frames has been lately developed by Molins et al. (1998). The absence of interpolation errors allows using large elements without the necessity of intermediate nodes. However, it is necessary to use a great number of control sections for the integration along the element which may introduce precision problems and errors similar to those obtained with the finite element method when the structure is discretized in the great number of element. Mari (1991) found that similar precision may be obtained by using 2n control sections with the generalized matrix formulation, while n elements are used with the finite element method.

2.1.2 Modeling the cyclic behavior of concrete

The computational analysis of reinforced concrete structures subjected to dynamic or cyclic loadings requires realistic stress-strain material models to reproduce the real behavior of the structure. Research on the cyclic response of concrete intents to provide efficient models capable of predicting all the hysteretic characteristics of the material subjected to cyclic loading. Since the first works attempting to characterize the cyclic behavior of concrete were published (Sinha et al. 1964), a significant research effort has been devoted to that

field, which has increased even more with the recent development of computational methods applied to reinforced concrete structures.

Numerous concrete models have been proposed in the last years. In the macroscopic level, three broad categories can be distinguished (CEB 1996): models derived from the theory of elasticity, models based on the theory of plasticity and models based on the continuum damage theory. Also, some coupled models based on the association of plasticity and continuum damage theory have been recently developed. Although it has been proved that the models derived from theory of plasticity and continuum damage theory can accurately simulate the observed behavior of concrete, its application in the engineering practice is reduced. This is motivated by the great amount of parameters that are usually needed and the difficulty to obtain them through conventional laboratory tests. In the context of this study, only simplified models which are essentially mathematical formulations derived from the generalization of test results for concrete under various loading histories are treated. Many of these models have been documented in the literature, like Sinha et al. (1964), Karsan and Jirsa (1969), Yankelevsky and Reinhardt (1987), Mander, Priestley and Park (1988), Bahn and Hsu (1998), Chang and Mander (1994), Mansour and Hsu (2005), Palermo and Vecchio (2003) among others. Most of them refer only to the compressive cyclic behavior of concrete and only a few consider the cyclic tension response.

Sinha et al. (1969) carried out an experimental investigation on the behavior of plain concrete under cyclic compression loading. A series of forty-eight tests were performed on concrete cylinders to obtain information about the properties of the envelope curve and the unloading and reloading curves, and analytical stress-strain relations for cyclic loading were derived. They assumed the property of uniqueness of the stress-strain relations (i.e. if the envelope, the unloading and the reloading curve passing through any point in the stress-strain plane remain independent of the previous load history, then the stress-strain relationship is unique) to predict behavior of concrete subjected to an arbitrary compression load history. This hypothesis was refuted by subsequent experimental evidence.

Karsan and Jirsa (1969) developed an experimental study of the strength and behavior of plain concrete subjected to repetitions of compressive stress to multiple levels. A total of 46 short rectangular columns were tested under cyclically varying axial loads. This was carried out in order to determine the stress-strain envelope and the unloading and reloading curves. The test results indicated that the stress-strain paths under cyclic loading generally do not exceed the envelope curve; furthermore, this curve can be modeled as the stress-strain curve obtained under monotonic loading to failure. The authors reported that the loading and unloading curves starting from a point within the stress-strain domain were not unique and that the value of stress and strain at the peak of the previous loading cycle had to be known to estimate the response. They considered the residual plastic strain as principal parameter to determine the unloading curve equation and proposed an empirical formula to correlates the residual plastic strain with the point on the envelope from which unloading starts.

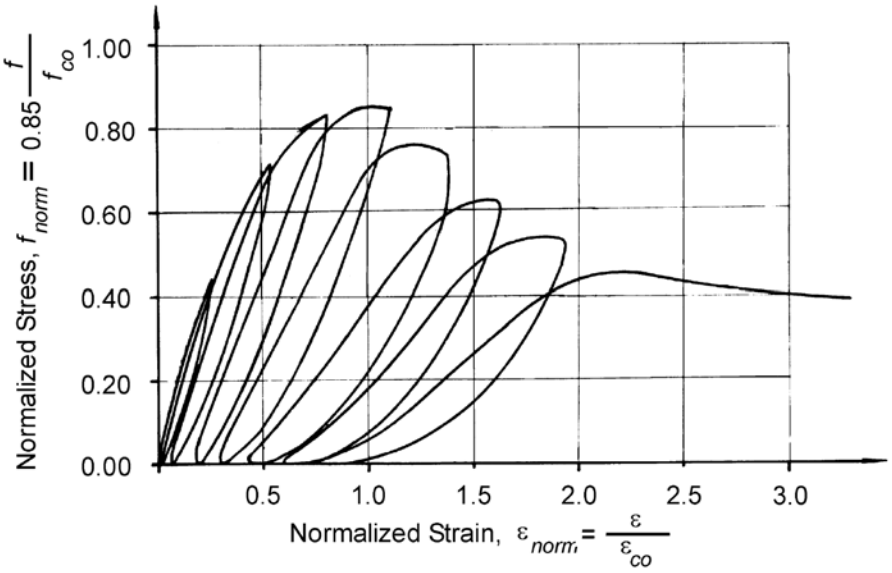

Figure 2.3 – Typical result of a cyclic compression test (Karsan and Jirsa,1969)

When reloading starts from zero stress to meet the envelope curve, it is found that the reloading curve becomes rather flat in most of its range and may be represented by a simple straight line (Sinha et al.1964) or a second-order parabola (Karsan and Jirsa, 1969).

Yankelevsky and Reinhardt (1987) proposed a simple uniaxial stress-strain model, based on geometrical properties of the loading history curves in the uniaxial stress-strain plane. They modeled the complete unloading-reloading cycle by a set of pieced linear curves defined by a set of six geometrical loci (called focal points) in the stress-strain plane.

Mander, Priestley and Park (1988) developed a stress-strain model for concrete subjected to uniaxial reversed compressive loading with incursions in tension and confined by transverse reinforcement. They used a modified expression of the equation suggested by Popovics (1973) for monotonic compression loading. The unloading curve was derived by the parameter adjustment, based on selected experimental unloading curves for confined and unconfined concrete. For the reloading curve, a linear stress-strain relation is assumed between the point of zero stress and the unloading strain, while a parabolic transition curve is adopted between the unloading strain and the return to the monotonic stress-strain. Martinez-Rueda and Elnashai (1997) modified this model to include the effect of degradation in stiffness and strength due to cyclic loading.

Chang and Mander (1994) proposed an advanced model to simulate the hysteretic behavior of confined and unconfined concrete in both cyclic compression and tension for both ordinary as well as high strength concrete including for the first time, effects of degradation produced by partial looping and a crack-closing model. The equation used by the authors for the unloading and reloading curves was a general Ramberg-Osgood equation (1949) adjusted by a series of parameters: the slope at the origin and the slope at the end of each curve. The complete behavior of concrete under cyclic loading was defined through a series of rules for each kind of curve (envelopes curves, unloading curves and reloading curves). To define the cyclic properties of concrete in compression, statistical regression analysis was performed on the experimental data from Sinha et al. (1964), Karsan and Jirsa (1969), Spooner and Dougill (1975), Okamoto et al. (1976) and Tanigawa and Uchida (1979). The same expressions proposed by the authors for compression were used for the tension cyclic response.

Bahn and Hsu (1998) developed a parametric study and an experimental investigation on the behavior of concrete under random cyclic compressive loading. They studied in a semi-empirical way a set of parameters that control the overall shape of cyclic stress-strain curve. This was carried out by combining the theoretical simulation and a series of experimental results. A power type equation was proposed for the unloading curve and a linear relationship for the reloading curve.

A constitutive model for concrete consistent with a compression field approach (Modified Compression Field Theory, Vecchio and Collins, 1986) was proposed by Palermo and Vecchio (2003). The concrete cyclic model presented by the authors considers concrete in both compression and tension. The unloading and reloading curves are linked to the envelope curves, which are represented by the monotonic response curves. Unloading is modeled using a Ramberg-Osgood formulation, considering boundary conditions at the onset of unloading and at a zero stress. Reloading is modeled as a linear curve with degrading reloading stiffness. This model also considers the case of partial unloading-reloading and a linear crack-closing function. All the model parameters were statistically derived from tests developed by others authors.

An extension of the Softened Membrane Model (Hsu and Zhu, 2002) subjected to reversal cyclic shear stresses, has been presented by Mansour and Hsu (2005). This work includes a cyclic uniaxial constitutive relationship for concrete that takes into account a “softening” of the concrete compressive strength caused by a constant tensile strain in the orthogonal direction. The unloading and reloading curves were formed by a set of pieced linear curves.

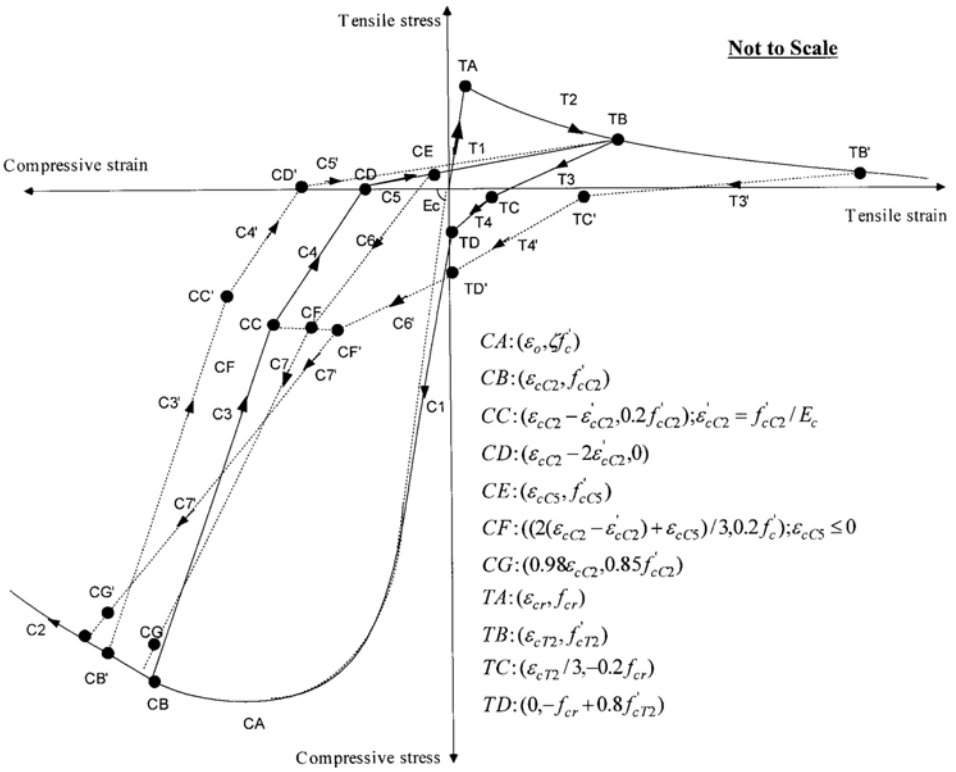

Figure 2.4 – Analytical model for cyclic stress-strain curves of concrete (Mansour and Hsu, 2005)

More recently, Sakai and Kawashima (2006) proposed an unloading and reloading model for concrete confined by transverse reinforcement. This model is based on tests results on reinforced concrete column specimens. It considers the effect of repeated unloading/reloading cycles and partial unloading-reloading by taking into account the number of cycles.

Under real cyclic or dynamic actions, concrete may experience complex loading processes involving not only full unloading-reloading cycles in compression or tension, but also partial unloading and reloading processes and mixed cycles involving compression and tension stresses and cracking. Some of the models available focus on particular aspects of the cyclic behavior. Thus, Karsan and Jirsa (1969), Yankelevsky and Reinhardt (1987), Mander, Priestley and Park (1988) or Bahn and Hsu (1998) are oriented to the compressive

regime. Moreover, Karsan and Jirsa (1969), Yankelevsky and Reinhardt (1987), Mander, Priestley and Park (1988) deal with only total unloading and reloading processes.

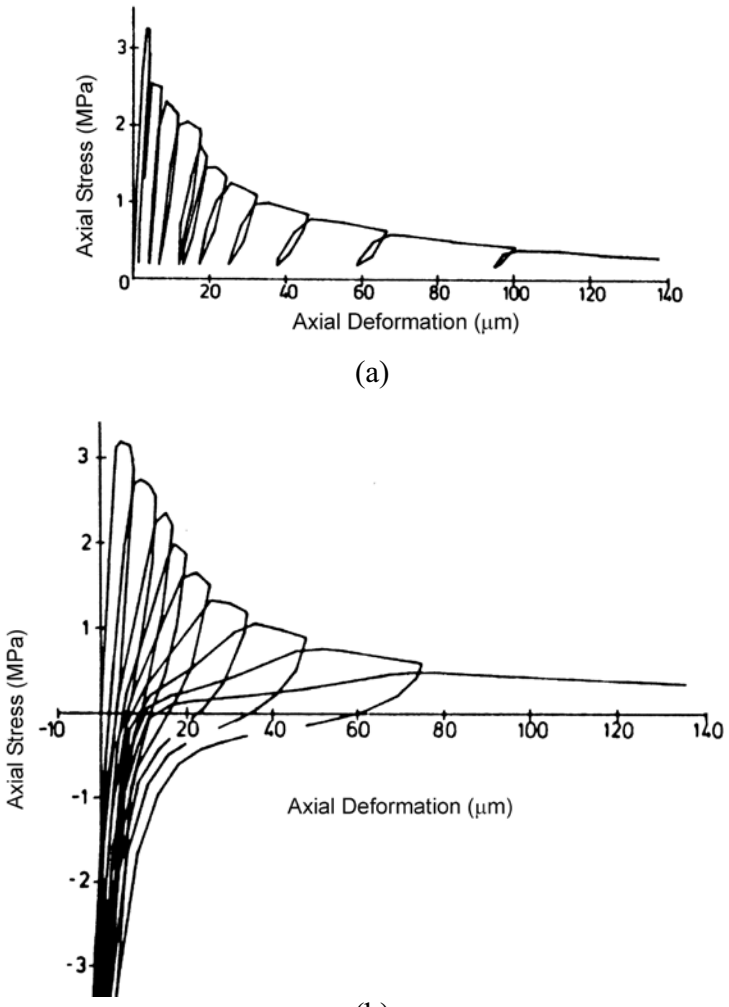

Figure 2.5 – Stress-strain response of concrete subjected to cyclic tensile loadings (a) and subjected to cyclic load reversals (Reinhardt, 1984)

Reinhardt (1984) presented a set of experiments for the characterization of concrete subjected to cyclic tensile loading (Fig. 2.5). Important characteristics of the concrete response include the following: 1) concrete responds essentially in a linear elastic manner until the tensile strength is reached. 2) After the peak tensile strength, the material presents a softening branch 3) unload-reload cycles initiating at strains in excess of the

correspondent to the peak tensile strength occur with a material stiffness significantly lower than the original material modulus.

2.1.3 Modeling the cyclic behavior of reinforcing steel

The behavior of the reinforcing steel is an important issue which may have a great influence in the overall behavior reinforced concrete members under cyclic or dynamic loadings. When subjected to cyclic loading, steel exhibits a loss of linearity prior to the attainment of the yield strength in the opposite direction. This characteristic is known as Bauschinger effect and has been observed that becomes more pronounced when increasing strain demand (Ma et al. 1976). Several models for the reinforcing steel accounting for the Bauschinger effect and other characteristics of the steel behavior have been proposed to date (Park et al. 1972, Aktan et al. 1973, Ma et al. 1976, Stanton and McNiven 1979, Filippou et al. 1983, Monti and Nuti 1992, Chang and Mander 1994, Hoehler and Stanton 2006). In all cases, these are phenomenological models where constitutive laws are calibrated on the basis of experimental data, based on either, Ramberg and Osgood (1943) or Menegotto and Pinto (1973) models. More recently, models based on the natural coordinates system have been developed; such is the case of those proposed by Dodd and Restrepo-Posada (1995) or Balan et al. (1998).

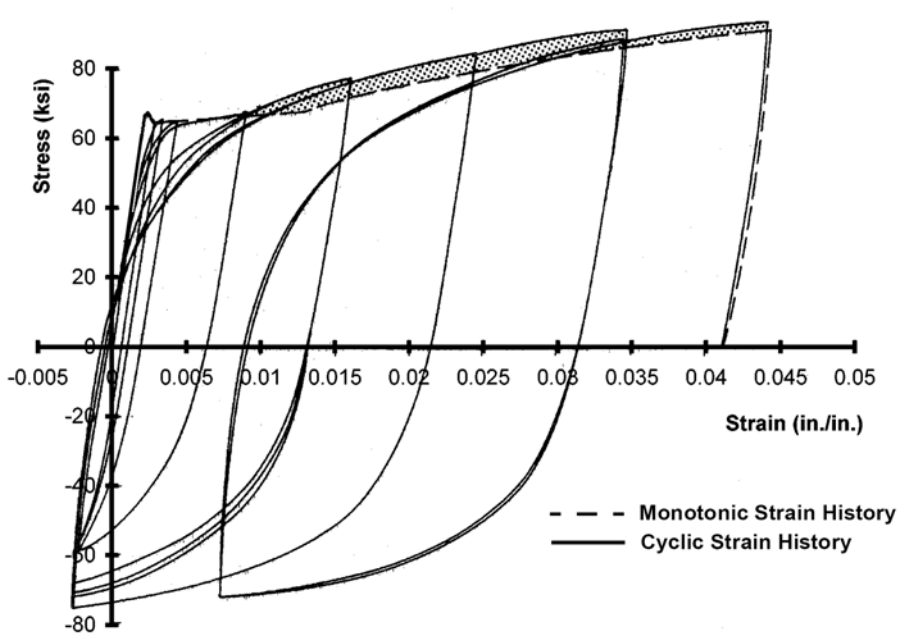

Figure 2.6 – Response of reinforcing steel subjected to reversed cyclic loading (Ma et al., 1976)

The model proposed by Ramberg and Osgood (1943) uses a single non linear equation to characterize the observed curvilinear response of reinforcing steel subjected to monotonic loading. The model defines the normalized strain as a function of the normalized stress with the following expression:

$$\varepsilon_{norm} = \beta\sigma_{norm}(1+\alpha|\sigma_{norm}|^{n-1}) \tag{2.1}$$

where ε_{norm} and σ_{norm} are the normalized strain and stress. The model may be extended for the case of reversed cyclic loading by introducing into the previous equation the strain and stress at the load reversal point. This model has shown acceptable accuracy predicting the one dimensional steel response. On the other hand, the explicit dependence on the stress makes more difficult its implementation.

Menegotto and Pinto (1973) proposed a model for the reinforcing steel subjected to load reversals where the response is defined by the following equation:

$$\sigma^* = b\varepsilon^* - \frac{(1-b)\varepsilon^*}{\left(1+\varepsilon^{*R}\right)^{1/R}} \tag{2.2}$$

where the effective strain and stress ε^*, σ^* are a function of the unload0reload interval, b is the ratio of the initial to final tangent stiffness and R is a parameter that defines the shape of the unloading curve.

2.2 Non linear analysis of masonry structures subjected to cyclic loading

During the last two decades, the capabilities of the non linear analysis for the assessment of masonry structures has been increased with the introduction of sophisticated methods for the modelization of the complex behavior of masonry. These methods are based in two main approaches, namely the macro-modeling and the micro-modeling. The first does not take into consideration any distinction between masonry units and joints, by means of averaging the effect of the mortar joints through the formulation of an equivalent continuous material. These average material properties are usually obtained by means of homogenization techniques (Pegon and Anthoine, 1997; Luciano and Saco, 1997; Milani et al, 2006; among others). The micro-modeling approach consists in modeling individually the mortar joints and the masonry units (Lourenço, 1996). In some cases, simplifications on the micro-modeling have been introduced, by means of using zero-thickness interfaces for the joints (Lourenço and Rots, 1997; Lofti and Shing, 1994). Although these methods allow the reproduction of the complex non linear behavior of masonry, the great computational effort required constrains the applicability of them to masonry panels and small structures. These limitations are even more evident when the assessment of complex masonry structures by means of time history analysis is considered. Alternative methods which may permit the time history non linear analysis of masonry wall structures, with a reasonable grade of accuracy and computational time consuming is still necessary.

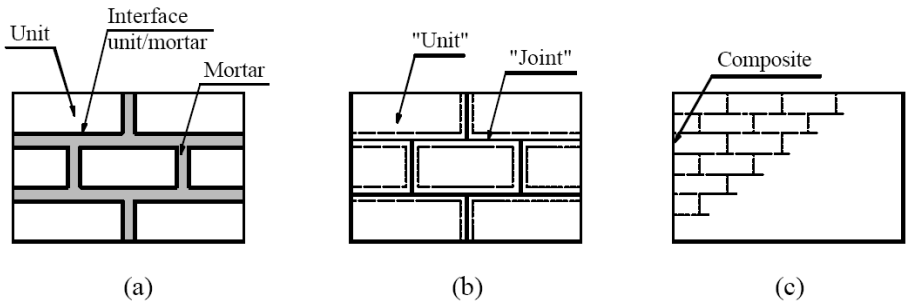

Figure 2.7 – Computational strategies for masonry: (a) detailed micro-modelling; (b) simplified micro-modelling; (c) macro-modelling (Lourenço, 1996)

A great number of existing masonry structures may be modeled as a set of linear elements, form spatial frames, like in the case of masonry arches. Molins and Roca (1998) presented a numerical model for the study of masonry arches and spatial frames, which considers both geometric and material nonlinearities, on the framework of the Generalized Matrix Formulation. In Roca et al. (2005), the authors extended the method to the modelization of buildings composed of masonry bearing walls. The building system is modeled as an equivalent frame system, where each wall panel is modeled as a unique element with only two nodes with six degrees of freedom per node. The main aspects that need to be addressed when one-dimensional members are used to model 2D wall systems are: 1) the capability of the one-dimensional beam formulation (in this case, Timoshenko's approach including shear deformation) to describe the axial behavior of wall panels with aspect ratios (height to base ratio) lower than the unity; and 2) the adequate description of the connection between the elements used to describe the wall panels and those referring to spandrels or lintels. In the first case, the authors shown that the Timoshenko's approach produce displacement results with errors of 3% with respect to a 2D finite element model in the case of wall panels with aspect ratios of 0.5. The second aspect was addressed by considering the method proposed by Kwan (1991).

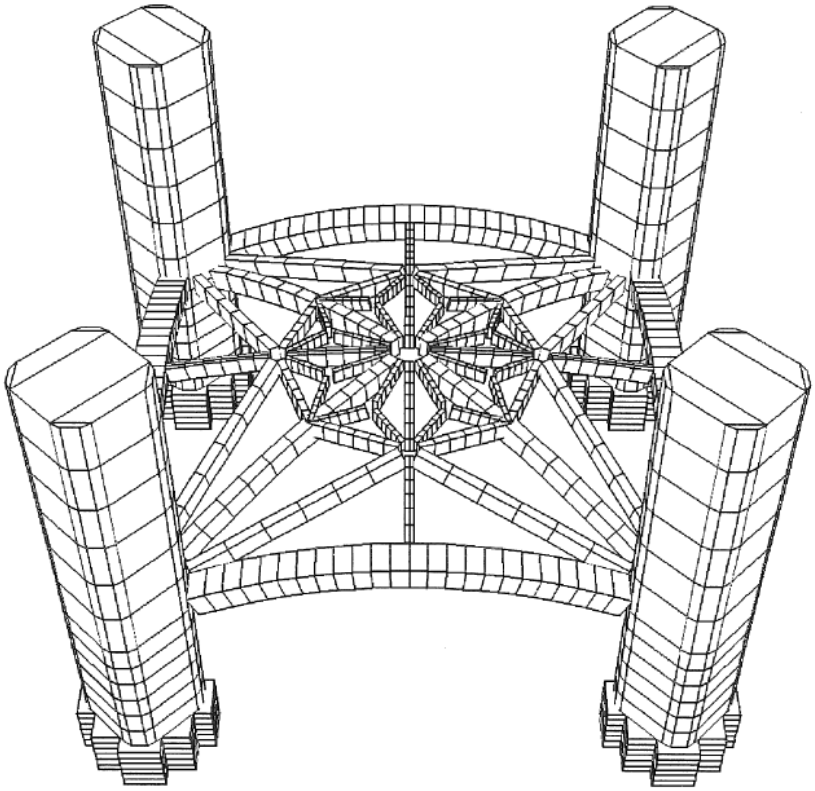

Figure 2.8 – Model of the vault of a choir inside an existing gothic church (Molins and Roca, 1998)

2.2.1 Modeling the cyclic behavior of masonry

A significant number of papers have been presented during the last years on the characterization of the behavior of masonry subjected to monotonic compression or shear-compression loading (Sinha, 1978; Magenes and Calvi, 1992; Calvi et al., 1996; Samarasinghe and Hendry, 1980; Page, 1981, 1983; Ganz and Thürlimann, 1983; Mann and Müller, 1982; Dhanasekar et al., 1985; Syrmankezis and Asteris, 2001; among others). However, only a few works have been presented on the behavior of masonry under cyclic loadings. This is the case of the works by Naraine and Sinha (1989), AlShebani and Sinha (1999, 2000) and Oliveira et al. (2006). Naraine and Sinha (1989) investigated the deformation characteristics of fired clay brick masonry with low levels of compressive strength under cyclic loading. This investigation was later extended to the deformation

characteristics of sand plast (a form of calcium silicate) brick masonry with higher levels of compressive strength subjected to uniaxial cyclic loading (AlShebani and Sinha, 1999) and biaxial cyclic loadings AlShebani and Sinha (2000). Oliveira et al (2006) researched on brittleness, energy dissipation and stiffness degradation of masonry prisms under cyclic loading. Other authors, as Chen et al. (1978) or Macchi (1985), have also reported on the cyclic behavior of brick masonry with focus on seismic design of buildings. In all cases, the behavior shown by brick masonry subjected to uniaxial cyclic loading presents significant similarity to that of concrete. The latter has been investigated since long time by Karsan and Jirsa (1969) and others.

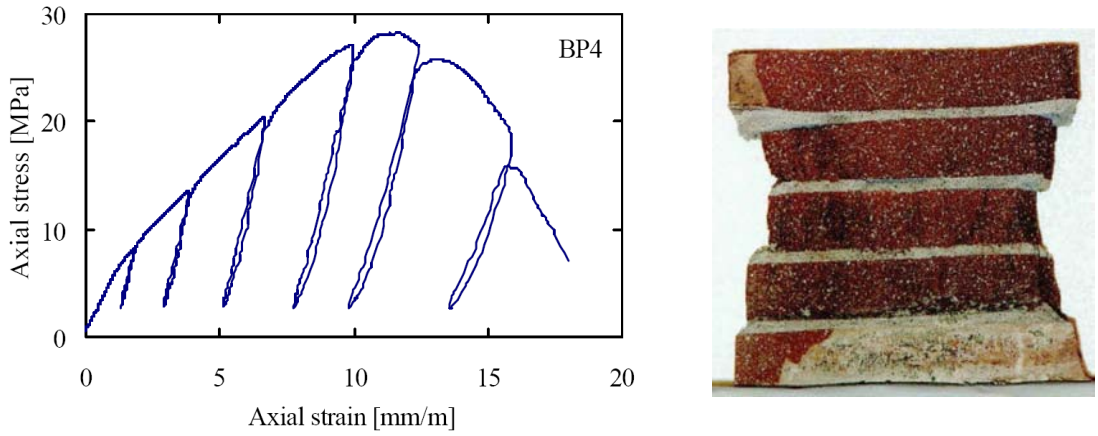

(a) (b)

Figure 2.9 – Masonry prisms subjected to cyclic compressive loading (Oliveira, 2002) (a) typical stress-strain curve obtained (b) view of the specimen after the test.

The tensile bond strength of the unit-mortar interface is an essential mechanical property of masonry, since most of the non linear behavior is initiated with the cracking in the mortar joints. It must be remarked that the non linear behavior of the joints is controlled by the unit-mortar interface. Moreover, the masonry strength can be generally equated to the tensile bond strength between the joint and the unit because this value is in most of the cases lower than the tensile strength of the unit. However, there are only a few numbers of works in the literature which address this issue. Van der Pluijm (1997) carried out a series of monotonic direct tensile tests in masonry specimens of solid clay and calcium-silicate

units. It was observed that the cracked specimens exhibited a bond area smaller than the cross sectional area of the specimen, and it concentrates at the inner part of the specimen, which it was attributed to the combiner effect of setting the mortar in its plastic phase and due to the effect of shrinkage. The most important material parameters concerning modeling are (Oliveira, 2002) the tensile strength and the fracture energy, defined as the energy necessary to create a unitary area of crack along the unit-mortar interface (i.e. area below the tensile stress-strain diagram). To the author knowledge, there are no experiments available in the literature regarding the behavior of masonry subjected to direct cyclic tensile loading.

2.3 Time integration schemes

2.3.1 Introduction

The mathematical expressions governing the dynamic response of the structural systems are known as the equations of motion of the structure. These equations may be formulated from the application of basic principles of the classic mechanics, like the D'alembert principle of dynamic equilibrium for example. This principle states that a structural system is in equilibrium when the forces acting on it, including the inertia forces, comply with the static equilibrium equations at each time instant. The inertia forces obtained from the Newton's second law of motion may be expressed as (Clough and Penzien, 1995):

$$\left(F_I\right)_j(t) = -m_j \ddot{d}_j(t) \qquad j = 1,2,...,n \tag{2.3}$$

where m_j, j=1,2, ...,n are the masses of the system and $\ddot{d}_j$ are the absolute accelerations. By considering also the elastic forces, the viscous damping forces and the dynamic forces acting on the structure, the system of equations of dynamic equilibrium is

$$\mathbf{M}\ddot{\mathbf{d}}(t) + \mathbf{C}\dot{\mathbf{d}}(t) + \mathbf{K}\mathbf{d}(t) = \mathbf{F}(t) \tag{2.4}$$

where $\mathbf{M}$ is the mass matrix of the structure, $\mathbf{C}$ is the damping matrix, $\mathbf{K}$ is the stiffness matrix of the structure and $\mathbf{d}(t)$, $\dot{\mathbf{d}}(t)$ and $\ddot{\mathbf{d}}(t)$ are respectively, the vector of displacements, the vector of velocities and the vector of accelerations of the structure.

The dynamic response of a structural system is obtained by solving the differential equation of motion that governs the behavior. The usual procedures for the solution of the equations of motion are the modal analysis, the analysis through the time domain, the analysis through the frequency domain and direct integration of the equation of motion by means of step-by-step integration techniques. Because superposition is applied to obtain the response of the structural system in the first three techniques, neither of these methods is suited for the use in analysis of non linear response. Although there are some attempts to extend the modal analysis to nonlinear analysis by updating the modal characteristics in each step of time (Mohraz et al, 1991; Leger and Dussolt, 1992), the step by step procedures are the only ones well suited to analysis of nonlinear response because they avoid any use of superposition. There are a great variety of step-by-step integration procedures, but in all of them the loading and the response history are divided into a sequence of time intervals or "steps". The response during each step is therefore calculated from the initial conditions (displacement and velocity) at the beginning of the step and from the history of loading during the step. Therefore, the response of each step is an independent analysis problem and there is no need to combine response contribution within the step. Non linear behavior may be considered easily by this approach simply by assuming that the structural properties remain constant during each step. Any desired degree of refinement in the nonlinear behavior may be reached by considering the time steps short enough. It can also be applied to any kind of nonlinearity, including those produced by changes in mass properties, damping properties and the more common nonlinearities due to changes in stiffness. The literature on this subject is vast, therefore only the main aspects of the most important step-by-step methods are outlined in the following paragraphs.

2.3.2 Step-by-step integration methods: basic concepts

Step-by-step procedures attempt to determine the dynamic history response, either for linear or non linear systems. This response is obtained from eq. 2.4, for a discrete set of time instants t_i instead of a function continuous in time. In general, these methods consist on the expression of the accelerations and velocities for a time step as a function of the actual displacement and the accelerations, velocities and displacements known for the previous step.

The methods may be classified either explicit or implicit. In the explicit or "open" methods the new response values calculated in each step depends only on quantities obtained in the preceding step, so that the analysis proceeds directly from one step to the next. On the other hand, in an implicit method the expressions that provide the new values for a given step include one or more values pertaining to that same step. At this point, the problem of the stability of the solution, intended in the way that the solution progress within some limits for the time interval Δt selected, becomes important. While in the case of the implicit algorithms, the solution is not artificially amplified whichever is the time interval selected (unconditionally stable algorithms), for the explicit methods there is a critical time interval over which the solution is artificially amplified (conditionally stable schemes).A fundamental result obtained by Dahlquist (1963) says that it is not possible the unconditional stability for the explicit schemes. As a result, the application of explicit algorithms is limited to the cases where small time step intervals are required, like in the case of impulse loadings.

For linear problems, it is possible to present, for each time step, an equation in the form:

$$\mathbf{Y}_{i+1} = \mathbf{A}\mathbf{Y}_i + \mathbf{Z}_{i+\alpha} \tag{2.5}$$

where the $\mathbf{Y}_i$ represents the dynamic response of the structure, $\mathbf{A}$ is the characteristic matrix of the integration scheme or "amplification matrix" and $\mathbf{Z}_{i+\alpha}$ refers to the external

forces included in the analysis for the in order to obtain the response at the time t_{i+1}, acting in this time interval. Based on equation 2.5, it is possible to analyze the stability of a time integration scheme (Barbat and Canet, 1994). The stability of the step-by-step procedure applied to linear systems became determined by following criterion

$$\rho(\mathbf{A}) = \max|\lambda_i| \leq 1 \tag{2.6}$$

where $\rho(\mathbf{A})$is the spectral radius of the amplification matrix, defined as the maximum absolute value of all eigenvalues. The spectral radius allows obtaining a clear indication of the behavior of the numerical solution and the amount of damping introduced as a function of the set of parameters that characterize the time integration scheme. This criterion for verifying the unconditional stability of time step procedures is valid for linear dynamics. That is not the case of non linear dynamics and a further criterion for the stability of time integration algorithms, as the conservation of energy, should be applied.

The accuracy of the algorithm is defined as the order of magnitude of the error as a function of the time interval considered.

Stability and accuracy are the most discussed properties of the step-by-step procedures. In the case of linear dynamic systems, the main topic is the order of accuracy of the solution, because the unconditional stability criterion is easy to be satisfied by most of the algorithms. On the other hand, in the case of nonlinear dynamic systems, the interest is focused on the numerical stability of the solution. Algorithms which are unconditionally stable in the linear regime often lose this stability in the nonlinear case (Kuhl and Chrisfield, 1999).

2.3.3 Explicit schemes. Central difference method

The central difference method is the most used explicit method for the solution of dynamic problems. As was stated before, in this kind of methods, the equation of equilibrium is

written in the time t_i in order to obtain the response of the structure at the time t_{i+1}. The solution is simplified, but on the other hand, it presents the problem of conditional stability. This means that for time intervals greater than a critical time step (Δt_{cr}), the solution becomes unstable and the convergence is not possible.

The equations that define this method are:

$$\ddot{\mathbf{d}}_i = \frac{1}{\Delta t^2}\left(\mathbf{d}_{i+1} - 2\mathbf{d}_i + \mathbf{d}_{i-1}\right) \tag{2.7}$$

$$\dot{\mathbf{d}}_i = \frac{1}{2\Delta t}\left(\mathbf{d}_{i+1} - \mathbf{d}_{i-1}\right) \tag{2.8}$$

which, together with the differential equation of motion for the instant t_i

$$\mathbf{M}\ddot{\mathbf{d}}_i + \mathbf{C}\dot{\mathbf{d}}_i + \mathbf{K}\mathbf{d}_i = \mathbf{F}(t_i) \tag{2.9}$$

allow to obtain $\mathbf{d}_{i+1}$ as:

$$\hat{\mathbf{M}}\mathbf{d}_{i+1} = \mathbf{P}_i \tag{2.10}$$

where

$$\begin{aligned} \hat{\mathbf{M}} &= \left(\frac{1}{\Delta t^2}\mathbf{M} + \frac{1}{2\Delta t}\mathbf{C}\right) \\ \mathbf{P}_i &= \mathbf{F}(t_i) + \left(\frac{2}{\Delta t^2}\mathbf{M} - \mathbf{K}\right)\mathbf{d}_i + \left(\frac{1}{2\Delta t}\mathbf{C} - \frac{1}{\Delta t^2}\mathbf{M}\right)\mathbf{d}_{i-1} \end{aligned} \tag{2.11}$$

Considering the problem of single degree of freedom undamped system without applied forces, the equation of motion is written as

$$\ddot{x} + \omega^2 x = f \tag{2.12}$$

The central difference method could be written as

$$\begin{bmatrix} x_{i+1} \\ x_i \end{bmatrix} = \mathbf{A} \begin{bmatrix} x_i \\ x_{i-1} \end{bmatrix} \tag{2.13}$$

with the amplification matrix

$$\mathbf{A} = \begin{bmatrix} 2 - \omega^2 \Delta t^2 & -1 \\ 1 & 0 \end{bmatrix} \tag{2.14}$$

From the analysis of the eigenvalues, if can be concluded only if $\Delta t < \frac{2}{\omega_{\max}}$, where $\omega_{\max}$ is the higher frequency of the system. This simple case shows one of the shortcomings of this method: it is necessary to work with small time steps. This is not a problem when applied to impact load problems, where the time steps are small.

Gutierrez and López Cela (1998) describe a technique to provide unconditional stability to the central difference method, by truncating the higher vibration modes produced by the discretization of the structure.

2.3.4 Implicit schemes

In the following paragraphs, the most significant implicit time step procedures are presented as well as the historical evolution of the subject. In general, the parameters used for comparison are based on its behavior when applied to linear problems, mainly the relative error in period, amplitude decay and the spectral radius (unconditional stability)

Houbolt's method

Houbolt (1950) was one of the firsts in developing a specific method for the resolution of the equations of motion by means of direct integration. This method consist of approximating the displacement field by a cubic parabola in time, between four consecutive time steps (Fig. 2.11), according to the following set of equations:

$$\mathbf{d}(\tau) = a\tau^3 + b\tau^2 + c\tau + d \tag{2.15}$$

$$a = \frac{1}{6\Delta t^3}\left[-\mathbf{d}_{i-2} + 3\mathbf{d}_{i-1} - 3\mathbf{d}_i + \mathbf{d}_{i+1}\right] \tag{2.16}$$

$$b = \frac{1}{2\Delta t^2}\left[\mathbf{d}_{i-1} - 2\mathbf{d}_i + \mathbf{d}_{i+1}\right] \tag{2.17}$$

$$c = \frac{1}{6\Delta t}\left[\mathbf{d}_{i-2} - 6\mathbf{d}_{i-1} + 3\mathbf{d}_i + 2\mathbf{d}_{i+1}\right] \tag{2.18}$$

Where $\tau = t - t_i$. By taking derivatives once and twice of equation 2.15 and for the particular case of $\tau = \Delta t$ lead to:

$$\dot{\mathbf{d}}_{i+1} = 3a\Delta t^2 + 2b\Delta t + c \tag{2.19}$$

$$\ddot{\mathbf{d}}_{i+1} = 6a\Delta t + 2b \tag{2.20}$$

By substituting the values of a, b, c and d the following equations are obtained:

$$\dot{\mathbf{d}}_{i+1} = \frac{1}{6\Delta t}\left[11\mathbf{d}_{i+1} - 18\mathbf{d}_i + 9\mathbf{d}_{i-1} - 2\mathbf{d}_{i-2}\right] \tag{2.21}$$

$$\ddot{\mathbf{d}}_{i+1} = \frac{1}{\Delta t^2}\left[2\mathbf{d}_{i+1} - 5\mathbf{d}_i + 4\mathbf{d}_{i-1} - \mathbf{d}_{i-2}\right] \tag{2.22}$$

These expressions, together with the equation of motion for the instant t_{i+1} allow obtaining the displacements, velocities and accelerations for the step $i+1$.

$$\mathbf{M}\ddot{\mathbf{d}}_{i+1} + \mathbf{C}\dot{\mathbf{d}}_{i+1} + \mathbf{K}\mathbf{d}_{i+1} = \mathbf{F}(t_{i+1}) \tag{2.23}$$

It is important to notice that in the Houbolt method, there are no additional parameters besides the time step to control the damping and accuracy characteristics of the method. In addition, the second members of equations 2.21 and 2.22 only consider the values of displacement that correspond to the actual step and previous steps. This is problematic at the beginning of the analysis, because the initial values for the first three steps should be known. A modified version of the Houbolt method was presented by Chung and Hulbert (1994), with a more convenient single-step form which avoids this problem.

Analyzing the behavior of the algorithm for the case undamped free vibrations of a single degree of freedom system, the following equation may be written

$$\begin{bmatrix} x_{i+1} \\ x_i \\ x_{i-1} \end{bmatrix} = A \begin{bmatrix} x_i \\ x_{i-1} \\ x_{i-2} \end{bmatrix} \tag{2.24}$$

where the amplification matrix is

$$A = \begin{bmatrix} 5\mu & -4\mu & \mu \\ 1 & 0 & 0 \\ 0 & 1 & 0 \end{bmatrix} \quad \mu = \frac{1}{2+\omega^2\Delta t^2} \tag{2.25}$$

Therefore, the Houbolt scheme is unconditionally stable no matter what is time step considered for the numerical integration.

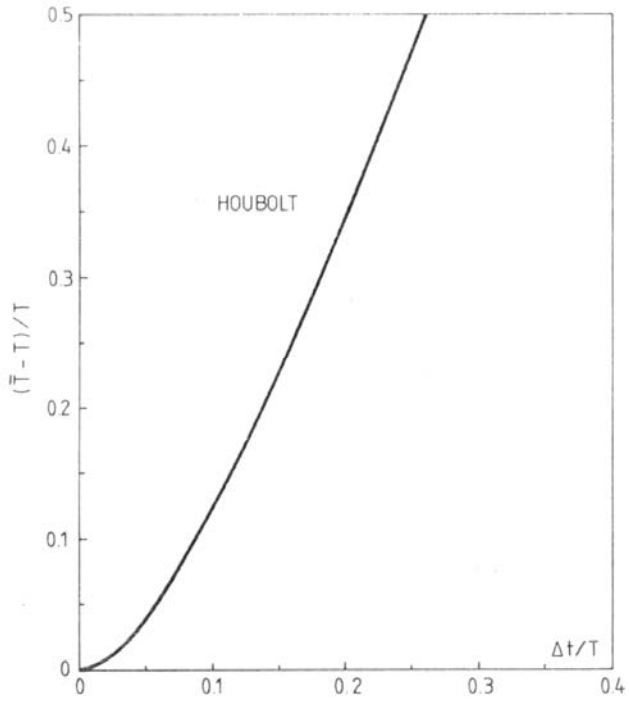

(a)

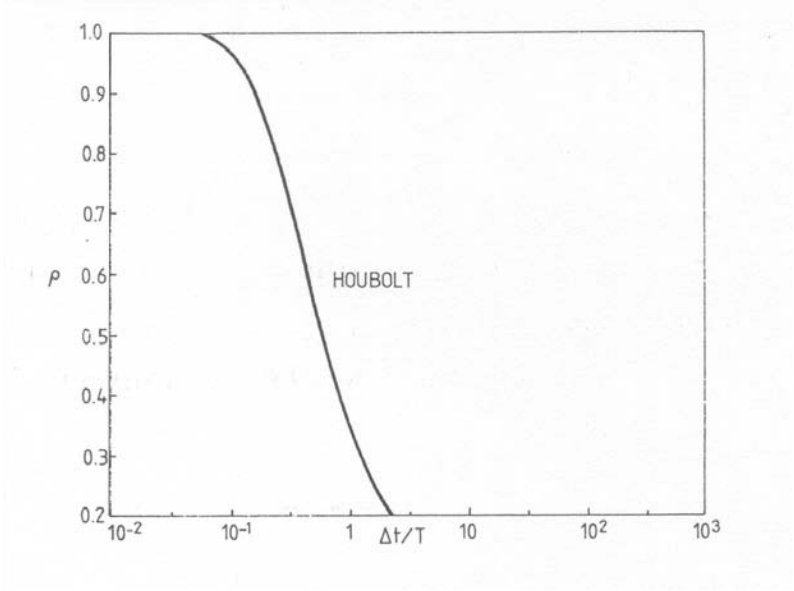

(b)

Figure 2.10– Houbolt algorithm (a) period elongation (b) spectral radius characteristics (Barbat and Canet, 1994)

Fig 2.10 shows the variation of the spectral radius with the time step considered. It can be observed that the value of the spectral radius considerably decreases below the unit, which

means that artificial damping is introduced. This property of the Houbolt method was recognized from the beginning as an essential feature in order to control the influence on the higher modes on the final response. The method is second order accurate and the time step is the only parameter used to control the numerical dissipation of the method.

Wilson's method

The method developed by Wilson (1968), introduces a new parameter θ under the hypothesis of a linear variation of the acceleration between the time t_i and the time $t_{i+\theta\Delta t}$:

$$\ddot{\mathbf{d}}(\tau) = \ddot{\mathbf{d}}_i + \frac{\tau}{\theta\Delta t}\left(\ddot{\mathbf{d}}_{i+\theta} + \ddot{\mathbf{d}}_i\right) \tag{2.26}$$

Where $\tau = t - t_i$. By integrating, the following expressions for velocities and displacements may be on obtained:

$$\dot{\mathbf{d}}(\tau) = \dot{\mathbf{d}}_i + \frac{\tau^2}{2\theta\Delta t}\ddot{\mathbf{d}}_{i+\theta} + \left(\tau - \frac{\tau^2}{2\theta\Delta t}\right)\ddot{\mathbf{d}}_i \tag{2.27}$$

$$\mathbf{d}(\tau) = \mathbf{d}_i + \tau\dot{\mathbf{d}}_i + \frac{\tau^3}{6\theta\Delta t}\ddot{\mathbf{d}}_{i+\theta} + \left(\frac{\tau^2}{2} - \frac{\tau^3}{6\theta\Delta t}\right)\ddot{\mathbf{d}}_i \tag{2.28}$$

Considering the particular case $\tau = \theta\Delta t$ leads to

$$\dot{\mathbf{d}}_{i+\theta} = \dot{\mathbf{d}}_i + \frac{\theta\Delta t}{2}\left(\ddot{\mathbf{d}}_{i+\theta} + \ddot{\mathbf{d}}_i\right) \tag{2.29}$$

$$\mathbf{d}_{i+\theta} = \mathbf{d}_i + \theta\Delta t\dot{\mathbf{d}}_i + \frac{\theta^2\Delta t^2}{6}\ddot{\mathbf{d}}_{i+\theta} + \frac{\theta^2\Delta t^2}{3}\ddot{\mathbf{d}}_i \tag{2.30}$$

therefore

$$\ddot{\mathbf{d}}_{i+\theta} = \frac{6}{\theta^2 \Delta t^2}\left(\mathbf{d}_{i+\theta} - \mathbf{d}_i\right) - \frac{6}{\theta \Delta t}\dot{\mathbf{d}}_i - 2\ddot{\mathbf{d}}_i \tag{2.31}$$

$$\dot{\mathbf{d}}_{i+\theta} = \frac{3}{\theta \Delta t}\left(\mathbf{d}_{i+\theta} - \mathbf{d}_i\right) - 2\dot{\mathbf{d}}_i - \frac{\theta \Delta t}{2}\ddot{\mathbf{d}}_i \tag{2.32}$$

From the latest equations and by imposing the dynamic equilibrium condition at instant $t = t_i + \theta \Delta t$ leads to:

$$\mathbf{M}\ddot{\mathbf{d}}_{i+\theta} + \mathbf{C}\dot{\mathbf{d}}_{i+\theta} + \mathbf{K}\mathbf{d}_{i+\theta} = \mathbf{F}_{i+\theta} \tag{2.33}$$

Which allows obtaining $\mathbf{d}_{i+\theta}$, and later $\mathbf{d}_{i+1}$, $\dot{\mathbf{d}}_{i+1}$ and $\ddot{\mathbf{d}}_{i+1}$ by considering $\tau = \Delta t$

Analyzing the behavior of the algorithm for the case undamped free vibrations of a single degree of freedom system, the following equation may be written:

$$\begin{bmatrix} \ddot{x}_{n+1} \\ \dot{x}_{n+1} \\ x_{n+1} \end{bmatrix} = \boldsymbol{A} \begin{bmatrix} \ddot{x}_i \\ \dot{x}_i \\ x_i \end{bmatrix} \tag{2.34}$$

with the amplification matrix

$$\boldsymbol{A} = \begin{bmatrix} 1 - \frac{\theta^2 \mu}{3} - \frac{1}{\theta} & -\theta \frac{\mu}{\Delta t} & -\frac{\mu}{\Delta t^2} \\ \left(1 - \frac{1}{2\theta} - \frac{\theta^2 \mu}{6}\right)\Delta t & 1 - \frac{\theta \mu}{2} & -\frac{\mu}{2\Delta t} \\ \left(\frac{1}{2} - \frac{1}{6\theta} - \frac{\theta^2 \mu}{18}\right)\Delta t^2 & \left(1 - \frac{\theta \mu}{6}\right)\Delta t & 1 - \frac{\mu}{6} \end{bmatrix} \quad \mu = \frac{1}{2 + \omega^2 \Delta t^2} \tag{2.35}$$

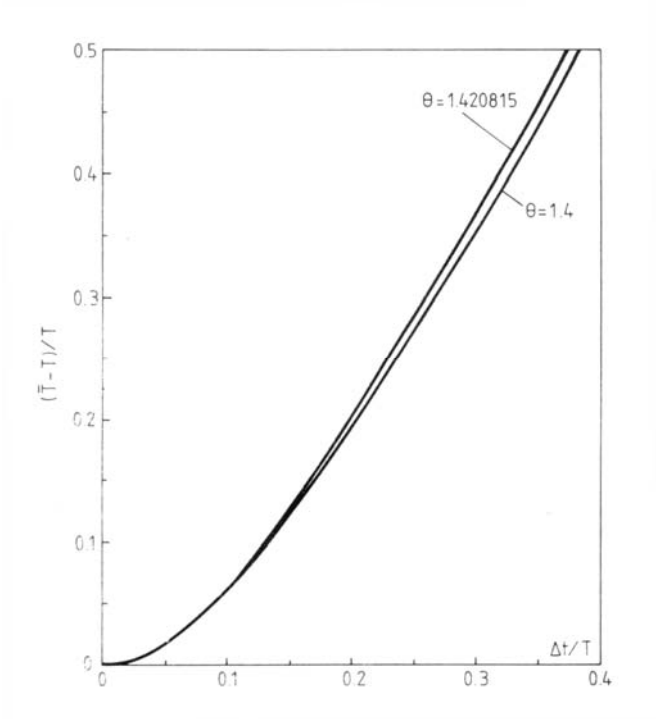

(a)

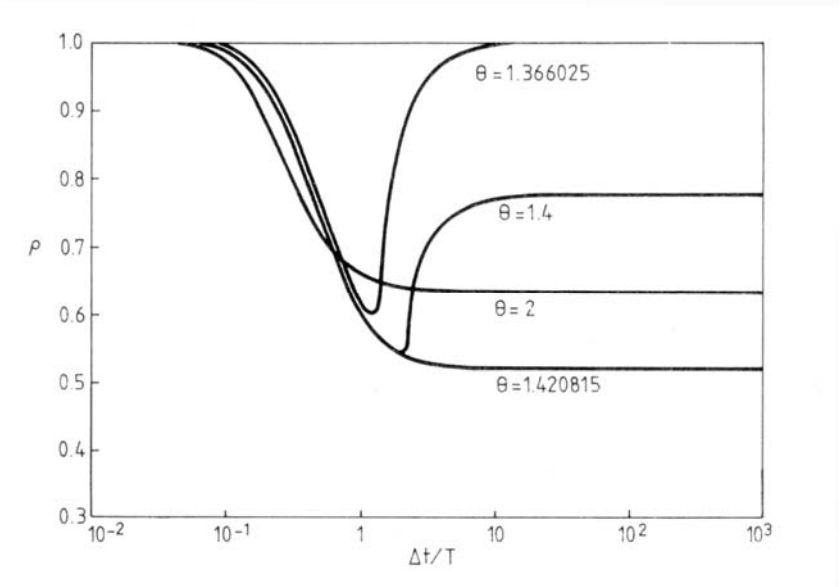

Figure 2.11– Wilson's algorithm (a) period elongation (b) spectral radius characteristics (Barbat and Canet, 1994)

The algorithm is second order accurate and it is unconditionally stable for values of θ greater than 1.37. The value recommended by Bathe and Wilson (1973) is θ = 1.4. It has been observed that for values of θ<1 the method presents an excessive level of damping over the lower modes of vibration. Therefore, in order to comply with the unconditional stability condition and to get lower damping over the first modes of vibration, it is necessary to impose the equation of motion outside the of the time interval considered (θ>1).

An advantage of this method compared with the Houbolt scheme, is that it is only necessary to know the initial conditions for a given instant, while in the Houbolt method, the conditions corresponding to the first three steps are required to start the process.

Fig 2.11 show the damping characteristics of the Wilson's method (spectral radius variation with the time step)

Newmark's Method

The method proposed by Newmark (1959), one of the most widely extended methods in common practice, follows the basic idea of numerical energy dissipation of the higher modes.

Considering the variation of the acceleration between the instants t_i and $t_{i+1} = t_i + \Delta t$ and defining $\tau = t - t_i$ with, the vector of acceleration at the instant t may be expressed as:

$$\ddot{\mathbf{d}}(\tau) = \ddot{\mathbf{d}}_i + f(\tau)\left(\ddot{\mathbf{d}}_{i+1} - \ddot{\mathbf{d}}_i\right) \tag{2.36}$$

where

$$\begin{aligned} f(\tau) &= 0 \quad \tau = 0 \\ f(\tau) &= 1 \quad \tau = \Delta t \end{aligned} \tag{2.37}$$

By integrating the previous equation, operating, and making $\tau = \Delta t$ the following equations for velocities and displacements are obtained (Barbat and Canet, 1994)

$$\dot{\mathbf{d}}_{i+1} = \dot{\mathbf{d}}_i + (1-\gamma)\Delta t\ddot{\mathbf{d}}_i + \gamma\Delta t\ddot{\mathbf{d}}_{i+1} \tag{2.38}$$

$$\mathbf{d}_{i+1} = \mathbf{d}_i + \dot{\mathbf{d}}_i\Delta t + \left[\left(\frac{1}{2}-\beta\right)\ddot{\mathbf{d}}_i + \beta\ddot{\mathbf{d}}_{i+1}\right]\Delta t^2 \tag{2.39}$$

The previous relationships represent the Newmark's difference equations which, together with the equation of motion for the instant t_{i+1} allow obtaining the response of the structure for this instant. It is evident from eq. 2.38 that the parameter γ provides a linearly varying weighting between the influence of the initial and final accelerations on the change of velocity; the factor β similarly provides for weighting the contributions of these initial and final accelerations to the change of displacement. The properties of unconditional stability, artificial damping and order of accuracy become determined by the values adopted for these parameters.

Analyzing the behavior of the algorithm for the case undamped free vibrations of a single degree of freedom system, the following equation may be written:

$$\begin{bmatrix} x_{i+1} \\ \dot{x}_{i+1} \\ \ddot{x}_{i+1} \end{bmatrix} = \boldsymbol{A}\begin{bmatrix} x_i \\ \dot{x}_i \\ \ddot{x}_i \end{bmatrix} \tag{2.40}$$

where the amplification matrix is:

$$A = \frac{1}{1+\beta\omega^2\Delta t^2}\begin{bmatrix} 1 & \Delta t & \left(\frac{1}{2}-\beta\right)\Delta t \\ -\gamma\omega^2\Delta t & 1-(\gamma-\beta)\omega^2\Delta t^2 & \left[1-\gamma-\left(\frac{1}{2}\gamma-\beta\right)\omega^2\Delta t^2\right]\Delta t \\ -\omega^2 & -\omega^2\Delta t & -\left(\frac{1}{2}-\beta\right)\omega^2\Delta t^2 \end{bmatrix} \tag{2.41}$$

Bathe and Wilson (1973) proved that the algorithm is unconditionally stable for values

$$\gamma \geq \frac{1}{2} \quad \beta \geq \frac{1}{4}\left(\frac{1}{2}+\gamma\right)^2 \tag{2.42}$$

The factor γ controls the amount of artificial damping introduced by the time step procedure and it is higher if the parameter increases. There is no artificial damping for the particular case γ=1/2 and β=1/4, which is widely known as the constant average acceleration method.

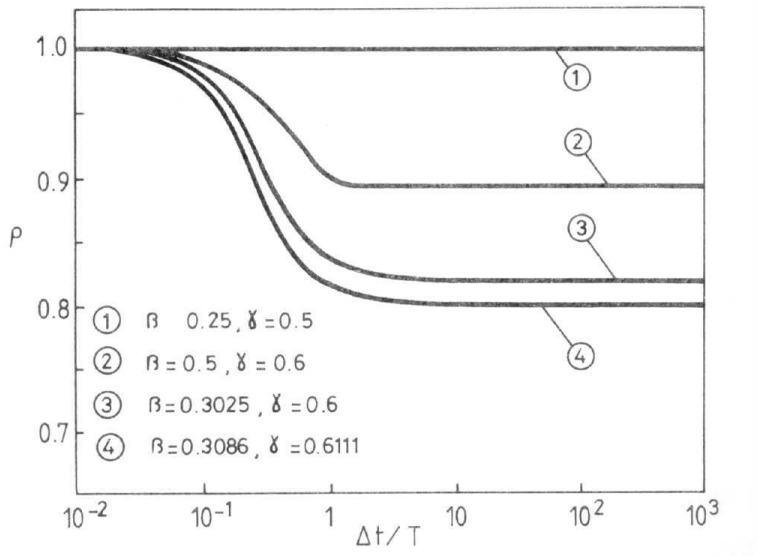

Figure 2.12– Newmark's algorithm spectral radius characteristics (Barbat and Canet, 1994)

The main shortcoming of the Newmark's method comes from the loose of second order accuracy for values of the parameters different of the constant average acceleration method. Accordingly to Bathe and Wilson (1973), the dissipative properties of this family of algorithms are considered inferior when compared with the Houbolt and Wilson methods, basically because the lower vibration modes are severely affected. On the other hand, the method shows adequate artificial damping properties over the higher modes.

The Hilber, Hughes and Taylor "α" method

The loose of the second order accuracy of the Newmark's method, has been eliminated for the first time by Hilber et al (1977) through the proposal of an alternative scheme (HHT). The main novelty of this method is the addition of a new dissipation coefficient α in the differential equation of motion. The equations in finite differences considered for an undamped system with multiple degrees of freedom are written as:

$$\mathbf{M}\ddot{\mathbf{d}}_{i+1} + (1+\alpha)\mathbf{K}\mathbf{d}_{i+1} - \alpha\mathbf{K}\mathbf{d}_i = \mathbf{F}_{i+1} \tag{2.43}$$

with

$$\ddot{\mathbf{d}}_{i+1} = \frac{1}{\beta\Delta t^2}(\mathbf{d}_{i+1} - \mathbf{d}_i) - \frac{1}{\beta\Delta t}\dot{\mathbf{d}}_i - \left(\frac{1}{2\beta} - 1\right)\ddot{\mathbf{d}}_i \tag{2.44}$$

$$\dot{\mathbf{d}}_{i+1} = \frac{\gamma}{\beta\Delta t}(\mathbf{d}_{i+1} - \mathbf{d}_i) + \left(1 - \frac{\gamma}{\beta}\right)\dot{\mathbf{d}}_i + \left(1 - \frac{\gamma}{2\beta}\right)\Delta t\ddot{\mathbf{d}}_i \tag{2.45}$$

These expressions allow obtaining the values of displacements, velocities and accelerations for the time instant t_{i+1}. Considering the case α=0, obviously this family of algorithms is reduced to the Newmark scheme. It has been studied that this algorithm is really affective for negative values of the parameter.

The amplification matrix of this method is written as:

$$A=\frac{1}{D}\begin{bmatrix} 1 & \Delta t & \left(\frac{1}{2}-\beta\right)\Delta t \\ -\gamma\omega^2\Delta t & 1-\mu(\gamma-\beta)\omega^2\Delta t^2 & \left[1-\gamma-\mu\left(\frac{1}{2}\gamma-\beta\right)\omega^2\Delta t^2\right]\Delta t \\ -\omega^2 & -\mu\omega^2\Delta t & -\mu\left(\frac{1}{2}-\beta\right)\omega^2\Delta t^2 \end{bmatrix}$$

$$D=1+(1+\alpha)\beta\omega^2 \qquad (2.46)$$

$$\mu=1+\alpha$$

Hilber et al (1977) propose values of $\beta=\frac{1}{4}(1-\alpha)^2$, $\gamma=\frac{1}{2}-\alpha$ and $-\frac{1}{3}\le\alpha\le 0$ where the algorithm is unconditionally stable.

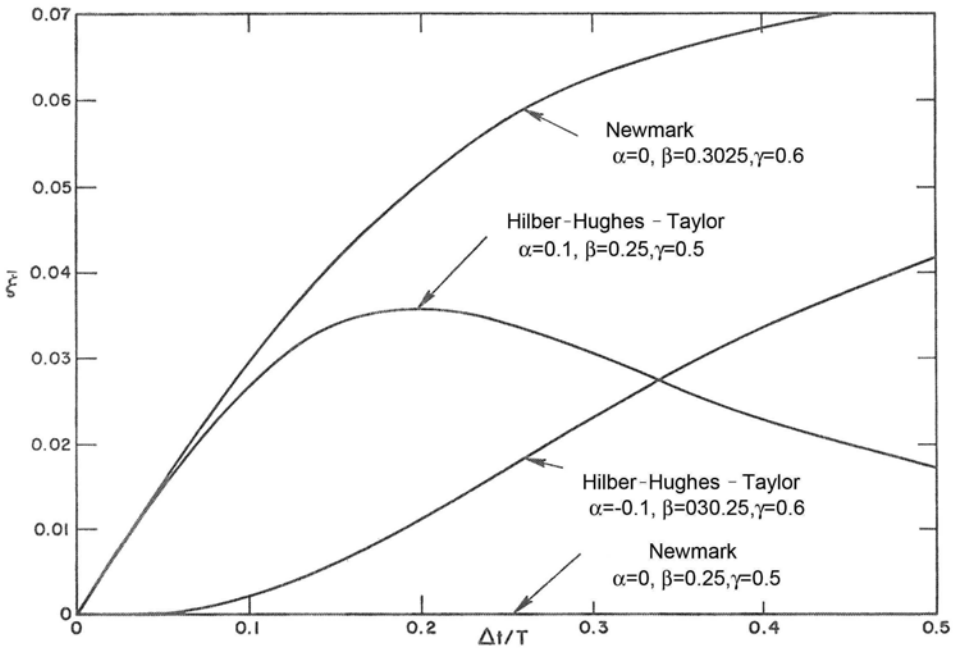

Figure 2.13– Algorithmic damping introduced by the method (Hilber et al., 1977)

Figure 2.13 the presents the damping introduced versus $\Delta t/T$, allowing the comparison between the Newmark's method and the Hilber-Hughes-Taylor scheme. It should be noted that the Hilber-Hughes-Taylor scheme with negative values of the parameter, presents a zero slope at the origin and therefore progressively increase. This is a desirable property

which ensure an adequately dissipation of the higher modes, without affecting the lower modes. This is not the case of the Newmark scheme or Hilber-Hughes-Taylor with positive values of the parameter, which present positive slope at the origin. It should also be noted that the Hilber-Hughes-Taylor scheme with positive values of the parameter, presents the additional problem of the change in the curvature, which emphasizes the inefficiency of the method for this range of values (Hilber et al, 1977).

Bossak-Newmark Method

Wood et al (1981) proposed another variation of the Newmark method (the so-called Bossak-Newmark method), which includes, like in the Hilber, Hughes and Taylor method, a new parameter α_B in order to control the artificial damping. The equation of motion for the instant t_{i+1} proposed by the authors is:

$$\left(1-\alpha_B\right)\mathbf{M}\ddot{\mathbf{d}}_{i+1}+\alpha_B\mathbf{M}\ddot{\mathbf{d}}_i+\mathbf{C}\dot{\mathbf{d}}_{i+1}+\mathbf{K}\mathbf{d}_{i+1}=\mathbf{F}\left(t_{i+1}\right) \tag{2.47}$$

where the finite difference equations for accelerations and velocities are those previously shown for the Hilber, Hughes and Taylor method.

The unconditional stability of the method is guaranteed if the following parameters are used (Wood et al, 1981):

$$\begin{aligned} &\alpha_B \le \frac{1}{2} \\ &\beta \ge \frac{\gamma}{2} \ge \frac{1}{4} \\ &\alpha_B+\gamma \ge \frac{1}{2} \end{aligned} \tag{2.48}$$

The method is second order accurate only if $\alpha_B=\frac{1}{2}-\gamma$

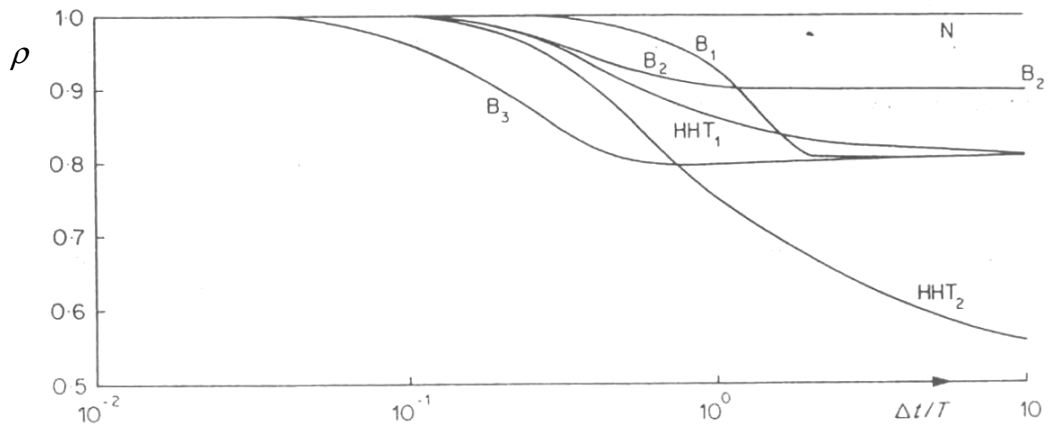

(a)

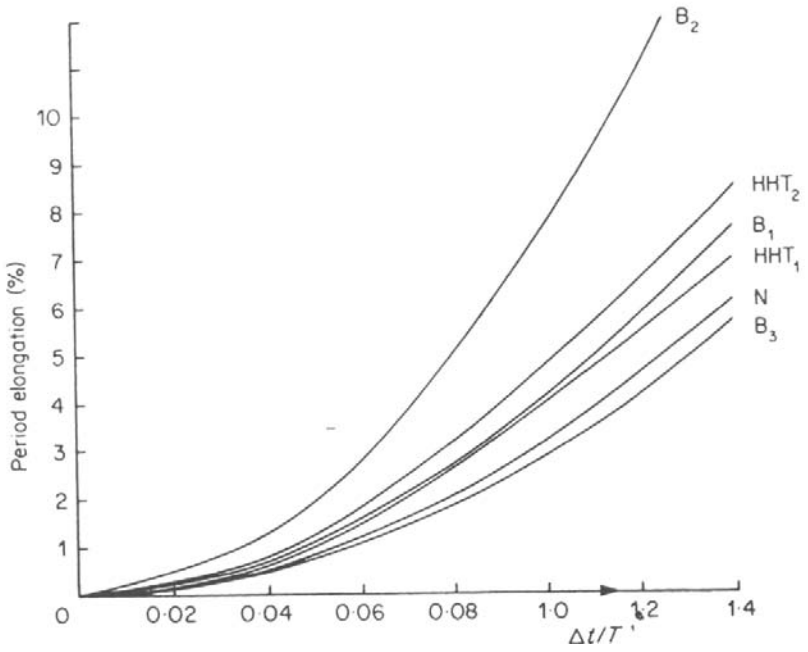

(b)

Figure 2.14– Newmark based algorithms comparison (a) spectral radius (b) period elongation (Wood et al, 1981)

N = Newmark's scheme

B_1 = Bossak's scheme $\alpha_B = -0.1,\ \beta = 0.3025,\ \gamma = 0.6$

B_2 = Bossak's scheme $\alpha_B = -0.1,\ \beta = 0.5,\ \gamma = 0.6$

B_3 = Bossak's scheme $\alpha_B = +0.1,\ \beta = 0.3025,\ \gamma = 0.6$

HHT_1 = Hilber-Hughes-Taylor scheme $\alpha_{HHT} = -0.1,\ \beta = 0.3025,\ \gamma = 0.6$

HHT_2 = Hilber-Hughes-Taylor scheme $\alpha_{HHT} = -0.3,\ \beta = 0.3025,\ \gamma = 0.6$

Collocations Schemes and "Overshooting"

Goudreau and Taylor (1972) discovered a characteristic of the Wilson family of algorithms, which makes them inappropriate for the analysis of problems with many degrees of freedom involving impact loading or loads suddenly applied: the solution suffer a significant overshoot at the initial instants of the response. Hilber y Hughes (1978) developed a study of this property for several methods developed till that moment. At the same time, the authors proposed a new family of schemes based on the basic idea of the Wilson scheme, called "Collocation Schemes". The basic equations of the proposed method are the following:

$$\mathbf{M}\ddot{\mathbf{d}}_{i+\theta} + \mathbf{K}\mathbf{d}_{i+\theta} = \mathbf{F}_{i+\theta} \tag{2.49}$$

$$\mathbf{d}_{i+\theta} = \mathbf{d}_i + \theta\Delta t\dot{\mathbf{d}}_i + (\theta\Delta t)^2\left[\left(\frac{1}{2}-\beta\right)\ddot{\mathbf{d}}_i + \beta\ddot{\mathbf{d}}_{i+\theta}\right] \tag{2.50}$$

$$\mathbf{d}_{i+1} = \mathbf{d}_i + \Delta t\dot{\mathbf{d}}_i + \Delta t^2\left[\left(\frac{1}{2}-\beta\right)\ddot{\mathbf{d}}_i + \beta\ddot{\mathbf{d}}_{i+1}\right] \tag{2.51}$$

$$\dot{\mathbf{d}}_{i+1} = \dot{\mathbf{d}}_i + \Delta t[(1-\gamma)\mathbf{d}_i + \gamma\mathbf{d}_{i+1}] \tag{2.52}$$

$$\ddot{\mathbf{d}}_{i+\theta} = (1-\theta)\ddot{\mathbf{d}}_i + \theta\ddot{\mathbf{d}}_{i+1} \tag{2.53}$$

$$\mathbf{F}_{i+\theta} = (1-\theta)\mathbf{F}_i + \theta\mathbf{F}_{i+1} \tag{2.54}$$

For the particular case with β=1/6 the method is reduced to the Wilson's scheme.

The studies developed by Hilber y Hughes (1978) revealed that the so-called "α" family of methods, which includes the HHT and the Bossak-Newmark families) show a better behavior concerning standard measures of dissipation and dispersion. In addition, it was

found that the property of overshooting reported by Goudreau y Taylor (1972) is an intrinsic characteristic of the Collocation schemes, while the "α" family of methods show good behavior of the initial response and lower levels of overshooting.

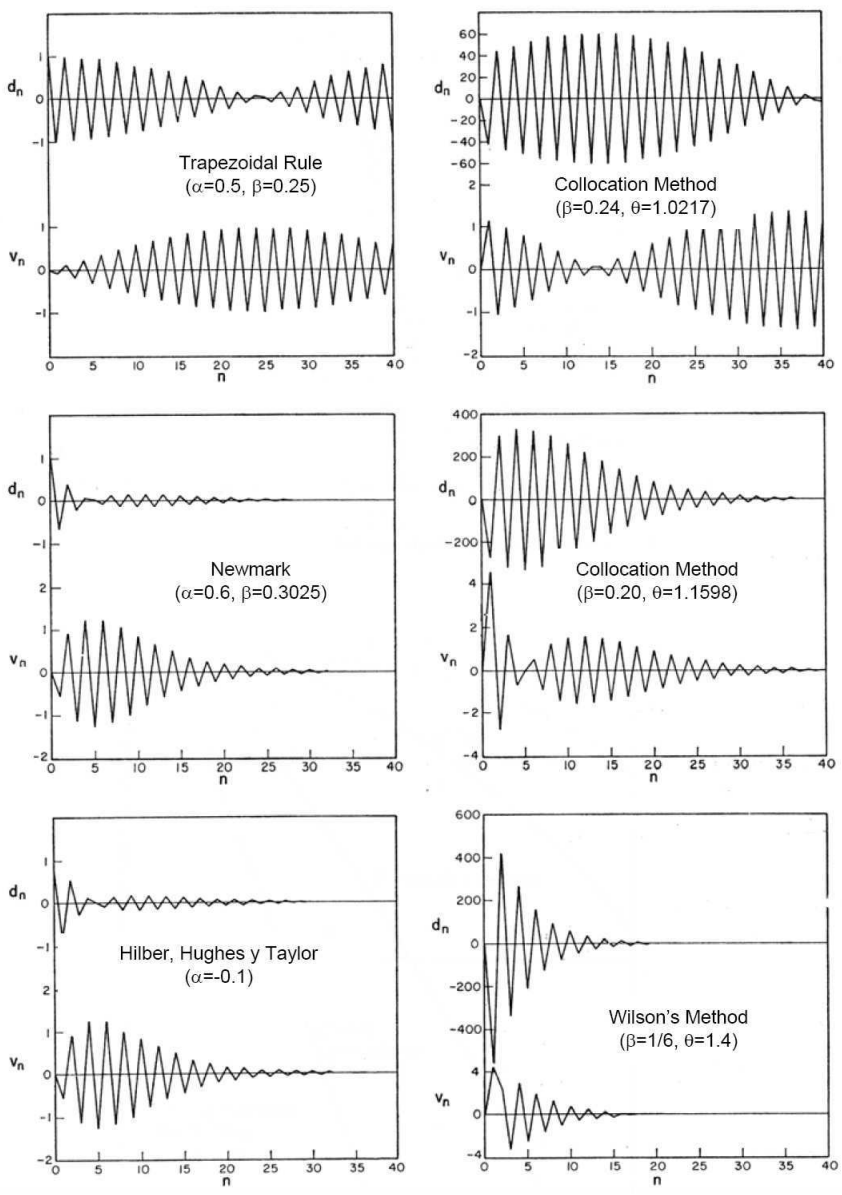

Figure 2.15 – Initial response and "overshoot" properties for different integration schemes (Hilber and Hughes, 1978)

Bazzi-Anderheggen "ρ" method

Bazzi and Anderheggen (1982) presented a new family of algorithms in two versions: an implicit and an explicit version. The implicit version of the algorithm includes only one parameter ρ in order to control the algorithmic damping introduced.

From the known values of $\mathbf{d}_i, \dot{\mathbf{d}}_i$ y $\ddot{\mathbf{d}}_i$ the values at the next step are written as:

$$\mathbf{d}_{i+1} = \mathbf{d}_i + \Delta\mathbf{d} \tag{2.55}$$

$$\dot{\mathbf{d}}_{i+1} = \frac{2}{\Delta t}\Delta\mathbf{d} - \dot{\mathbf{d}}_i + \frac{1-\rho}{1+\rho}\Delta t\ddot{\mathbf{d}}_i \tag{2.56}$$

$$\ddot{\mathbf{d}}_{i+1} = \frac{(1+\rho)(1+\rho^2)}{\Delta t}\left(\Delta\mathbf{d} - \Delta t\dot{\mathbf{d}}_n\right) + \left(1-\rho-\rho^3\right)\ddot{\mathbf{d}}_i \tag{2.57}$$

The increment in the displacements $\Delta\mathbf{d}$ is obtained after substituting in the equation of motion

$$\left(\mathbf{M} + \frac{\Delta t}{2}\mathbf{C} + \frac{\Delta t^2}{2(\rho+1)}\mathbf{K}\right)\Delta\mathbf{d} = \Delta t\mathbf{M}\dot{\mathbf{d}}_i + \frac{\rho-1}{2(\rho+1)}\Delta t^2\mathbf{M}\ddot{\mathbf{d}}_i + \frac{\Delta t^2}{2}\left(\mathbf{f}_i^* - \mathbf{q}_i - b*\mathbf{q}'_{i+1}\right) \tag{2.58}$$

with

$$\mathbf{f}_i^* = \frac{1}{\Delta t}\int_{t_i}^{t_{i+1}}\mathbf{f}(t)\mathrm{d}t \tag{2.59}$$

$$b^* = \frac{1}{\Delta t}\int_{t_i}^{t_{i+1}} b(t)\mathrm{d}t \tag{2.60}$$

where $\mathbf{f}(t)$ is the vector of external forces, $\mathbf{q}(t)$ is the vector of internal forces and $b(t)$ is a function non-dimensional of the time.

From the analysis of the spectral properties of the algorithm for a linear single degree of freedom system, it can be obtained that the algorithm is unconditionally stable if $\rho \leq 1$. The method is second order accurate and doesn't show problems of overshooting at the first stages of the analysis. Considering the particular case of $\rho = 1$, the method is identical to the trapezoidal rule.

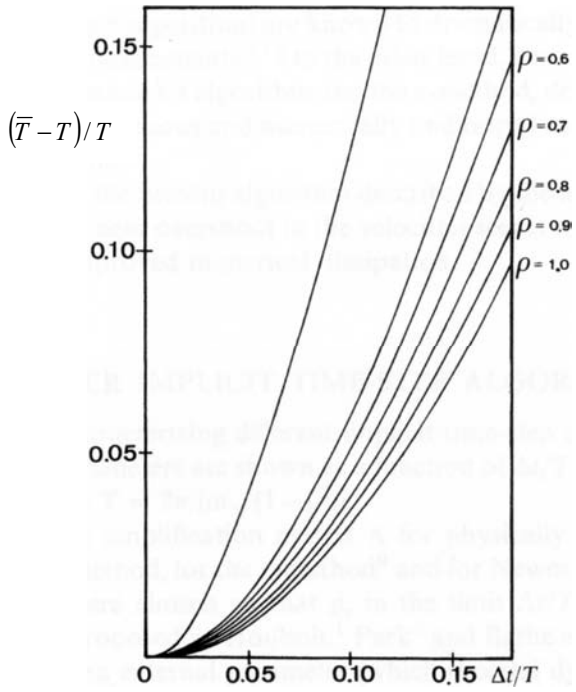

Figure 2.16 – Period elongation for different values of the parameter ρ (Bazzi and Anderheggen, 1982)

Zienkiewicz's scheme

Zienkiewicz et al. (1984) presented a general procedure to solve either dynamics problems or diffusion problems. The procedure proposed is based on the approximation of the residual weights allowing obtaining a family of general algorithms by means of polynomials of order p, which includes the Wilson and Newmark methods. For the solution of dynamic problems it is necessary to consider polynomials at least of order 2. Considering higher order polynomials, it appears a problem with the initial conditions, and it is necessary to know more than the "natural" initial conditions in velocities and displacements.

Considering a time step Δt where the function x is approximated by a polynomial in time as

$$\mathbf{x} = \mathbf{x}_n + \dot{\mathbf{x}}_n t + \ddot{\mathbf{x}}_n \frac{1}{2} t^2 + ... + \boldsymbol{\alpha}^{(p)} t^p \frac{1}{p!} \tag{2.61}$$

Or in a more compact form

$$\mathbf{x} = \sum_{q=0}^{p-1} \overset{q}{\mathbf{x}}_n \frac{t}{q!} + \boldsymbol{\alpha}_n^{(p)} t^p \frac{1}{p!} \tag{2.62}$$

where

$$\overset{q}{\mathbf{x}}_n = \left(\frac{d^q}{dt^q} \mathbf{x}_n \right) \qquad 0 < t < \Delta t \tag{2.63}$$

By assuming that $\mathbf{x}_n, \dot{\mathbf{x}}_n$, etc. are known at the beginning of the interval and $\boldsymbol{\alpha}_n^{(p)}$ is an unknown vector where $\mathbf{x}_{n+1}, \dot{\mathbf{x}}_{n+1}$, etc. may be determined as:

$$\begin{aligned}\mathbf{x}_{n+1} &= \sum_{q=0}^{p-1} \mathbf{x}_n^q \frac{\Delta t^q}{q!} + \boldsymbol{\alpha}_n^{(p)} \frac{\Delta t^p}{p!} = \hat{\mathbf{x}}_{n+1} + \boldsymbol{\alpha}_n^{(p)} \frac{\Delta t^p}{p!} \\ \dot{\mathbf{x}}_{n+1} &= \sum_{q=1}^{p-1} \mathbf{x}_n^q \frac{\Delta t^{q-1}}{(q-1)!} + \boldsymbol{\alpha}_n^{(p)} \frac{\Delta t^{p-1}}{(p-1)!} = \hat{\dot{\mathbf{x}}}_{n+1} + \boldsymbol{\alpha}_n^{(p)} \frac{\Delta t^{p-1}}{(p-1)!}\end{aligned} \tag{2.64}$$

the vector $\boldsymbol{\alpha}_n^{(p)}$ may be obtained by means of

$$\boldsymbol{\alpha}_n^{(p)} = \left(\frac{\Delta t^{p-2}}{(p-2)!}\theta_{p-2}\mathbf{M} + \frac{\Delta t^{p-1}}{(p-1)!}\theta_{p-1}\mathbf{C} + \frac{\Delta t^p}{p!}\theta_p \mathbf{K} \right)^{-1} \left(\bar{\mathbf{f}} - \mathbf{M}\tilde{\ddot{\mathbf{x}}}_{n+1} - \mathbf{C}\tilde{\dot{\mathbf{x}}}_{n+1} - \mathbf{K}\tilde{\mathbf{x}}_{n+1} \right) \tag{2.65}$$

Where the values of $\tilde{\mathbf{x}}_{n+1}, \tilde{\dot{\mathbf{x}}}_{n+1}$ y $\tilde{\ddot{\mathbf{x}}}_{n+1}$ come determined by

$$\begin{aligned}\tilde{\mathbf{x}}_{n+1} &= \sum_{q=0}^{p-1} \mathbf{x}_n^q \frac{\Delta t^q}{q!}\theta_q \\ \tilde{\dot{\mathbf{x}}}_{n+1} &= \sum_{q=1}^{p-1} \mathbf{x}_n^q \frac{\Delta t^{q-1}}{(q-1)!}\theta_{q-1} \\ \tilde{\ddot{\mathbf{x}}}_{n+1} &= \sum_{q=2}^{p-1} \mathbf{x}_n^q \frac{\Delta t^{q-2}}{(q-2)!}\theta_{q-2}\end{aligned} \tag{2.65}$$

The accuracy and stability of the method becomes determined by the proper selection of the parameters θ_q with $q = 1 \ldots p$, and the time interval Δt.

If a quadratic polynomial is considered, this resulting algorithm includes the Newmark scheme ($\gamma = \theta_1$ and $\beta = \theta_2/2$) and the requirements for unconditional stability are:

$$\begin{aligned}\theta_1 &\geq \tfrac{1}{2} \\ \theta_2 &\geq \theta_1\end{aligned} \tag{2.66}$$

Although the algorithm is very similar to the Newmark scheme, it shows some benefits, both physically and in a computational sense. In first place, only the values of

displacements and velocities are necessary to start the process. Second, the term $\boldsymbol{\alpha}_n^{(2)}$ represents the average acceleration in the time interval Δt and the equilibrium equation is satisfied on the average of the time interval.

If a cubic algorithm is considered, it is necessary to include three parameters θ_1, θ_2 and θ_3 providing initial conditions for $\mathbf{x}_n, \dot{\mathbf{x}}_n$ and $\ddot{\mathbf{x}}_n$. In this case, the second order algorithms of Houbolt, Wilson, HHT and Bossak-Newmark are also included. Table 2.1 summarizes the relationships between the parameters of the mentioned methods and the theta values.

Algorithm	**Theta values**
Houbolt	θ_1=2 unconditionally stable θ_2=11/3 θ_3=3
Wilson	$\theta_1=\theta_W$ unconditionally stable for θ_W=1.366 $\theta_1=\theta_W^2$ $\theta_1=\theta_W^3$
Bossak-Newmark (no physical damping) γ_B=1/2−α_B	θ_1=1-α_B θ_2=2/3-α_B+2β_B θ_3=6β_B
Bossak-Newmark (with physical damping) γ_B=1/2−α_B β_B=1/6−α_B/2	θ_1=1−α_B θ_2=1−2α_B θ_3=1−3α_B
Hilber-Hughes-Taylor (no physical damping) γ_H=1/2−α_H	θ_1=1 θ_2=2/3+2β_H−2α_H^2 θ_3=6β_H(1+α_H)

Table 2.1 – Correspondence with parameters of other methods (Zienkiewicz et al., 1984)

In later communications Katona et al. (1985) presented a method, the so-called beta-*m*, which is basically a generalization of the Newmark's method, obtained from the developed in Taylor's series (i.e. it can be demonstrated that the Newmark scheme is Taylor series exact in the term $\ddot{x}_n$ plus an approximation for the term $\dddot{x}_n$). From a development in Taylor series up to order *m* the same number of parameters β_0, β_1, ..., β_{m-1} are obtained. The results obtained with this method doesn't differ from those presented previously by Zienkiewicz et al. (1984) and Wood (1984), regarding stability and accuracy.

Hoff and Pahl Method

Hoff and Pahl (1988 a) presented a method with a similar procedure to the one presented by Zienkiewicz et al. (1984) and may be intended as an extension of this last method. From the same basis of the residual weights method, it can be obtained a new algorithm with controllable numerical dissipation and second order accuracy, from the proper selection of six parameters. Initially the selection of these parameters should be arbitrary but in later communications the method was reduced to a one independent parameter. This last method is known as the θ_1-method and the basic equations are (Hoff y Pahl, 1988 b):

$$\begin{aligned} &\mathbf{M}\ddot{\mathbf{d}}(t)+\mathbf{C}\dot{\mathbf{d}}(t)+\mathbf{K}\mathbf{d}(t)=\mathbf{p}(t) \\ &\mathbf{d}(0)=\mathbf{d}_0 \\ &\dot{\mathbf{d}}(0)=\dot{\mathbf{d}}_0 \end{aligned} \tag{2.67}$$

$$\left[\mathbf{M}+\left(\frac{3}{2}-\theta_1\right)\Delta t\mathbf{C}+\frac{1}{4\theta_1^2}\Delta t^2\mathbf{K}\right]\Delta\ddot{\mathbf{d}}=\mathbf{p}_n+\theta_0\left(\mathbf{p}_{n+1}-\mathbf{p}_n\right)-\mathbf{M}\ddot{\mathbf{d}}_n-\mathbf{C}\left(\dot{\mathbf{d}}_n+\theta_1\Delta t\ddot{\mathbf{d}}_n\right) - \mathbf{K}\left(\mathbf{d}_n+\theta_1\Delta t\dot{\mathbf{d}}_n+\frac{1}{2}\Delta t^2\ddot{\mathbf{d}}_n\right) \tag{2.68}$$

$$\begin{aligned}
\ddot{\mathbf{d}}_{n+1} &= \ddot{\mathbf{d}}_n + \Delta\ddot{\mathbf{d}} \\
\dot{\mathbf{d}}_{n+1} &= \dot{\mathbf{d}}_n + \Delta t\ddot{\mathbf{d}}_n + \left(\frac{3}{2} - \theta_1\right)\Delta t\Delta\ddot{\mathbf{d}} \\
\mathbf{d}_{n+1} &= \mathbf{d}_n + \Delta t\dot{\mathbf{d}}_n + \frac{1}{2}\Delta t^2\ddot{\mathbf{d}}_n + \frac{1}{4\theta_1^2}\Delta t^2\Delta\ddot{\mathbf{d}}
\end{aligned} \tag{2.69}$$

$$0.95 \le \theta_1 \le 1 \tag{2.70}$$

The method is second order of accuracy for any arbitrary physical damping, presents good numerical dissipation characteristics, no overshooting of the solution and it is unconditionally stable in the range indicated. For the case $\theta_1 = 1$ the method becomes the Newmark's trapezoidal rule. The authors also presented an interesting formulation of the scheme in the non linear case.

The generalized-α method

Chung and Hulbert (1993) presented a method called the generalized-α, for the numerical integration of the equation of motion, with numerical dissipation properties by means of additional parameters following the basic idea of the Hilber-Hughes-Taylor and Bozzak-Newmark methods. The basic form of this family of algorithms becomes defined by the following expressions:

$$\mathbf{M}\ddot{\mathbf{d}}_{i+1-\alpha_m} + \mathbf{C}\dot{\mathbf{d}}_{i+1-\alpha_f} + \mathbf{K}\mathbf{d}_{i+1-\alpha_f} = \mathbf{F}\left(t_{i+1-\alpha_f}\right) \tag{2.71}$$

$$\mathbf{d}_{i+1} = \mathbf{d}_i + \Delta t\dot{\mathbf{d}}_i + \Delta t^2\left[\left(\frac{1}{2} - \beta\right)\ddot{\mathbf{d}}_i + \beta\ddot{\mathbf{d}}_{i+1}\right] \tag{2.72}$$

$$\dot{\mathbf{d}}_{i+1} = \dot{\mathbf{d}}_i + \Delta t\left[(1-\gamma)\ddot{\mathbf{d}}_i + \gamma\ddot{\mathbf{d}}_{i+1}\right] \tag{2.73}$$

where

$$\mathbf{d}_{i+1-\alpha_f} = (1-\alpha_f)\mathbf{d}_{i+1} + \alpha_f \mathbf{d}_i \tag{2.74}$$

$$\dot{\mathbf{d}}_{i+1-\alpha_f} = (1-\alpha_f)\dot{\mathbf{d}}_{i+1} + \alpha_f \dot{\mathbf{d}}_i \tag{2.75}$$

$$\ddot{\mathbf{d}}_{i+1-\alpha_m} = (1-\alpha_m)\ddot{\mathbf{d}}_{i+1} + \alpha_m \ddot{\mathbf{d}}_i \tag{2.76}$$

$$t_{i+1-\alpha_f} = (1-\alpha_f)t_{i+1} + \alpha_f t_i \tag{2.77}$$

The resulting equation of motion is a combination of the HHT and Bossak-Newmark equations and for the particular cases $\alpha_m = 0$ the algorithm is reduced to the HHT method, while considering $\alpha_f = 0$ the algorithm is reduced to the Bossak-Newmark scheme. If $\alpha_f = \alpha_m = 0$ the resulting algorithm is the Newmark's scheme.

By analyzing the eigenvalues of the amplification matrix of the algorithm, it may be obtained that the method is unconditionally stable when:

$$\begin{aligned} &\alpha_m \le \alpha_f \le \frac{1}{2} \\ &\beta \ge \frac{1}{4} + \frac{1}{2}(\alpha_f - \alpha_m) \end{aligned} \tag{2.78}$$

The method is second order accurate if

$$\gamma = \frac{1}{2} - \alpha_m + \alpha_f \tag{2.79}$$

The method presented, allows varying the numerical dissipation over the higher modes from the case of nil dissipation ($\rho(\mathbf{A}) = 1$) to the case of asymptotic annihilation of the solution ($\rho(\mathbf{A}) = 0$), where the response of the higher modes is completely eliminated after the first time step. The authors also found that the method doesn't show the overshoot of the solution on the first steps reported by Hilber and Hughes (1978). From figures 2.17 to

2.19 it can be concluded that the method shows better numerical dissipation properties and lower errors in period when compared with other numerical dissipation schemes, without excessive increase in the complexity of the algorithm.

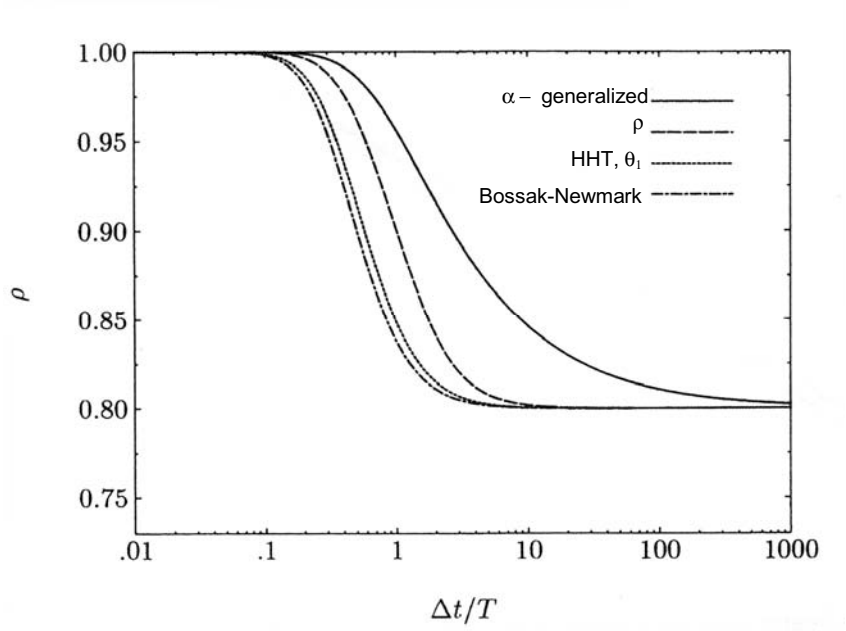

Figure 2.17 – Spectral radius for different dissipative algorithms (Chung and Hulbert, 1993)

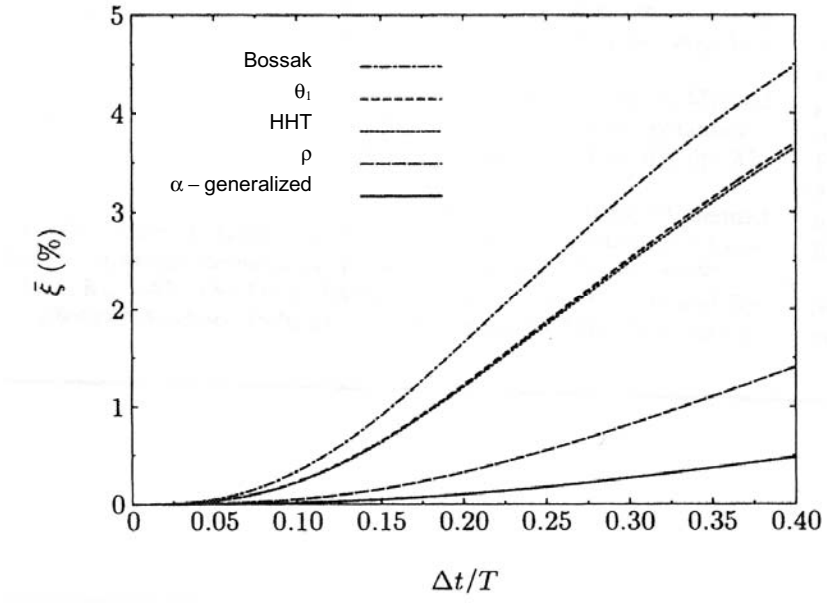

Figure 2.18 – Algorithmic damping for different dissipative schemes (Chung and Hulbert, 1993)

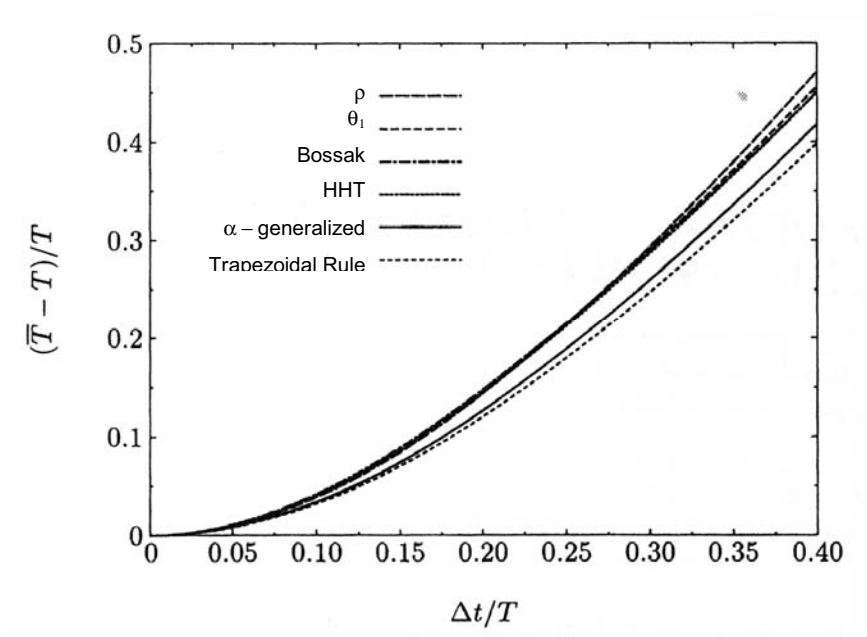

Figure 2.19 – Error in the period for different dissipative algorithms (Chung and Hulbert, 1993).

Conservation of energy algorithms

In the case of non linear problems, the main interest of the researchers is focused on the numerical stability of the solution. This is basically due to the fact that many algorithms which are unconditionally stables for linear problems, frequently loose this property in the non linear case. Although the spectral stability is a necessary condition to guarantee the unconditional stability of the integration scheme, it is not enough in the case of non linear problems. A further condition shall be applied. A sufficient condition for the unconditional stability in the non linear regime is the conservation or decay in the total energy of the system in each time step (Kuhl y Crisfield, 1999). This energy condition may be expressed by the following inequality:

$$U_{n+1} - U_n + K_{n+1} - K_n \leq W_{ext} \tag{2.80}$$

where U_{n+1} and U_n represent the strain energy at the end and at the beginning of the time step, K_{n+1} and K_n the corresponding kinetic energy and W_{ext} represents the work produced by the external forces within the time step. The notion of "energy conserving" will be related herein to Hamiltonian systems ($W_{ext} = 0$). This corresponds to the conservation of the sum of total energy including the work done by the external and damping forces for a general dynamical system.

In principle, there are three groups of algorithms which should satisfy the energy criterion:

1. Numerical dissipation algorithms. This group of algorithms employs numerical dissipation to satisfy the inequality (2.80). These well known methods posses controllable high frequency dissipation for linear dynamics by the algorithmic design. Examples of this algorithms have been extensively described (Newmark, HHT, Bossak, Generalized-α).

2. Enforced conservation of energy algorithms. These algorithms fulfill the stability criterion by enforcing the conservation of energy. The "Constraint Energy Method" by Hughes et al. (1978) was designed as an extension of the trapezoidal rule (Newmark, 1959) with the constraint of energy conservation via method of Lagrange multipliers. Kuhl and Ramm (1996) observed that this algorithm conserves the total energy perfectly, but leads to final failure in the Newton-Raphson iteration equilibrium. A variant of this method was developed by Kuhl and Ramm (1996), which consist of the inclusion of conservation of momentum and angular momentum theorems as constrains (via Lagrange multipliers) in a numerical dissipation scheme with the approximations of the Newmark's scheme. In any case, these methods only lead to convergent solutions if the base algorithm is stable.

3. Energy conservation algorithms. Currently, the effort of the researchers to guarantee the stability of the integration scheme is focused on this group of algorithms. The basis of this method was accounted for the first time on the "Energy-Momentum Method" by Simo and Tarnow (1992). The original application to continua was later applied to rigid body dynamics (Simo and Wong, 1991), trusses (Crisfield and Shi, 1994) and beams (Simo et al. 1995; Galvanetto and Crisfield, 1996; Crisfield et al., 1997). This method is second order accurate and conserves the total energy of the system and linear as well as angular momentum. More recently, the "Modified Energy Momentum Method" was proposed after adding terms of numerical dissipation within the algorithm, in order to guarantee to decay in the total energy in contact problems (Armero and Petöcz, 1998). Similar properties of numerical dissipation and total energy decay presents the "Generalized Energy-Momentum Method" developed by Kuhl and Crisfield (1999) over the base of the generalized-α method (Chung y Hulbert, 1993).

Chapter 3

Cyclic constitutive model for concrete and masonry

The computational analysis of reinforced concrete and masonry structures subjected to dynamic or cyclic loadings requires realistic stress-strain material models to reproduce the real behavior of the structure. Research on the cyclic response of concrete and masonry aims at providing an efficient model capable of predicting all the hysteretic characteristics of the material in cyclic loading. Since the first works attempting to characterize the cyclic behavior of concrete were published (Sinha et al., 1964), a significant research effort has been devoted to that field, which has increased even more with the recent development of computational methods applied to these structures. In this chapter, a constitutive model for the description of the response of concrete and masonry under general cyclic loading is presented. Compared to previous ones, the model presents several advantages. It affords to consider all the hysteretic characteristics of the complex behavior of concrete and masonry in a simple and practical way. It can be used to simulate the cyclic response of the material subject to general load conditions, including partial unloading or reloading or mixed hysteretic loops involving the transition from compression to tension stresses or vice-versa. Moreover, all the required input data can be obtained through conventional laboratory monotonic compression and tension tests. This is an important issue which determines the applicability of the present model in engineering practice. The model has been validated by comparison with available experimental results provided by different authors for both, concrete and masonry. The proposed model for concrete has been recently published in the form of a journal paper (Sima et al., 2008).

3.1 Cyclic constitutive model for concrete

3.1.1 Proposed model for concrete in cyclic compression

3.1.1.1 Envelope curve

It is commonly accepted by most researchers (Karsan and Jirsa, 1969; Yankelevsky and Reinhardt, 1987; Bahn and Hsu, 1998; among others) that the envelope curve for a concrete subjected to axial cyclic compression can be approximated by the monotonic stress-strain curve. In turn, the monotonic curve adopted as envelope should verify some desirable characteristics: (1) the slope at the origin should be equal to the initial modulus of deformation, (2) it should describe correctly the ascending and the descending post peak (softening) branch and (3) it should permit to adjust the post peak behavior to experimental results.

The properties of the monotonic stress-strain curve of concrete have been studied by many researchers. Some classical references on this topic are Hognestand et al. (1955), Popovics (1973) or Tsai (1988). A more extensive list of contributions can be found in Chang and Mander (1994).

Experimental results have shown that the monotonic compression curve of concrete presents a linear response until approximately a half of the compressive strength. Due to that, a first linear relation is considered herein until the elastic limit is reached. An exponential type equation is considered for the envelope stress-strain curve of concrete beyond the elastic limit. It has been observed that such exponential equation fits well the experimental results. This curve is defined by a set of parameters that can be obtained in a monotonic compression test, including (1) the initial modulus of concrete E_0, (2) the strain at the elastic limit ε_0 and (3) the coordinates at the peak of the stress-strain curve (ε_c', f_c').

The following equation is adopted for the stress-strain envelope curve of concrete:

$$\begin{cases} \sigma = \varepsilon E_0 & \varepsilon \le \varepsilon_0 \\ \sigma = \left[\varepsilon_0 (1 - A) + A\varepsilon e^{\left(\frac{\varepsilon_0 - \varepsilon}{\varepsilon_c'} \right)} \right] E_0 & \varepsilon > \varepsilon_0 \end{cases} \tag{3.1}$$

where

$$A = \frac{f_c' - \varepsilon_0 E_0}{E_0 \left(\varepsilon_c' e^{\frac{\varepsilon_0}{\varepsilon_c'} - 1} - \varepsilon_0 \right)} \tag{3.2}$$

This equation is a special case of the equation proposed by Mazars and Pijaudier-Cabot (1989) for a damage model for concrete and is used by many authors for concrete models (Faría et al., 1998; Saetta et al., 1999; among others) and later extended to masonry models (Saetta et al., 2000; Berto et al., 2000). The original parameters have been rewritten in terms of the set of parameters obtained in a 1D monotonic compressive test (as is previously mentioned).

Eq. (3.1) can be rewritten as

$$\sigma = (1 - \delta^-) E_0 \varepsilon \tag{3.3}$$

where

$$\delta^- = \left[1 - \frac{\varepsilon_0}{\varepsilon} (1 - A) - A\, e^{\left(\frac{\varepsilon_0 - \varepsilon}{\varepsilon_c'} \right)} \right] \tag{3.4}$$

The compression damage parameter δ^- represents the material degradation in compression and varies from 0 (material without deterioration) to 1 (completely damaged material).

Even when this curve presents a good agreement with typical monotonic stress-strain curves of concrete, it does not allow the adjustment of the softening branch to experimental results. Carrying out this adjustment is very important in some cases like in confined concrete modeling. Because of that, the possibility to optionally including a new point $(\varepsilon_{op}, f_{op})$ to define the descending branch as a new variable is considered (Fig. 3.1). A new descending branch is proposed herein, which has been obtained by adjusting an exponential curve to zero slope at the peak stress point and to the new point $(\varepsilon_{op}, f_{op})$. This equation can be written as follows:

$$\sigma = \left[B + C\varepsilon e^{\left(\frac{\varepsilon_0 - \varepsilon}{\varepsilon_0'}\right)} \right] E_0 \qquad \varepsilon > \varepsilon'_c \tag{3.5}$$

where

$$B = \frac{f_{op}\varepsilon_c' e^{\left(\frac{\varepsilon_0}{\varepsilon_c'}-1\right)} - \varepsilon_{op} f_c' e^{\frac{\varepsilon_0}{\varepsilon_c'}\left(1-\frac{\varepsilon_u}{\varepsilon_0}\right)}}{E_0\left[\varepsilon_c' e^{\left(\frac{\varepsilon_0}{\varepsilon_c'}-1\right)} - \varepsilon_{op} e^{\frac{\varepsilon_0}{\varepsilon_c'}\left(1-\frac{\varepsilon_u}{\varepsilon_0}\right)}\right]} \tag{3.6}$$

and

$$C = \frac{f_c' - f_{op}}{E_0\left[\varepsilon_c' e^{\left(\frac{\varepsilon_0}{\varepsilon_c'}-1\right)} - \varepsilon_{op} e^{\frac{\varepsilon_0}{\varepsilon_c'}\left(1-\frac{\varepsilon_u}{\varepsilon_0}\right)}\right]} \tag{3.7}$$

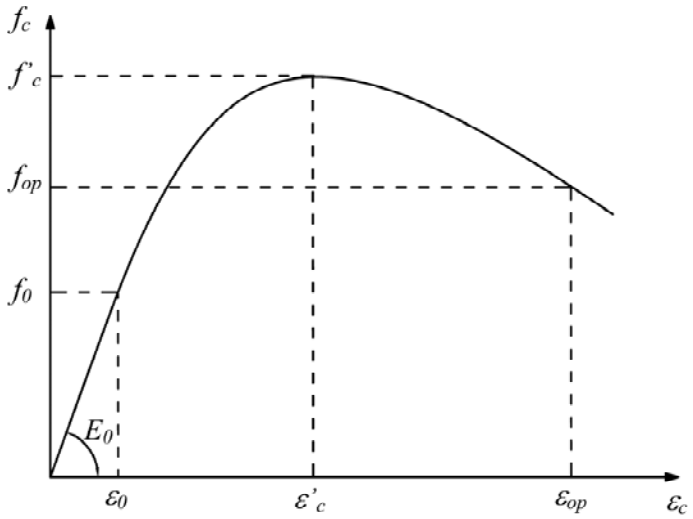

Figure 3.1 – Envelope curve of concrete

The equation (3.5) can be rewritten in terms of the compressive damage as follows:

$$\sigma = \left(1 - \delta^{-}\right) E_0 \varepsilon \tag{3.8}$$

where

$$\delta^{-} = \left[1 - \frac{B}{\varepsilon} - C e^{\left(\frac{\varepsilon_0 - \varepsilon}{\varepsilon'_c}\right)}\right] \qquad \varepsilon > \varepsilon'_c \tag{3.9}$$

3.1.1.2 Unloading and reloading curves

As it has been observed by many researchers (Sinha et al., 1964; Karsan and Jirsa, 1969; Bahn and Hsu, 1998), when a concrete specimen is monotonically loaded up to a certain strain level and then unloaded to a zero stress level in a typical cyclic test, the unloading curve is concave from the unloading point and characterized by high stiffness at the beginning (Fig. 3.2). The stiffness gradually decreases and becomes very flat at low stress levels and the residual plastic strains are considerably reduced. When reloading is

performed from zero stress up to the envelope curve, it has been observed that the curve is rather flat in almost all of its length. Depending on the compression damage level, a great amount of energy may be dissipated in a complete cycle. The aim of modeling the shape of the unloading and reloading curves is to capture the damage accumulation and the energy dissipation of the material due to cyclic loading.

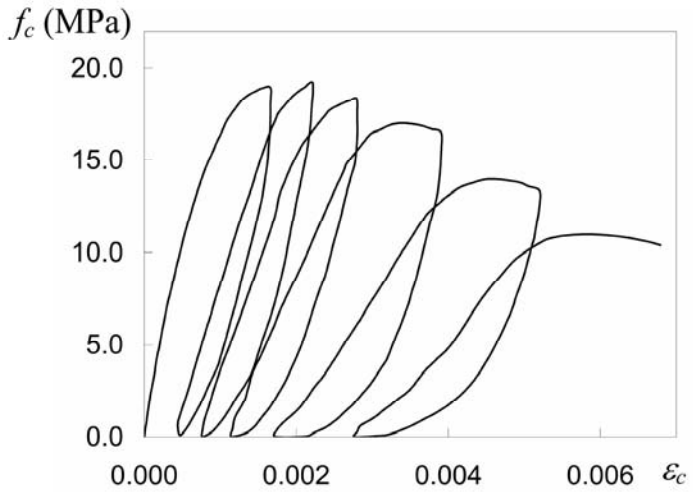

Figure 3.2 – Typical cyclic compression test from Karsan and Jirsa (1969)

The shape of the unloading and reloading curves depends on the amount of non recoverable damage in the concrete. Many models consider the unloading strain as the parameter that defines the unloading and reloading path and determines the degree of damage caused by the cycling (Karsan and Jirsa, 1969; or Palermo and Vecchio, 2003). Several types of curves have been used to reproduce the unloading curve also, like the Ramberg-Osgood equation used by Palermo and Vecchio (2003) or Chang and Mander (1994), the power type used by Bahn and Hsu (1998) or the multilinear curve proposed by Yankelevsky and Reinhardt (1987) or Mansour and Hsu (2005). In turn, reloading can be accurately modeled by a linear curve as is done by most researchers (Palermo and Vecchio, 2003; Bahn and Hsu, 1998; among others). Herein, an exponential type equation is proposed for the unloading curve of concrete and a linear type equation is used for the reloading curve (Fig. 3.3). The equation proposed for the unloading branch includes the main features of the unloading curves obtained experimentally, such as the curvature of the unloading curve, the

initial unloading stiffness, the final unloading stiffness and the unloading strain–plastic strain ratio. It has been observed that these characteristics vary with the accumulation of damage. Some previous works ignore this fact and consider as constants one or more characteristics. Chang and Mander (1994) consider the initial unloading stiffness equal to the initial modulus of deformation of the concrete. Palermo and Vecchio (2003) assigned to the initial unloading stiffness a value equal to the initial tangent stiffness of the concrete and a value equal to the 7.1 % of the initial tangent stiffness of the concrete to the final unloading stiffness. Herein, none of these important characteristics are previously fixed. The final unloading stiffness and the unloading strain–plastic strain ratio are explicitly related to the damage accumulation in the concrete. As a consequence, the curvature of the unloading curve and the initial unloading stiffness are implicitly related to the damage accumulation.

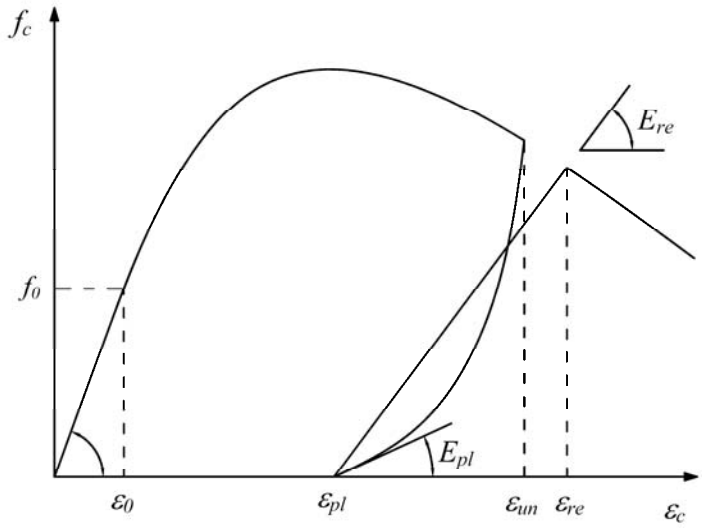

Figure 3.3 – Complete unloading-reloading cycle in compression

The proposed unloading curve is given by the equation:

$$\sigma = D^1 e^{D^2\left(1-\frac{\varepsilon-\varepsilon_{pl}}{\varepsilon_{un}-\varepsilon_{pl}}\right)} E_0\left(\varepsilon-\varepsilon_{pl}\right) \tag{3.10}$$

where

$$D^1 = \frac{r(1-\delta_{un})}{(r-1)} \qquad D^2 = Ln\left[\frac{R(1-\delta_{un})(r-1))}{r}\right] \tag{3.11}$$

with $r = \varepsilon_{un}/\varepsilon_{pl}$ and $R = E_{pl}/E_0.\varepsilon_{pl}$ is the strain at zero stress, E_{pl} is the stiffness at the end of the unloading curve and (Fig. 3.3), δ_{un} is the compressive damage δ^- at the unloading point which is the only parameter used here to define the complete unloading-reloading path. The dependence of the other variables with this parameter has been determined in a semi empirical way. A series of cyclic test on plain concrete under compressive loadings have been reproduced with this model and statistical regression has been performed as is later shown. The tests considered are those performed by Sinha et al. (1964), Karsan and Jirsa (1969), Spooner and Dougill (1975), Okamoto et al. (1976), Tanigawa et al. (1979), Buyukozturk and Tseng (1984) and Bahn and Hsu (1998).

The reloading response is modeled by a linear curve as is done by most researchers (Palermo and Vecchio, 2003; Bahn and Hsu, 1998; Sakai and Kawashima, 2006; among others). This approach is in agreement with experimental results.

A meaningful feature included in the model, which is not always considered by other authors, is the degradation in reloading stiffness with load cycling. As has been observed in test results, the reloading curve does not return to the envelope curve at the previous maximum unloading strain and further straining is needed to taking up again the envelope curve. It has been found that the relationship between the reloading compressive damage δ_{re} (defined as the compressive damage δ^- at the reloading strain ε_{re}) and the unloading compressive damage δ_{un} presents a linear behavior (Fig. 3.4). The difference between δ_{un} and δ_{re} describes the damage accumulated in each cycle. The effect of cyclic stiffness degradation and its dependence with the unloading compressive damage can be observed in Fig. 3.5. It can be noted that the unloading strain–plastic strain ratio presents a linear dependence with the unloading compressive damage (Fig. 3.6). Increasing in the unloading

compressive damage produces a decrease in the final unloading stiffness. This relationship can be adequately modeled also by a second order parabola (Fig. 3.7).

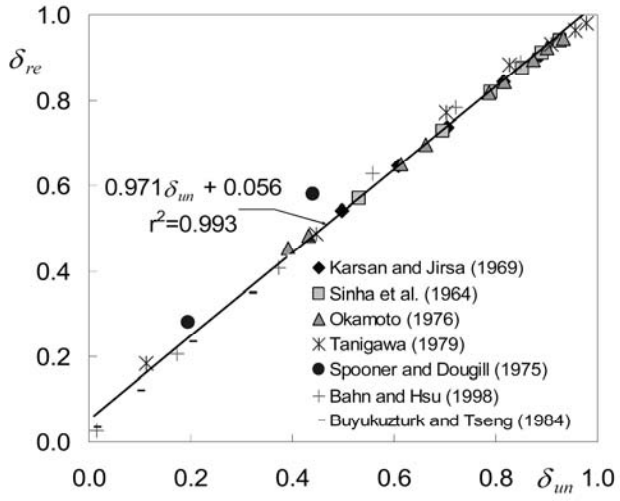

Figure 3.4 - Relationship between the reloading damage and the unloading damage obtained by means of statistical regression on selected experimental results.

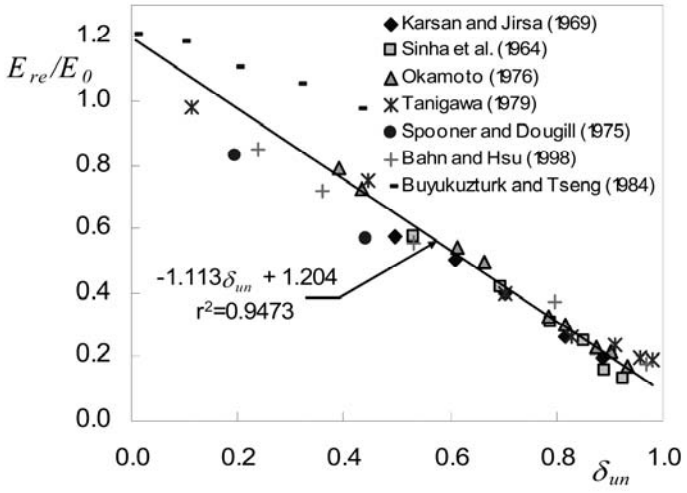

Figure 3.5 - Relationship between the reloading stiffness and the unloading damage obtained by statistical regression on selected experimental results.

A linear variation between the unloading damage δ_{un} and the reloading damage δ_{re} has been considered for the compressive damage δ^- during the unloading path. For the reloading path, the compressive damage has been maintained as a constant, which is in

agreement with experimental data (i.e. the test results suggest that the reloading curve becomes non linear only beyond the point of intersection with the unloading curves, often referred to as the common point). These relationships can be expressed as follows:

$$\delta^{-} = \delta_{un} + \frac{\delta_{re} - \delta_{un}}{\varepsilon_{pl} - \varepsilon_{un}}\left(\varepsilon - \varepsilon_{un}\right) \tag{3.12}$$

for the unloading path, and

$$\delta^{-} = \delta_{re} \tag{3.13}$$

for the reloading path.

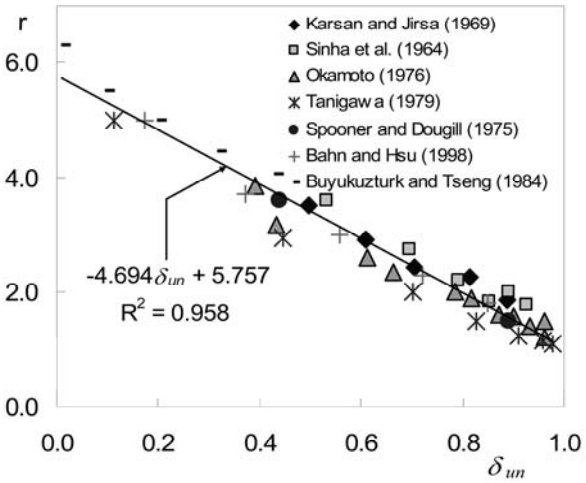

Figure 3.6 - Relationship between the unloading strain-plastic strain ratio and the unloading damage obtained by means of statistical regression on selected experimental results.

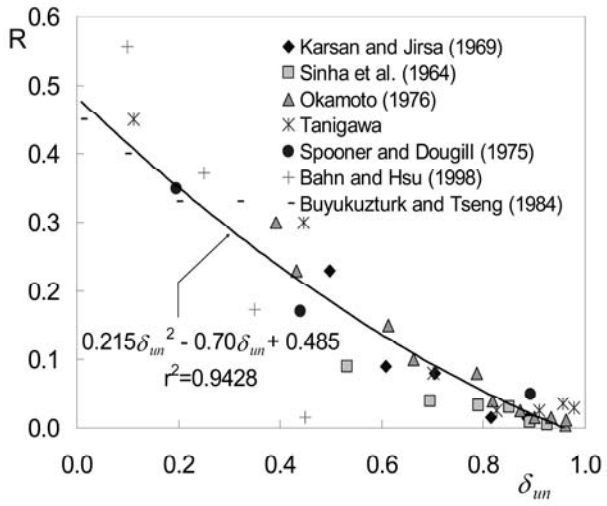

Figure 3.7 – Relationship between the final unloading stiffness – initial unloading stiffness ratio and the unloading damage obtained by means of statistical regression on selected experimental results.

3.1.1.3 Partial unloading and reloading

Most of the models available in the literature do not consider the behavior of concrete in the case of partial unloading and partial reloading. In other cases, this issue has been considered in a simplified way. There exists a lack of experimental information considering the general case of partial unloading followed by partial reloading. The curves proposed herein for the general case of partial unloading-reloading cycles are based on the tests results by Bahn and Hsu (1998), who developed a series of tests in order to study the response of concrete under random load cycles.

As is suggested by these experimental results, when a partial unloading occurs followed by reloading to meet the envelope curve, the reloading path can be modeled by the linear relationship connecting the reversal point with the point in the envelope curve that corresponds to a damage defined by eq. (3.12) for the reversal point (ε'_{rev})

$$\delta_{rev} = \delta_{un} + \frac{\delta_{re} - \delta_{un}}{\varepsilon_{pl} - \varepsilon_{un}} \left(\varepsilon_{rev} - \varepsilon_{un} \right) \tag{3.14}$$

where ε_{rev} is the strain at the reversal point (Fig. 3.8). The compressive damage remains equal to δ_{rev} during the reloading path.

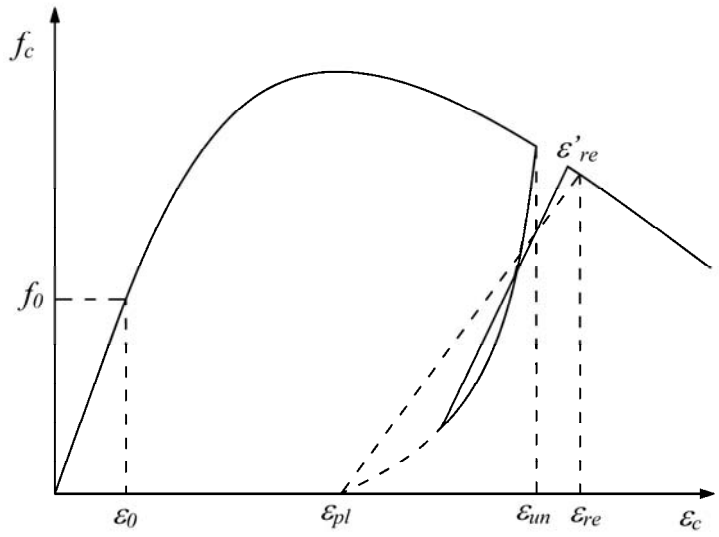

Figure 3.8 – Reloading from partial unloading in compression.

When a partial reloading is performed, the following unloading path is modeled by eq. (3.10) but substituting the unloading strain and the slope at zero stress as follows (curve 3 in Fig. 3.9):

$$\sigma = B^1 e^{A^1\left(1-\frac{\varepsilon-\varepsilon_{pl}}{\varepsilon^1_{un}-\varepsilon_{pl}}\right)} E_0\left(\varepsilon-\varepsilon_{pl}\right) \tag{3.15}$$

where

$$A^1 = Ln\left[\frac{R^1}{B^1}\right] \qquad B^1 = \frac{f^1_{un}}{E_0\varepsilon^1_{un}\left(1-r^1\right)} \tag{3.16}$$

with $r^1 = \varepsilon^1_{un}/\varepsilon_{pl}$ and $R^1 = E^1_{pl}/E_0$, where ε^1_{un} and f^1_{un} are the coordinates of the reversal point, and

$$E_{pl}^{1} = \frac{E_{re} - E_{pl}}{\varepsilon_{re} - \varepsilon_{pl}} \left(\varepsilon_{un}^{1} - \varepsilon_{pl} \right) + E_{pl} \tag{3.17}$$

is the new stiffness at the end of the unloading curve. A linear interpolation as in eq. (3.12) is performed for the damage in the unloading path.

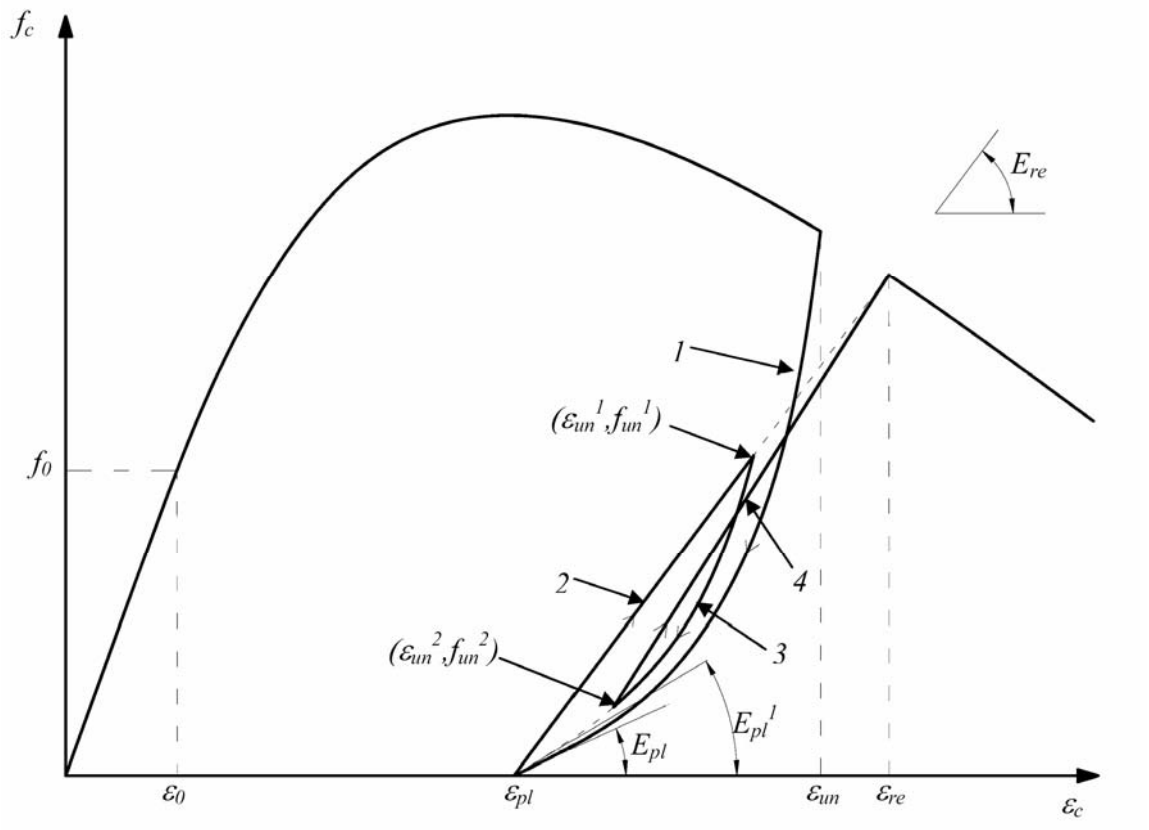

Figure 3.9 – Partial reloading followed by partial unloading for concrete in compression.

Curve 4 (Fig. 3.9) describes partial reloading from a partial unloading branch. A linear response curve is assumed from the coordinates of the new reversal point $\left(\varepsilon_{un}^{2}, f_{un}^{2} \right)$ until the point of return to the envelope curve defined for the complete cycle.

3.1.2 Proposed model for concrete in cyclic tension

In the pre-peak branch, a linear elastic relationship represents well the behavior in tension and most researchers have used this approach. The post peak behavior is in some cases modeled as an abrupt fall to zero stress (perfect-brittle material). However, this simplification in the post peak behavior does not agree with the experimental results and can produce incoherent results when it is applied in a computational model.

Several expressions have been documented in the literature to represent the softening branch, including straight lines (Bazant and Oh, 1983), polylinear curves (Rots et al., 1985), exponential curves (Gopalaratman and Shah, 1985), polynomial curves (Lin and Scordelis, 1975) or combinations of them (Cornelissen et al., 1985).

The response of concrete under cyclic tension has been studied in detail by Reinhardt (1984) and Reinhardt et al. (1986). More than 100 tests were performed on plain concrete under cyclic tension and numerical expressions for the softening branch and the unloading and reloading curves were derived. It was observed (like in the case of plain concrete under cyclic compression loadings) that the reloading curve does not return to the envelope curve at the previous maximum unloading strain and further straining is needed to taking up again the envelope curve. This phenomenon is less important than in compression. The energy dissipated in a tension cycle without incursions in the compression zone can be neglected when it is compared with the energy dissipated in a complete compression cycle. However, some authors (Okamura and Maekawa, 1991; Hordijk, 1991; or Palermo and Vecchio, 2003) have provided an accurate approximation of the complete unloading-reloading cycle in tension.

The tension envelope curve adopted for the present formulation consists of a linear elastic relation until reaching the tensile strength, followed by an exponential curve to represent the softening branch

$$\sigma = E_0 \varepsilon_{ct} e^{\alpha\left(1-\frac{\varepsilon}{\varepsilon_{ct}}\right)} \tag{3.18}$$

where ε_{ct} is the tensile strain that corresponds with the tensile strength (Fig. 3.10) and α is defined by the following expression:

$$\alpha = \left(\frac{G_f E_0}{l^* f_{ct}^{\ 2}} - \frac{1}{2}\right)^{-1} \geq 0 \tag{3.19}$$

where G_f is the fracture energy (considered as a material property), f_{ct} is the tensile strength of concrete and l^* is a "characteristic length" or "crack band width" introduced to guarantee the objectivity of the results with respect to the size of the finite element mesh (Oliver, 1989)

Like in compression, it is useful to rewrite the expression (3.18) to define the damage in tension as:

$$\sigma = \left(1-\delta^+\right) E_0 \varepsilon \tag{3.20}$$

where

$$\delta^+ = 1 - \frac{\varepsilon_{ct}}{\varepsilon} \cdot e^{\alpha\left(1-\frac{\varepsilon}{\varepsilon_{ct}}\right)} \tag{3.21}$$

The tensile damage parameter δ^+ measures the material degradation in tension and varies from 0 (material without deterioration) to 1 (completely damaged material).

In reinforced concrete, the tension stiffening effect can be modeled through an adequate adjustment of the fracture energy in (3.19).

The cyclic behavior is modeled herein in a simplified way. A straight line is used for the unloading branch in tension. The same curve is considered for the reloading branch when there is no incursion in compression during a cycle. Based on experimental data from Reinhardt (1984), the following criterion is proposed to account for the stiffness deterioration:

$$\frac{E_{new}}{E_0} = \left(\frac{\varepsilon}{\varepsilon_{ct}} \right)^{-1.05} \tag{3.22}$$

where E_{new} is defined in Fig. 3.10.

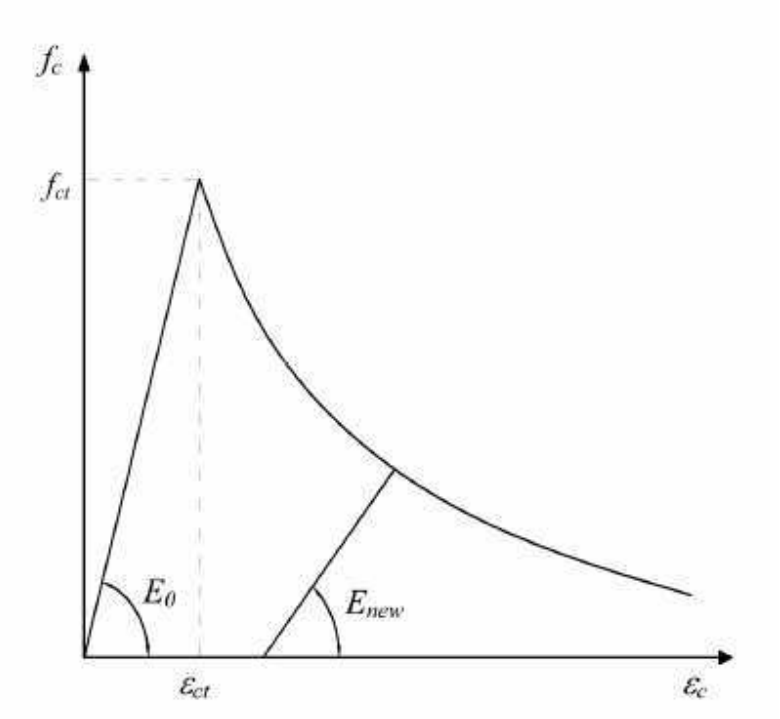

Figure 3.10 – Tension envelope curve for concrete.

3.1.3 Transition curves

A series of tests attempting to characterize the effect of damage in tension when the specimen is loaded in compression were developed by Ramtani et al. (1992). These test

results have shown that completely closing the cracks requires a certain amount of compression. Once the crack is closed, the stiffness of the concrete is no affected by accumulated damage in tension.

The transition curve from tension to compression once the damage in tension is produced, closing the cracked zones, is assumed to be linear which is in agreement with experimental results (Légeron et al., 2005). The crack closure mechanism is governed by the "crack closure stress" σ_f (see Fig. 3.11) which is the stress at which the crack is supposed to be completely closed. It has been observed that the crack closure stress is strongly affected by the concrete strength and placement methods (crack roughness). For monolithic structures with no previous damage in compression, σ_f is in the range of the tensile strength (Légeron et al., 2005) and can be taken as

$$\sigma_f = \sigma_f^0 = -\frac{f_c^{'}}{10} \tag{3.23}$$

In the case of concrete with dry joints, σ_f can be significantly lower.

The increasing of compression damage may produce a decrease in the magnitude of this variable (Mazars et al., 2004). A simple linear variation of σ_f with the compression damage is considered herein as follows:

$$\sigma_f = \left(1 - \delta^{-}\right)\sigma_f^0 \tag{3.24}$$

where σ_f^0 is the initial crack closure stress (considered as input data by the user).

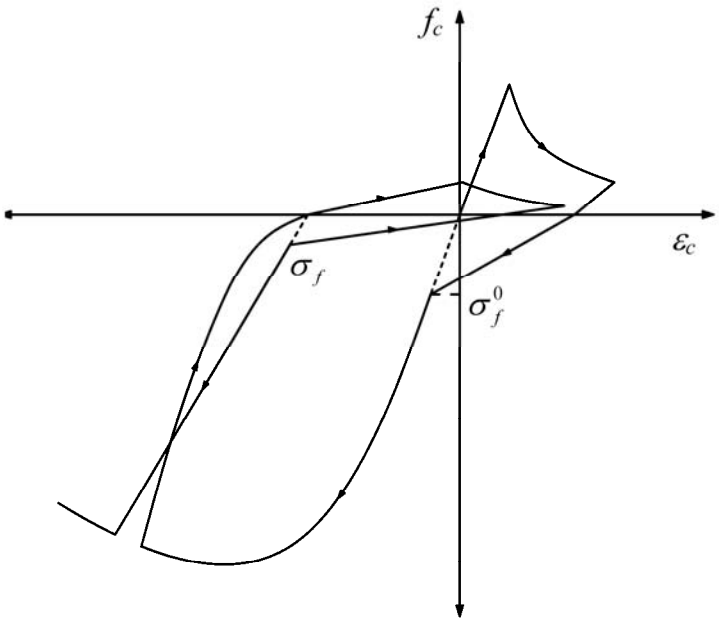

Figure 3.11 – Clack-closing model.

3.1.4 Model Verification. Comparison with test results

Several uniaxial cyclic test results have been compared with predictions obtained by means of the model presented. These tests cover several concrete strengths and a variety of cyclic histories, including both cyclic compression and cyclic tension. In the case of cyclic compression, results from works performed by Okamoto et al. (1976) and Tanigawa et al. (1979) have been considered. In the case of cyclic tension and cyclic tension with small incursions in compression, the model is compared with test results from Reinhardt (1984). In all cases, the present model shows satisfactory agreement with the experimental results.

In Fig. 3.12 to 3.14, experimental tests carried out by Okamoto et al. (1976) and Tanigawa et al. (1979) are reproduced and compared with the model results and with those provided by Chang and Mander (1994) and Yankelevsky and Reinhardt (1987). The mechanical characteristics considered for the model are summarized in Table 3.1.

In all cases the strains where the unloading curves start in the experimental results have been considered as the reverse points for the model.

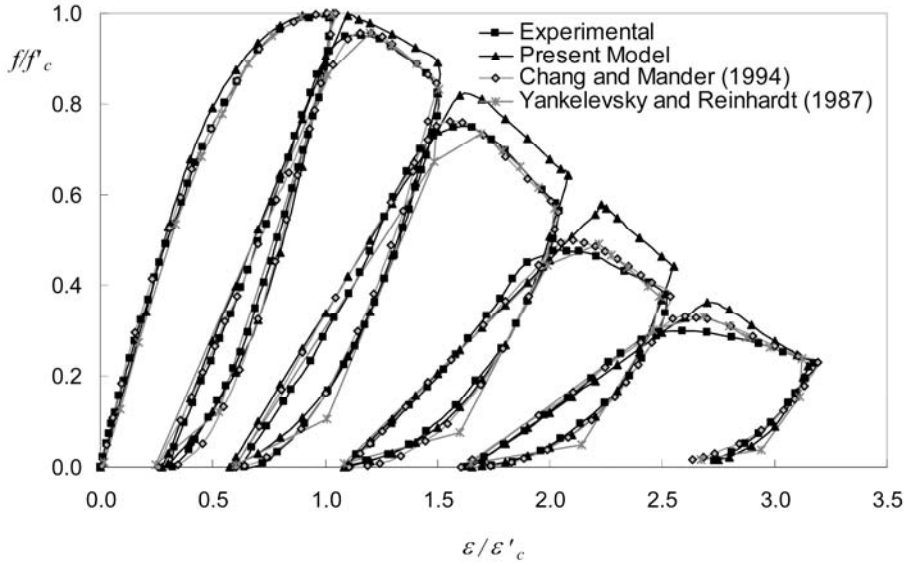

Figure 3.12 – Cyclic compression test by Okamoto et al. (1976), $f_c^{'} = 30.0$ MPa.

Table 3.2 summarizes the dissipated energy obtained with the proposed model and is compared against experimental results and numerical results obtained by Chang and Mander (1994) and Yankelevsky and Reinhardt (1987).

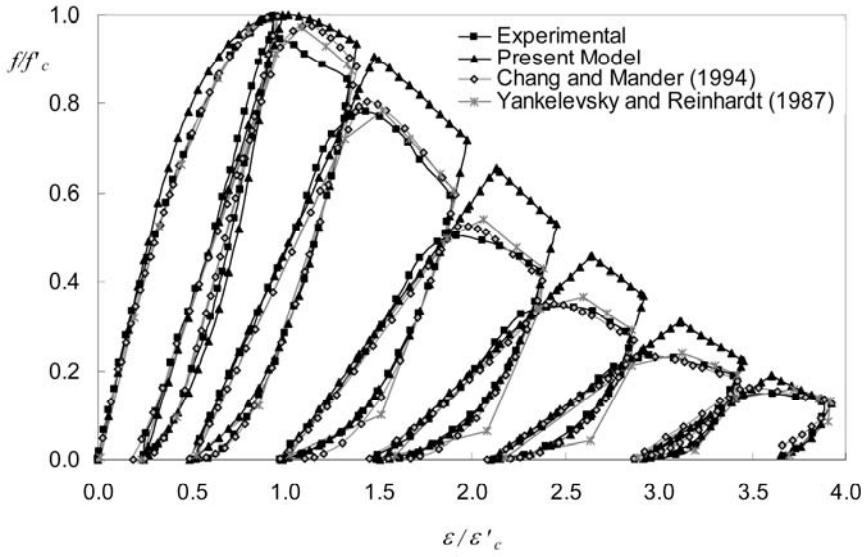

Figure 3.13 – Cyclic compression test by Okamoto et al. (1976), $f_c^{'} = 40.0$ MPa.

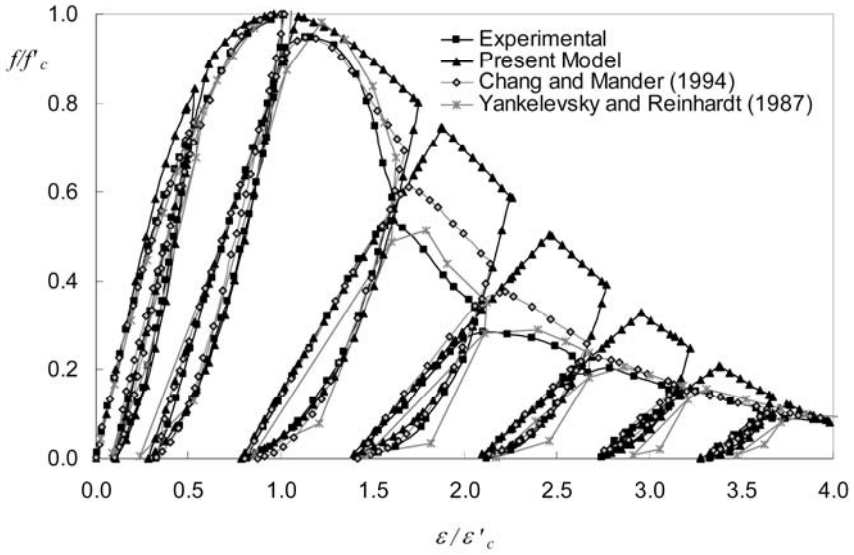

Figure 3.14 – Cyclic compression test by Tanigawa et al. (1979), $f_c^{'} = 40.0$ MPa.

Okamoto et al. (1976) f'_c = 30.0 Mpa - Fig. 3.12							
	Experimental	Present Model		Chang and Mander		Yankelevsky and Reinhardt	
Cicle Nr.	Nmm/mm^2	Nmm/mm^2	Error (%)	Nmm/mm^2	Error (%)	Nmm/mm^2	Error (%)
1	1054.5	1402.5	33%	1212.0	15%	1123.5	7%
2	1318.5	1492.5	13%	1429.5	8%	1392.0	6%
3	1090.5	1053.0	-3%	1159.5	6%	1212.0	11%
4	708.0	631.5	-11%	837.0	18%	840.0	19%
Total	4171.5	4579.5	10%	4638.0	11%	4567.5	9%
Okamoto et al. (1976) f'_c =40.0 Mpa - Fig. 3.13							
	Experimental	Present Model		Chang and Mander		Yankelevsky and Reinhardt	
Cicle Nr.	Nmm/mm^2	Nmm/mm^2	Error (%)	Nmm/mm^2	Error (%)	Nmm/mm^2	Error (%)
1	1828.0	1838.7	1%	1197.8	-34%	1075.3	-41%
2	2447.3	2137.6	-13%	1864.5	-24%	1582.8	-35%
3	1729.0	1696.8	-2%	1675.3	-3%	1761.3	2%
4	1139.8	1135.5	0%	1230.1	8%	1341.9	18%
5	623.7	705.4	13%	705.4	13%	744.1	19%
6	234.4	223.7	-5%	260.2	11%	348.4	49%
Total	8002.2	7737.6	-3%	6933.3	-13%	6853.8	-14%
Tanigawa et al. (1979) $f'c$ =40.0 Mpa - Fig. 3.14							
	Experimental	Present Model		Chang and Mander		Yankelevsky and Reinhardt	
Cicle Nr.	Nmm/mm^2	Nmm/mm^2	Error (%)	Nmm/mm^2	Error (%)	Nmm/mm^2	Error (%)
1	552.0	664.0	20%	294.0	-47%	354.0	-36%
2	1406.0	1614.0	15%	1122.0	-20%	1536.0	9%
3	1528.0	1770.0	16%	1710.0	12%	1182.0	-23%
4	762.0	698.0	-8%	922.0	21%	774.0	2%
5	364.0	348.0	-4%	352.0	-3%	356.0	-2%
6	166.0	140.0	-16%	142.0	-14%	150.0	-10%
7	100.0	118.0	18%	64.0	-36%	54.0	-46%
Total	4778.0	5234.0	10%	4542.0	-5%	4352.0	-9%

Table 3.2 – Dissipated energy calculated for the compressive verification examples.

In figures 3.15 to 3.17 three of the experimental tests performed by Reinhardt (1984) are reproduced. The average compressive strength of the concrete specimens measured in 150 mm cubes was $f_c = 47.1$ MPa (corresponding to a compressive strength measured in standard cylinders of $f_c^{'} = 40.0$ MPa) with a standard deviation of $s = 2.83$ MPa and the tensile strength was $f_{ct} = 3.20$ MPa with a standard deviation of $s = 0.30$ MPa. The original curves were presented in the stress-displacement plane. To transform these curves to the stress-strain plane, the displacement data have been modified by considering the gauge length of the extensometers (35 mm). The average fracture energy reported by the authors was $G_f = 135\,\text{N/m}$. The model results have been obtained considering the same concrete characteristics of the experimental test. The characteristic length l^* has been considered equal to 35 mm. Concrete specimens were submitted to cyclic tension with different lower stress values.

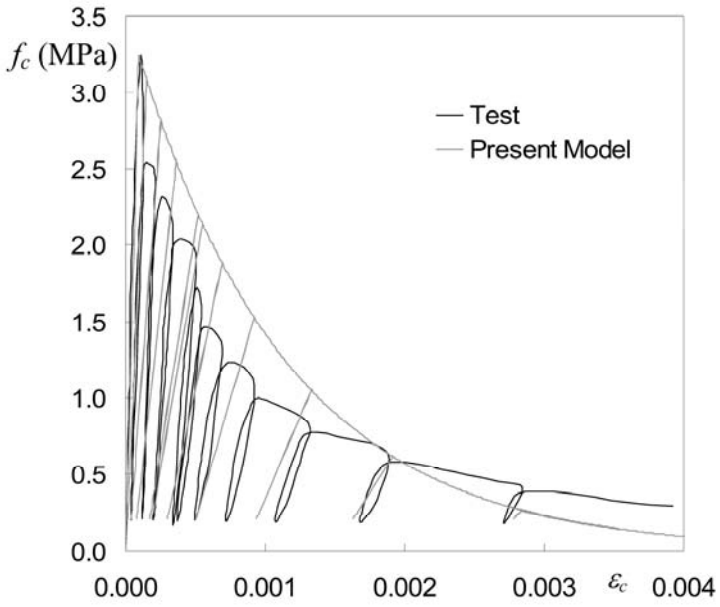

Figure 3.15 – Cyclic tension test by Reinhardt (1984)

In the first case (Fig. 3.15) the lower stress considered is 5 % of the tensile strength. In this case, the unloading and the reloading curves in the model coincide and there is no energy dissipation during a cycle. However, in the experimental results it can be observed that the

amount of energy dissipated in a cycle is really small. Based on these observations it can be concluded that the present model for unloading-reloading in tension is a satisfactory approximation of the real behavior.

In the second case (Fig. 3.16) the lower stress considered is compressive and amounts to 15 % of the tensile strength. In the experimental curve, the unloading and the reloading path of one cycle are significantly different, exhibiting a large hysteresis loop. This feature can be accurately simulated with the model by considering an adequate crack closure stress. A value σ_f^0 of 0.25 f_{ct} has been considered in this case.

In Fig. 3.17, experimental results of a test with large incursions in compression are presented. The lower stress considered is equal to the tensile strength. The loops produced in this case are still larger and the proposed model seems to be a satisfactory approximation.

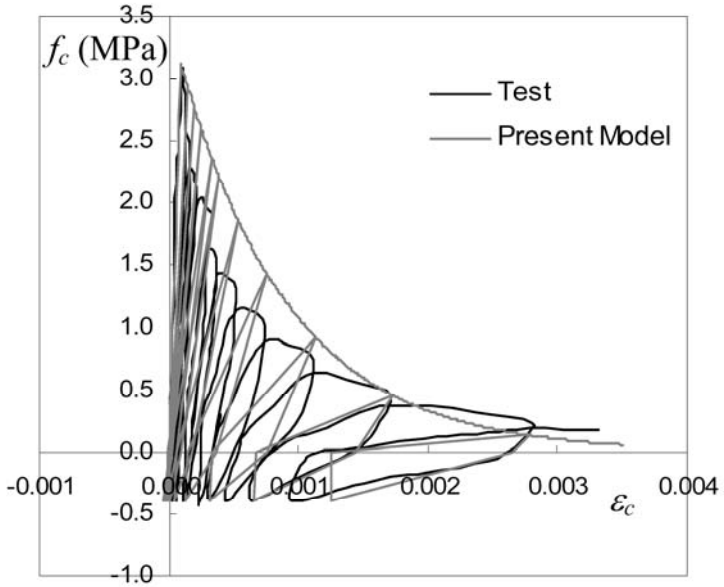

Figure 3.16 – Cyclic tension test with small incursions in compression by Reinhardt (1984)

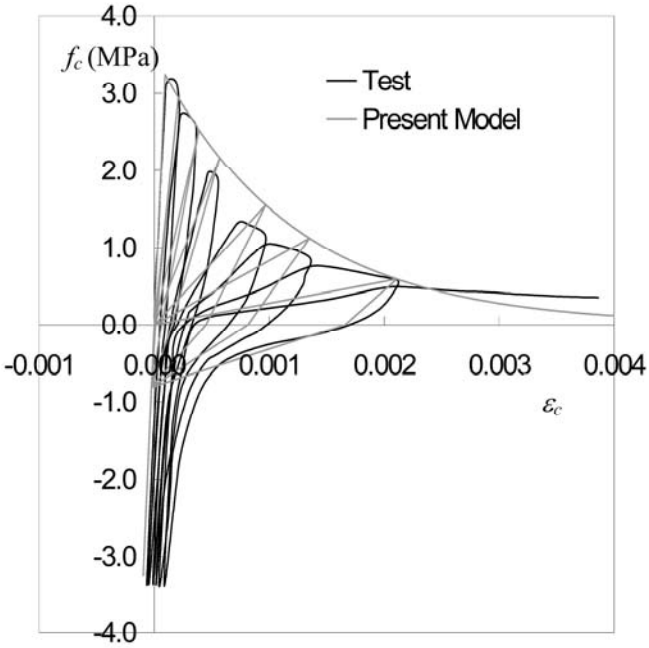

Figure 3.17 – Cyclic tension test with high incursions in compression by Reinhardt (1984)

3.2 Cyclic constitutive model for masonry

A significant number of papers have been presented during the last years on the characterization of the behavior of masonry subjected to monotonic compression or shear-compression loading. (Priestley and Elder, 1983; Magenes, 1992; Naraine and Sinha, 1989, 1991a, 1991b; Ewing and Kowalski, 2004; among others). However, only a few works have been presented on the behavior of masonry under cyclic compressive loadings. This is the case of the works by Naraine and Sinha (1989, 1991a, 1991b), AlShebani and Sinha (1999, 2000) and Oliveira et al. (2006). Naraine and Sinha (1989, 1991a, 1991b) investigated the deformation characteristics of fired clay brick masonry with low levels of compressive strength under cyclic loading. This investigation was later extended to the deformation characteristics of sand plast (a form of calcium silicate) brick masonry with higher levels of compressive strength subjected to uniaxial cyclic loading (AlShebani and Sinha, 1999; and biaxial cyclic loadings AlShebani and Sinha, 2000). Oliveira et al (2006) researched on brittleness, energy dissipation and stiffness degradation of masonry prisms under cyclic loading. Other authors, as Chen et al. (1978) or Macchi (1985), have also reported on the cyclic behavior of brick masonry with focus on seismic design of buildings.

In all cases, the behavior shown by brick masonry subjected to uniaxial cyclic loading presents significant similarity to that of concrete. The latter has been investigated since long time by Karsan and Jirsa (1969) and others.

Based on these results, the basic procedure proposed by Sima et al. (2008) and previously presented for the derivation of a uniaxial cyclic constitutive loading of concrete has been adopted herein. This procedure consists of the modelization of experimental results available in the literature in order to obtain, by means of linear regression, the necessary model parameters for the material.

The basic set of equations (eq. 3.1 to 3.24) used to describe the complete cyclic behavior of concrete previously presented is also used for the masonry.

In the case of compressive loading, the dependence of the other variables with the parameter has been determined in a semi empirical way. The cyclic compression experimental test performed by Naraine and Sinha (1989) over brick masonry panels have been reproduced with this model and statistical regression has been performed in order to obtain the proper dependency of the variables with the level of damage when the unloading starts.

The reloading curve has been modeled by a linear equation. It has been observed in test results (Naraine and Sinha, 1989) that the reloading curve does not return to the envelope curve at the previous maximum unloading strain and further straining in needed to taking up again the envelope curve. It has been found that the relationship between the reloading compressive damage δ_{re} (defined as the compressive damage δ^{-} at the reloading strain ε_{re}) and the unloading compressive damage δ_{un} shows a linear behavior (Fig. 3.18)

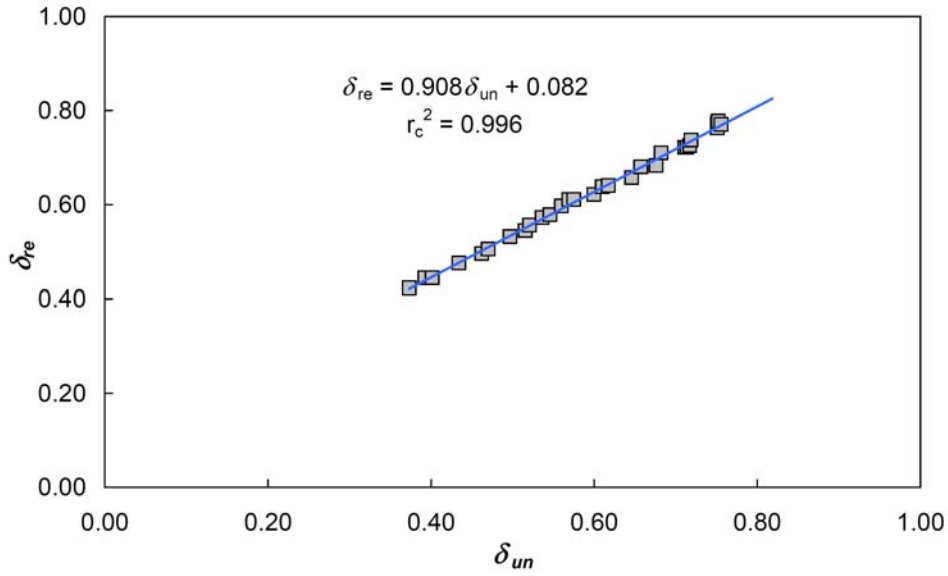

Figure 3.18 - Relationship between the reloading damage and the unloading damage obtained by means of statistical regression on experimental results by Naraine and Sinha (1989).

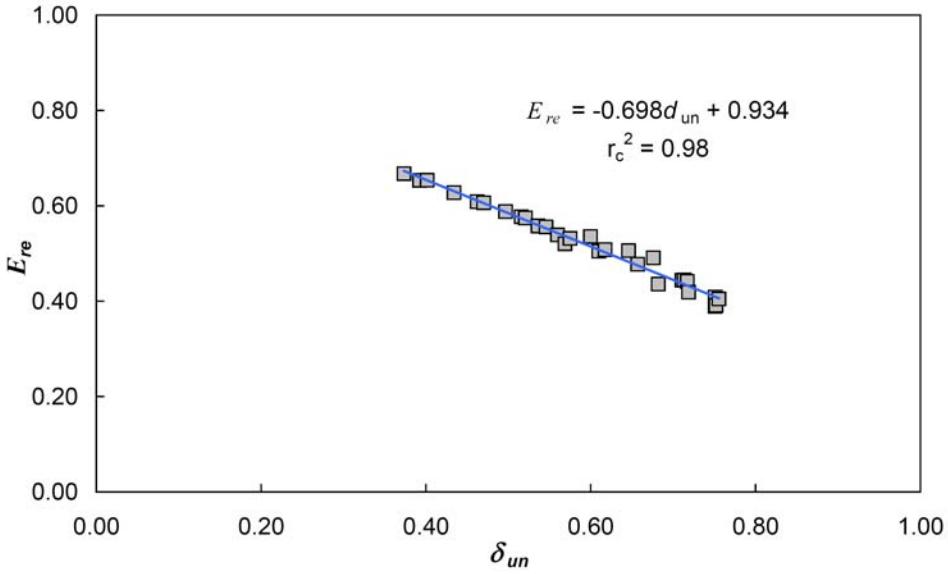

Figure 3.19 - Relationship between the reloading stiffness and the unloading damage obtained by statistical regression on experimental results by Naraine and Sinha (1989).

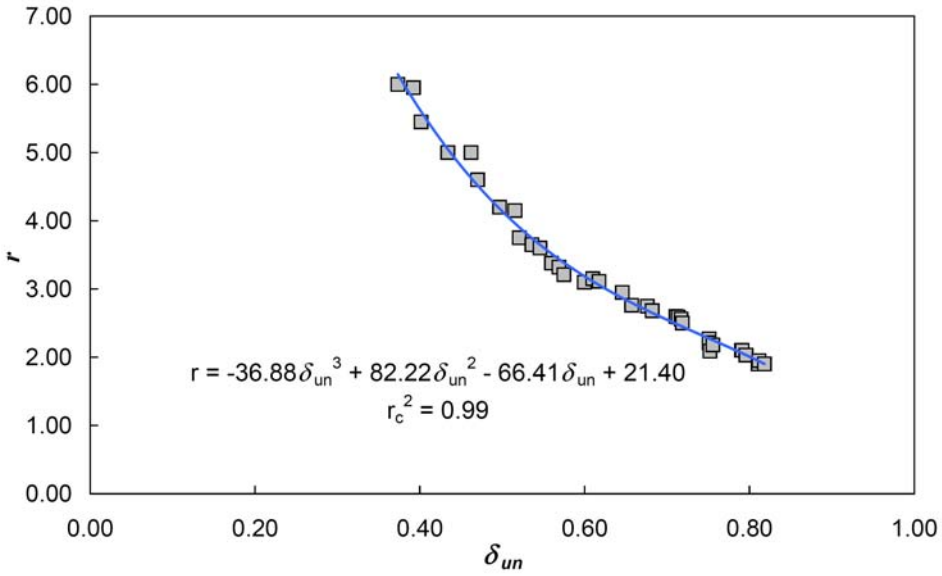

Figure 3.20 - Relationship between the unloading strain-plastic strain ratio and the unloading damage obtained by means of statistical regression on experimental results by Naraine and Sinha (1989).

The difference between δ_{un} and δ_{re} represents the damage accumulated in each cycle. The effect of cyclic stiffness degradation and its dependence with the unloading compressive damage may be observed in Fig. 3.19, while Figs. 3.20 and 3.21 give the obtained relationship between the parameter r (unloading strain-plastic strain ratio) and the unloading compressive damage, and the parameter R (final unloading stiffness-initial unloading stiffness ratio) and the unloading compressive damage, respectively.

Very good adjustments have been possible for the different parameters of the model, with correlation coefficients varying between 0.98 and 1 (Figs 3.18 to 3.21). As a result, the proposed model can be successfully applied to simulate the experimental results presented by Naraine and Sinha (1989) and a very good comparison is obtained between the cyclic experimental and numerical results (Fig. 3.22).

Due to the lack of experimental information regarding the general case of partial unloading-reloading, as well as for the cyclic behavior in tension, the envelope curve in tension proposed for concrete in Sima et al. (2008) and previously explained is adopted herein.

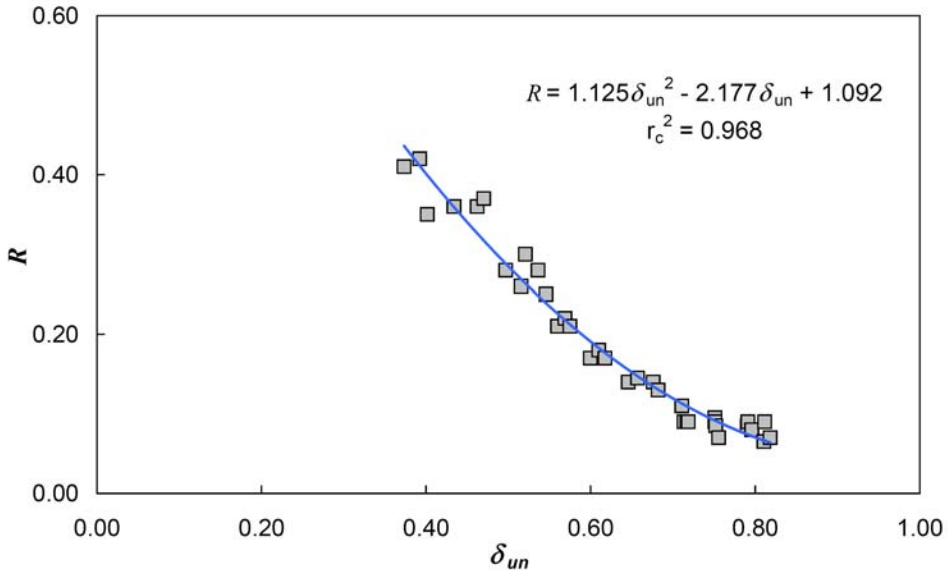

Figure 3.21 – Relationship between the final unloading stiffness – initial unloading stiffness ratio and the unloading damage obtained by means of statistical regression on results by Naraine and Sinha (1989)

To the author knowledge, there are no test results available in the literature regarding the cyclic tensile behavior of masonry. Therefore, the criterion proposed by Sima et al (2008) for concrete is adopted herein for the tensile cyclic behavior of masonry.

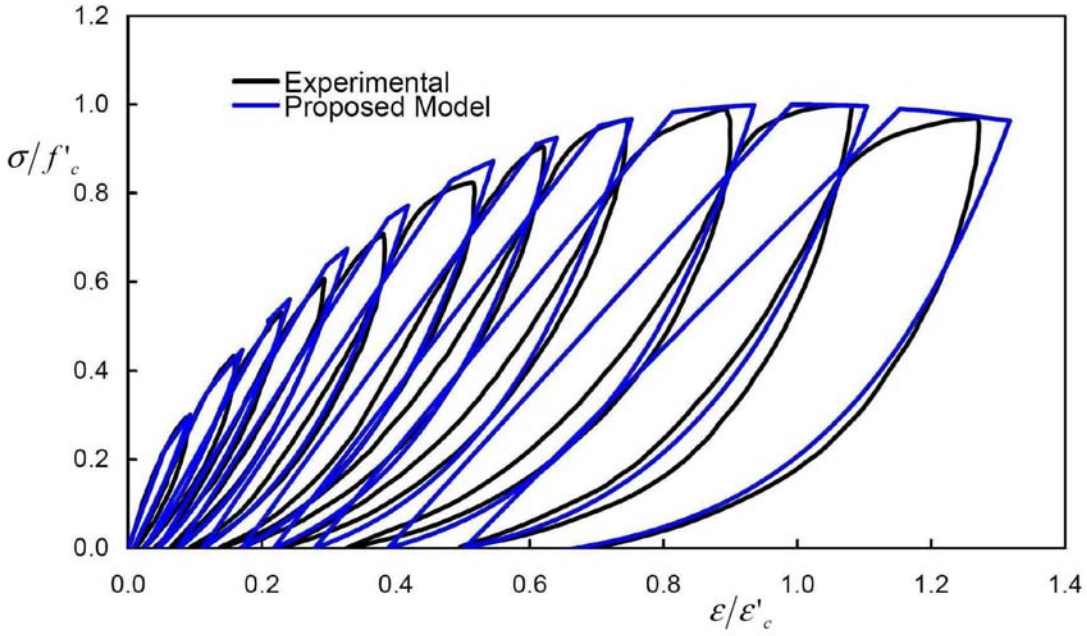

Figure 3.22 – Application of the proposed model for masonry under cyclic compressive loading to one of the test presented by Naraine and Sinha (1989)

Chapter 4

Structural analysis model

Analysis by of spatial frame structures by means of solid elements is the most general and versatile approach. However, it becomes too expensive, in the computational sense, when it is applied to non linear analysis of complex structures involving multiple members. In the case of reinforced concrete structures, the most common and economical strategy is the use of linear elements, either based on the concentrated plasticity approach or the fiber elements approach. In the case of spatial framed masonry structures, an alternative to the macro and micro modelization, which still require a large computational effort preventing their application to the study of large and complex masonry structures, would be the modelization of the masonry elements by means of equivalent frame elements. In the present work, the so-called Generalized Matrix Formulation has been used as the basic structural analysis model. It consists of a generalization of the flexibility based conventional matrix methods, in which the frame deformation shape is a result of the exact integration of the equilibrium and compatibility equations of an element. In this chapter, the main characteristics of this formulation are presented, as well as the extension to the non linear dynamic analysis by means of the direct integration of the equation of motion of the structure.

4.1 Basic formulation: Linear static analysis

As aforementioned, the Generalized Matrix Formulation (GMF) for curved elements with variable cross section has been chosen as the basic environment for the analysis of reinforced concrete framed structures. The main characteristics of the formulation are described in the following paragraphs. A more in deep explanation of the derivation of the GMF can be found in Molins (1996).

It must be remarked that the most commonly used procedures for the management of curved elements are based on the decomposition of members into polygons of straight elements with uniform cross section or use displacement formulations of the FEM with isoparametric curved elements. However, the first approach is a coarse and expensive approximation and the second one uses an assumed interpolation of the structure and its deformed shape. In the second case, the assumed interpolation constrains the possible geometries to a limited subset and thus involves an extra condition over imposed on the more general conditions of equilibrium and compatibility and the stress-strain relationship. As a result, the internal forces are calculated in such a way that the equilibrium cannot be satisfied within an element in a strict sense. Conversely, GMF is directly based on the equilibrium between external and internal forces at any point within an element and no additional hypothesis (to interpolate strains or stresses) over the displacements or stress field is required. The GMF can be seen also as a hybrid formulation in which sectional internal forces across the element are expressed as an interpolation of the external forces acting on it. However, the interpolation used for the internal forces is not arbitrarily defined; in fact, it is an exact expression directly derived from the consideration of the equilibrium upon an element. The main features of the basic formulation are summarized in the following paragraphs.

The equilibrium equation of the element is derived by considering a slice of element with infinitesimal length ds belonging to a member subjected to a distributed load $\boldsymbol{p}$ and a moment $\boldsymbol{m}$ along its axis, as is shown in Fig. 4.1. Acting on both ends of the slice, the

forces and moments $-\boldsymbol{R}$, $-\boldsymbol{M}$ and $\boldsymbol{R}+d\boldsymbol{R}$, $\boldsymbol{M}+d\boldsymbol{M}$ at point O and O' respectively, are in equilibrium with the applied loads. The equilibrium condition may be expressed as follows:

$$\begin{aligned} d\boldsymbol{R}+\boldsymbol{p}ds&=0\\ -\boldsymbol{R}\times d\boldsymbol{s}+d\boldsymbol{M}+\boldsymbol{m}ds&=0 \end{aligned} \tag{4.1}$$

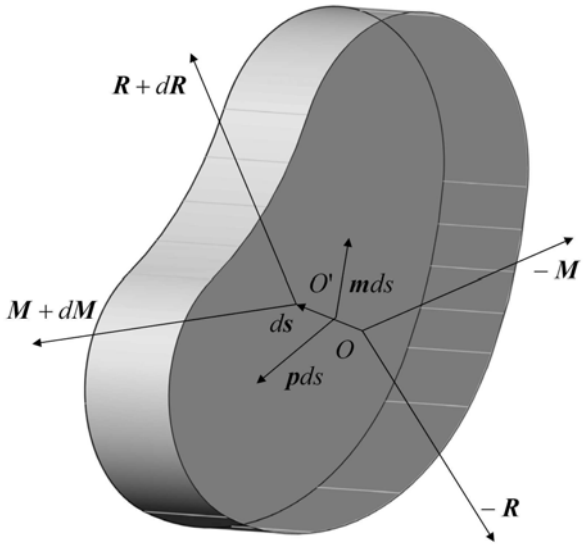

Figure 4.1 – Equilibrium over a slice of beam with a differential thickness

The equations of equilibrium of an element can be obtained by integrating the ordinary system of first-order equations (4.1). The solution of the system is formed by a solution of the homogeneous system plus a particular solution of the complete system. As a particular solution of the system, a cantilever configuration with free end at point B has been selected. Under these assumptions, integration of (4.1) leads to the following equation:

$$\begin{bmatrix} R_X\\ R_Y\\ R_Z\\ M_X\\ M_Y\\ M_Z \end{bmatrix} = \begin{bmatrix} 1 & 0 & 0 & 0 & 0 & 0\\ 0 & 1 & 0 & 0 & 0 & 0\\ 0 & 0 & 1 & 0 & 0 & 0\\ 0 & (Z-Z_B) & -(Y-Y_B) & 1 & 0 & 0\\ -(Z-Z_B) & 0 & (X-X_B) & 0 & 1 & 0\\ (Y-Y_B) & -(X-X_B) & 0 & 0 & 0 & 1 \end{bmatrix} \begin{bmatrix} R_{XB}\\ R_{YB}\\ R_{ZB}\\ M_{XB}\\ M_{YB}\\ M_{ZB} \end{bmatrix} + \begin{bmatrix} R_X^*\\ R_Y^*\\ R_Z^*\\ M_X^*\\ M_Y^*\\ M_Z^* \end{bmatrix} \tag{4.2}$$

Equation (4.2) can be rewritten in the following compact form:

$$\boldsymbol{\sigma}_{XY}(s) = \boldsymbol{N}(s, s_B)\boldsymbol{P}_B + \boldsymbol{\sigma}^*_{XY}(s) \tag{4.3}$$

Where $\boldsymbol{N}(s, s_B)$ is an interpolation matrix that describes the exact equilibrium forces between the transverse sections B and s, $\boldsymbol{\sigma}_{XY}(s)$ is the vector of sectional forces at any section of curvilinear coordinate s, and $\boldsymbol{\sigma}^*_{XY}(s)$ is the vector of forces produced by the distributed loads, $\boldsymbol{p}$ and $\boldsymbol{m}$, on a cantilever isostatic configuration, calculated as

$$\boldsymbol{\sigma}^*_{XY}(s) = \int_s^B \boldsymbol{N}(s, \xi)[\boldsymbol{p}, \boldsymbol{m}]^T d\xi \tag{4.4}$$

The kinematic compatibility is imposed by mean of the Navier-Bresse's equations (Marí, 1985):

$$\boldsymbol{\omega}(s) = \boldsymbol{\omega}(s_0) + \int_{s_0}^{s} \boldsymbol{\Omega}(\xi) d\xi \tag{4.5}$$

$$\boldsymbol{\lambda}(s) = \boldsymbol{\lambda}(s_0) + \boldsymbol{\omega}(s_0) \times (\boldsymbol{\Gamma}(s_0) - \boldsymbol{\Gamma}(s)) + \int_{s_0}^{s} (\boldsymbol{\Lambda}(\xi) + \boldsymbol{\Omega}(\xi) \times (\boldsymbol{\Gamma}(\xi) - \boldsymbol{\Gamma}(s))) d\xi \tag{4.6}$$

where $\boldsymbol{\lambda}(s)$ and $\boldsymbol{\omega}(s)$ are the vector of displacements and rotations of the reference axial curve at the point with curvilinear coordinate s; $\boldsymbol{\Lambda}(\xi) = (\varepsilon_X, \varepsilon_Y, \varepsilon_Z)$ and $\boldsymbol{\Omega}(\xi) = (\phi_X, \phi_Y, \phi_Z)$ are the vectors of sectional strains and sectional curvatures, in the curvilinear coordinate point ξ, and $\boldsymbol{\Gamma} = (X, Y, Z)$ is the reference vector of points belonging to the axial curve (Fig. 4.2).

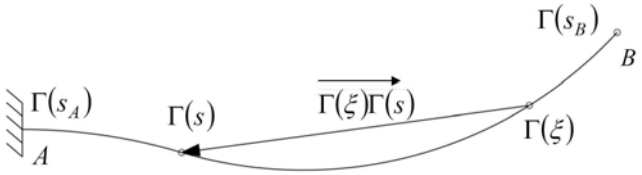

Figure 4.2 – Cantilever basic isostatic configuration

Applying (4.5) and (4.6) to the ends of the element, A and B, the following equation is obtained

$$\boldsymbol{u}_B = \boldsymbol{N}^T(s_A, s_B)\boldsymbol{u}_A + \int_A^B \boldsymbol{N}^T(s, s_B)\boldsymbol{\varepsilon}_{XY}\, ds \tag{4.7}$$

where $\boldsymbol{u}_A = (\boldsymbol{\lambda}_A, \boldsymbol{\omega}_A)^T$ and $\boldsymbol{u}_B = (\boldsymbol{\lambda}_B, \boldsymbol{\omega}_B)^T$ are the movement vectors at the ends A and B respectively, and $\boldsymbol{\varepsilon}_{XY}(s) = (\boldsymbol{\Lambda}, \boldsymbol{\Omega})^T$ is the strain vector of the section with curvilinear coordinate s.

The second term in equation (4.7) gives the movement of end B caused by the deformation of the element

$$\boldsymbol{d} = \boldsymbol{u}_B - \boldsymbol{N}^T(s_A, s_B)\boldsymbol{u}_A = \int_A^B \boldsymbol{N}^T(s, s_B)\boldsymbol{\varepsilon}_{XY}(s)\, ds \tag{4.8}$$

The constitutive relationship between sectional forces and sectional strains in local coordinates may be expressed as follows:

$$\boldsymbol{\sigma}_s = \boldsymbol{K}_s\left(\boldsymbol{\varepsilon}_s - \boldsymbol{\varepsilon}_s^0\right) + \boldsymbol{\sigma}_s^0 \tag{4.9}$$

where $\boldsymbol{\sigma}_s = (\boldsymbol{R}, \boldsymbol{M})^T = (N, V_y, V_z, M_x, M_y, M_z)^T$ are the sectional forces, and $\boldsymbol{\varepsilon}_s = (\boldsymbol{\Lambda}, \boldsymbol{\Omega})^T = (\varepsilon_x, \varepsilon_y, \varepsilon_z, \phi_x, \phi_y, \phi_z)^T$ are respectively the sectional axial strain, the shear

strains in the y and z axis, the twist and the bending curvatures, $\boldsymbol{K}_s$ is the sectional stiffness matrix, which depends on the shape of the section and on the elastic properties of the materials, $\boldsymbol{\sigma}_s^0$ is the vector of forces due to initial stresses and $\boldsymbol{\varepsilon}_s^0$ is the vector of initial strains of the section.

At this point, a series of hypothesis regarding the mechanical behavior of the element are introduced: (1) linear elastic response is assumed; (2) Bernoulli's hypothesis is maintained, so that the sections remain plane after deformation of the element, although, due to shear deformation, they do not necessarily remain perpendicular to the axis; (3) tangential forces (shear and torsion) and normal forces (axial and bending) are assumed to be completely uncoupled; (4) Saint Venant torsion is assumed.

The sectional stiffness matrix $\boldsymbol{K}_s$, is obtained by combining the equilibrium condition, the kinematic compatibility, and the material constitutive equations at the sectional level. The normal and shear behaviors are considered uncoupled in the constitutive relationships; thus, a uniaxial stress-strain constitutive equation can be used to describe the axial behavior at the filament level.

The lack of coupling between tangential and normal forces is observed in the absence of cross terms between the normal and the tangential constitutive relations in the sectional stiffness matrix:

$$\boldsymbol{K}_s = \begin{bmatrix} \iint_A E dA & 0 & 0 & 0 & \iint_A E z dA & -\iint_A E y dA \\ & GA_{S_y} & 0 & -GA_{S_y} z_c & 0 & 0 \\ & & GA_{S_z} & GA_{S_z} y_c & 0 & 0 \\ & & & GJ + G\left(A_{S_z} y_c^2 + A_{S_y} z_c^2\right) & 0 & 0 \\ & sym. & & & \iint_A E z^2 dA & -\iint_A E y z dA \\ & & & & & \iint_A E y^2 dA \end{bmatrix} \quad (4.10)$$

Where E is the Young's modulus of the material at point (y,z) of the cross-section, G is the shear modulus of the material, J is the torsional inertia of the section, (y_c, z_c) are the local coordinates of the shear center and A_{S_y}, A_{S_z} are the reduced areas of the section for shear forces in the local directions y and z (Fig. 4.3).

The terms in expression (4.10) referring to the normal sectional stiffness are well known and do not need further justification. The terms associated to the sectional behavior under tangent forces results from the combination of the equilibrium equation (4.11) and compatibility (4.12) with the stress-stress relationships (4.13):

$$\begin{aligned} &\Omega = M_x + z_c V_y - y_c V_z \\ &\gamma_y = \gamma_y^c + \phi_x z_c \qquad \gamma_z = \gamma_z^c - \phi_x y_c \end{aligned} \tag{4.11}$$

$$V_y = \gamma_y^c G A_{sy} \qquad V_z = \gamma_z^c G A_{sz} \tag{4.12}$$

$$\Omega = GJ\phi_x \tag{4.13}$$

Where Ω refers to the torsional moment applied to the shear center and γ_y^c and γ_z^c are the shear strains at the shear center.

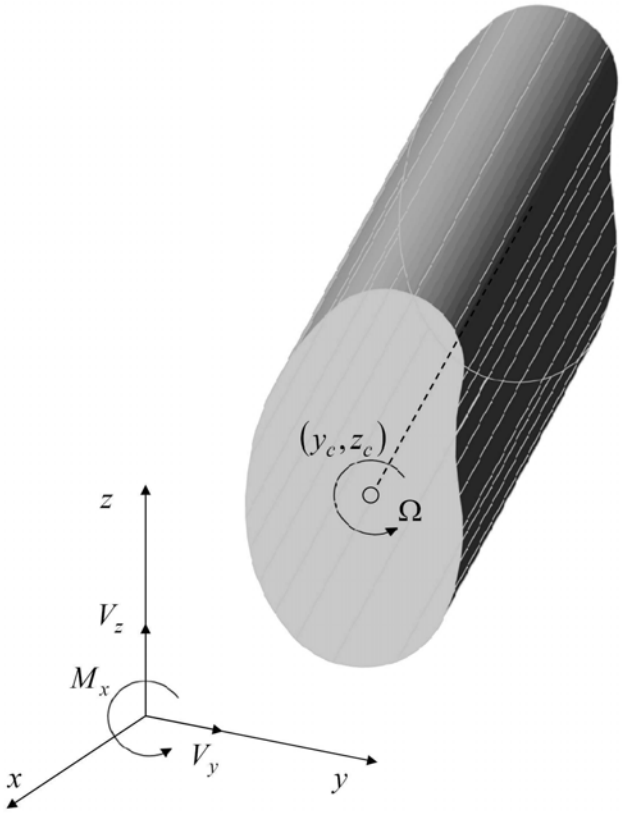

Figure 4.3 – Cross section local axes

The rotation matrix $\boldsymbol{C}$ is introduced to relate the sectional stress or strain vectors expressed in local coordinates (x, y, z) and global coordinates (X, Y, Z), so that

$$\boldsymbol{\varepsilon}_s = \boldsymbol{C}\boldsymbol{\varepsilon}_{XY} \qquad \boldsymbol{\sigma}_s = \boldsymbol{C}\boldsymbol{\sigma}_{XY} \tag{4.14}$$

where $\boldsymbol{C}^T = \boldsymbol{C}^{-1}$. Thus, the constitutive equation (4.9) may be rewritten as

$$\boldsymbol{C}\boldsymbol{\sigma}_{XY} = \boldsymbol{K}_s\left(\boldsymbol{C}\boldsymbol{\varepsilon}_{XY} + \boldsymbol{\varepsilon}_s^0\right) + \boldsymbol{C}\boldsymbol{\sigma}_{XY}^0 \tag{4.15}$$

The following equation for the strain vector in global coordinates may is obtained by solving equation (4.15)

$$\boldsymbol{\varepsilon}_{XY} = \boldsymbol{C}^T \boldsymbol{K}_s^{-1} \boldsymbol{C}\left(\boldsymbol{\sigma}_{XY} - \sigma_{XY}^0\right) - \boldsymbol{C}^T \boldsymbol{\varepsilon}_s^0 \tag{4.16}$$

Substituting (4.16) in equation (4.8) gives

$$\boldsymbol{d} = \boldsymbol{u}_B - \boldsymbol{N}^T(s_A, s_B)\boldsymbol{u}_A = \int_A^B \boldsymbol{N}^T(s, s_B)\left(\boldsymbol{C}^T \boldsymbol{K}_s^{-1} \boldsymbol{C}\left(\boldsymbol{\sigma}_{XY} - \boldsymbol{\sigma}_{XY}^0\right) - \boldsymbol{C}^T \boldsymbol{\varepsilon}_s^0\right) ds \tag{4.17}$$

The equilibrium equation (4.3) allows relating the internal section forces at any point with the forces $\boldsymbol{P}_A$ and $\boldsymbol{P}_B$ at the ends of the elements. This relation can be incorporated in equation (4.17) as follows:

$$\begin{aligned} \boldsymbol{d} = & \int_A^B \left(\boldsymbol{N}^T(s, s_B)\boldsymbol{C}^T \boldsymbol{K}_s^{-1} \boldsymbol{C}\boldsymbol{N}(s, s_B) P_B + \boldsymbol{N}^T(s, s_B)\boldsymbol{C}^T \boldsymbol{K}_s^{-1} \boldsymbol{C}\boldsymbol{\sigma}_{XY}^*\right) ds \\ & - \int_A^B \left(\boldsymbol{N}^T(s, s_B)\boldsymbol{C}^T \boldsymbol{K}_s^{-1} \boldsymbol{C}\boldsymbol{\sigma}_{XY}^0 - \boldsymbol{N}^T(s, s_B)\boldsymbol{C}^T \boldsymbol{\varepsilon}_s^0\right) ds \end{aligned} \tag{4.18}$$

This equation can be rewritten as:

$$\boldsymbol{d} = \boldsymbol{F}\boldsymbol{P}_B + \boldsymbol{d}^* + \boldsymbol{d}^0 \tag{4.19}$$

where $\boldsymbol{F} = \int_A^B \boldsymbol{N}^T \boldsymbol{C}^T \boldsymbol{K}_s^{-1} \boldsymbol{C}\boldsymbol{N}\, ds$ is the flexibility matrix of the element, $\boldsymbol{d}^* = \int_A^B \boldsymbol{N}^T \boldsymbol{C}^T \boldsymbol{K}_s^{-1} \boldsymbol{C}\boldsymbol{\sigma}_{XY}^*\, ds$ is the vector of displacements in B produced by the deformation of the element in its basic isostatic configuration under the effect of distributed loads, and $\boldsymbol{d}^0 = \int_A^B \boldsymbol{N}^T \boldsymbol{C}^T \left(\boldsymbol{K}_s^{-1} \boldsymbol{C}\boldsymbol{\sigma}_{XY}^0 - \boldsymbol{\varepsilon}_s^0\right) ds$ is the vector of displacements in B due to the initial strains and stresses.

To obtain the stiffness matrix of the element, the explicit relationship between forces and nodal displacements is formulated. Combining equation (4.9) and (4.19), the following relationship is obtained for the extreme B:

$$\boldsymbol{P}_B = -\boldsymbol{F}^{-1}\boldsymbol{N}^T(s_A, s_B)\boldsymbol{u}_A + \boldsymbol{F}^{-1}\boldsymbol{u}_B - \boldsymbol{F}^{-1}\left(\boldsymbol{d}^* + \boldsymbol{d}^0\right) \tag{4.20}$$

In the case of the extreme A, a similar result may be obtained by combining equation (4.20) with the equilibrium equation (4.3)

$$\boldsymbol{P}_A = \boldsymbol{N}(s_A, s_B)\boldsymbol{P}_B + \boldsymbol{P}_A^* \tag{4.21}$$

$$\boldsymbol{P}_A = \boldsymbol{N}(s_A, s_B)\left(-\boldsymbol{F}^{-1}\boldsymbol{N}^T(s_A, s_B)\boldsymbol{u}_A + \boldsymbol{F}^{-1}\boldsymbol{u}_B - \boldsymbol{F}^{-1}\left(\boldsymbol{d}^* + \boldsymbol{d}^0\right)\right) + \boldsymbol{P}_A^* \tag{4.22}$$

The following matrix expression is obtained by combining both results:

$$\begin{bmatrix}\boldsymbol{P}_A \\ \boldsymbol{P}_B\end{bmatrix} = \begin{bmatrix}\boldsymbol{N}(s_A, s_B)\boldsymbol{F}^{-1}\boldsymbol{N}^T(s_A, s_B) & -\boldsymbol{N}(s_A, s_B)\boldsymbol{F}^{-1} \\ -\boldsymbol{F}^{-1}\boldsymbol{N}^T(s_A, s_B) & \boldsymbol{F}^{-1}\end{bmatrix}\begin{bmatrix}\boldsymbol{u}_A \\ \boldsymbol{u}_B\end{bmatrix} - \begin{bmatrix}\boldsymbol{N}(s_A, s_B)\boldsymbol{F}^{-1}\left(\boldsymbol{d}^* + \boldsymbol{d}^0\right) - \boldsymbol{P}_A^* \\ \boldsymbol{F}^{-1}\left(\boldsymbol{d}^* + \boldsymbol{d}^0\right)\end{bmatrix} \tag{4.23}$$

which can be rewritten in a more compact form as

$$\boldsymbol{P} = \boldsymbol{K}\boldsymbol{u} + \boldsymbol{P}^{*0} \tag{4.24}$$

where $\boldsymbol{P}$ is the vector of forces at the extreme points, $\boldsymbol{K}$ is the stiffness matrix of the element, $\boldsymbol{u}$ is the vector of displacements at the extreme points and $\boldsymbol{P}^{*0}$ is the vector of reactions corresponding to the perfect clamping at the ends of the element due to initial strains and stresses.

This last equation allows the construction of the global equation of the structural problem following the conventional assemblage processes.

4.2 Solution strategy for the non-linear problem

The solution method for the non-linear problems in the framework of the GMF adopted herein was proposed by Molins (1996). It consist in the combination of an incremental process, in which some predefined load increments are gradually provided to the structure, together with an iterative method to solve the problem at each increment (Newton-Raphson). A remarkable feature of this solution strategy is that it combines a set of iterations at the global level with a secondary set for each individual element.

For the global iteration i of an increment of load k, a linear system of equation if formulated and solved, which takes the form:

$$\Delta \boldsymbol{u}_k^i = \left[\boldsymbol{K}_k^{i-1}\right]^{-1} \boldsymbol{P}_k^{i-1} \tag{4.25}$$

where $\Delta \boldsymbol{u}_k^i$ is the vector of nodal displacements, $\boldsymbol{K}_k^{i-1}$ is the global updated stiffness matrix of the structure and $\boldsymbol{P}_k^{i-1}$ is the vector of unbalanced forces evaluated after iteration $i-1$ as the difference between the external forces and the internal resisting ones. Once the previous linear system is solved, the different variables are updated with the obtained increments. The increment in displacements is added to the vector of total displacements according to:

$$\boldsymbol{u}_k^i = \boldsymbol{u}_k^{i-1} + \Delta \boldsymbol{u}_k^i \tag{4.26}$$

As in most of the flexibility based formulations (Backlund, 1976; Grelat, 1978; Carrascón et al., 1987; among others) the internal forces are obtained through the direct integration of the sectional forces. The implementation of this procedure on the GMF requires the following steps (Molins, 1996):

1. Compute the increment of forces at the ends of the beam elements from the vector of incremental nodal displacements obtained in the i iteration:

$$\begin{bmatrix} \Delta \boldsymbol{P}_A^i \\ \Delta \boldsymbol{P}_B^i \end{bmatrix} = \boldsymbol{K}^{i-1} \begin{bmatrix} \Delta \boldsymbol{u}_A^i \\ \Delta \boldsymbol{u}_B^i \end{bmatrix} \tag{4.27}$$

2. Compute the increment of sectional forces in local coordinates, by means of the equilibrium equation:

$$\Delta \boldsymbol{\sigma}_s^i(s) = \boldsymbol{C}(s)\boldsymbol{N}(s, s_B)\Delta \boldsymbol{P}_B^i \tag{4.28}$$

$$\boldsymbol{\sigma}_{s\,tot}^i(s) = \boldsymbol{\sigma}_{s\,tot}^{i-1}(s) + \Delta \boldsymbol{\sigma}_s^i(s) \tag{4.29}$$

3. Obtain the corresponding sectional strains by using the sectional flexibility matrix

$$\Delta \boldsymbol{\varepsilon}_s^i = \left[\boldsymbol{K}_s^{i-1}\right]^{-1} \Delta \boldsymbol{\sigma}_s^{i-1} \tag{4.30}$$

4. Add the strain increments to the vector of total strains

$$\boldsymbol{\varepsilon}_s^i = \boldsymbol{\varepsilon}_s^{i-1} + \Delta \boldsymbol{\varepsilon}_s^i \tag{4.31}$$

5. From the constitutive equation generate the internal forces and the updated sectional stiffness matrix

$$\boldsymbol{\sigma}_s^i(s) = \boldsymbol{f}\left(\boldsymbol{\varepsilon}_s^i\right) \tag{4.32}$$

$$\boldsymbol{K}_s^i = \frac{\partial \boldsymbol{f}}{\partial \boldsymbol{\varepsilon}_s^i} \tag{4.33}$$

6. Obtain the unbalanced forces and the unbalanced strains as

$$\boldsymbol{\sigma}_{s\,u}^{i}(s) = \boldsymbol{\sigma}_{s\,tot}^{i}(s) - \boldsymbol{\sigma}_{s}^{i}(s) \tag{4.34}$$

$$\boldsymbol{\varepsilon}_{s\,u}^{i}(s) = \left[\boldsymbol{K}_{s}^{i}\right]^{-1}\boldsymbol{\sigma}_{s\,u}^{i} \tag{4.35}$$

7. The latest unbalanced strains are considered as initial strains for the next iteration. Previously, the unbalanced displacements $\boldsymbol{d}_{u}^{i}$ caused by the unbalanced strains on the isostatic basic configuration are calculated as:

$$\boldsymbol{d}_{u}^{i} = \int_{A}^{B} \boldsymbol{N}^{T}\boldsymbol{C}^{T}\boldsymbol{\varepsilon}_{s\,u}^{i}(s)\,ds \tag{4.36}$$

Finally, the element unbalanced forces may be computed as

$$\begin{bmatrix}\boldsymbol{P}_{u\,A}^{i}\\ \boldsymbol{P}_{u\,B}^{i}\end{bmatrix} = -\begin{bmatrix}\boldsymbol{N}_{(A;B)}\boldsymbol{F}^{-1}\boldsymbol{d}_{u}^{i}\\ \boldsymbol{F}^{-1}\boldsymbol{d}_{u}^{i}\end{bmatrix} \tag{4.37}$$

8. The new vector of loads $\Delta\boldsymbol{P}_{u}^{i}$ to be applied to the structural system is obtained by assembling the unbalanced elementary forces (4.37). Therefore, the next iteration $i+1$ can be undertaken, and the process follows until convergence is obtained.

Even though this procedure should lead to a correct solution by itself, its efficiency and convergence speed are limited due to the fact that the computed strains in step 4 are not exact (i.e. the set of matrices $\boldsymbol{K}_{s}^{i-1}$, $\boldsymbol{C}$ and $\boldsymbol{N}$ have not been updated and do not guarantee either equilibrium or compatibility in the new state of the structure). The inclusion of a complementary iterative cycle at the element level, allows obtaining a more efficient solution procedure. Molins et al. (1998) observed that the number of global iterations required to reach convergence is significantly reduced, therefore the modified procedure is highly advantageous in the computational sense. This type of secondary iteration has been

previously used by Ciampi and Carlesimo (1986), Taucer et al. (1991) and Spacone (1994). In a later work, Neuenhofer and Filippou (1997) proposed a procedure that bypasses the need for iteration during the element state determination by accepting both residual displacements, which violate compatibility at the element ends, and unbalanced section forces, which violate strict equilibrium along the element during each iteration of the global equilibrium equation.

The secondary iterative cycle, carried independently for each element, maintains the same 8 steps with some minor modifications. The incremental sectional strains in step 3 are now computed for the element iteration j within a global iteration i as:

$$\Delta\boldsymbol{\varepsilon}_s^j = \left[\boldsymbol{K}_s^{j-1}\right]^{-1}\Delta\boldsymbol{\sigma}_s^j + \boldsymbol{\varepsilon}_{s\,u}^{j-1}(s) \tag{4.38}$$

After step 7, the unbalanced force at the end B is computed as

$$\Delta\boldsymbol{P}_{u\,B}^{j+1} = -\boldsymbol{K}^j\boldsymbol{d}_u^j \tag{4.39}$$

and the process is then repeated starting from the step 2 until the convergence is reached for the element iteration.

4.3 Dynamic analysis formulation

For the derivation of the GMF for dynamic analysis, a consistent mass matrix was proposed by Molins et al. (1998) which was obtained from the definition of a sectional mass matrix and a description of the displacement field in the element, as is explained in the following paragraphs. A remarkable feature of the proposed mass matrix is that it incorporates information related to the geometry, the stiffness distribution and the mass density within the element.

The sectional mass matrix proposed by Molins et al. (1998) takes the form:

$$\boldsymbol{M}_S(s)=\begin{bmatrix} \iint_A \rho dA & 0 & 0 & 0 & \iint_A \rho z dA & -\iint_A \rho y dA \\ & \iint_A \rho dA & 0 & -\iint_A \rho z dA & 0 & 0 \\ & & \iint_A \rho dA & \iint_A \rho y dA & 0 & 0 \\ & & & \iint_A \left(y^2+z^2\right)\rho dA & 0 & 0 \\ & Sym. & & & \iint_A \rho z^2 dA & -\iint_A \rho yz dA \\ & & & & & \iint_A \rho y^2 dA \end{bmatrix} \tag{4.40}$$

By assuming that the cross-sections are moved as rigid bodies in their plane, the inertial forces in local coordinates $\boldsymbol{f}_I(s)=\left[f_{Ix}(s),f_{Iy}(s),f_{Iz}(s),f_{Ixx}(s),f_{Iyy}(s),f_{Izz}(s)\right]^T$ of any cross section of curvilinear coordinate s, may be calculated as a function of the accelerations:

$$\boldsymbol{f}_I(s)=\boldsymbol{M}_S(s)\ddot{\boldsymbol{u}}(s) \tag{4.41}$$

where $\ddot{\boldsymbol{u}}(s)=\left[\ddot{u}_x(s),\ddot{u}_y(s),\ddot{u}_z(s),\ddot{\theta}_x(s),\ddot{\theta}_y(s),\ddot{\theta}_z(s)\right]^T$ is the acceleration vector of a point on the axis with curvilinear coordinate s.

By combining equations (4.3) and (4.16) it may be obtained the following expression which relates the sectional strains $\boldsymbol{\varepsilon}_{XY}(s)$ to the forces $\boldsymbol{P}_B$ at the end B and the forces $\boldsymbol{\sigma}^*_{XY}(s)$:

$$\boldsymbol{\varepsilon}_{XY}(s)=\boldsymbol{C}^T(s)\boldsymbol{K}_s^{-1}(s)\boldsymbol{C}(s)\left(\boldsymbol{N}(s,s_B)\boldsymbol{P}_B+\boldsymbol{\sigma}^*_{XY}(s)\right) \tag{4.42}$$

By assuming that the element does not carry distributed loads (i.e. $\boldsymbol{\sigma}^*_{XY}=0$ and $\boldsymbol{d}^*=0$), and combining equations (4.20) and (4.42) yields

$$\boldsymbol{\varepsilon}_{XY}(\xi)=\boldsymbol{C}^T(\xi)\boldsymbol{K}_s^{-1}(\xi)\boldsymbol{C}(\xi)\boldsymbol{N}(\xi,s_B)\left(\boldsymbol{F}^{-1}\boldsymbol{d}_B-\boldsymbol{F}^{-1}\boldsymbol{N}^T_{(A,B)}\boldsymbol{d}_A\right) \tag{4.43}$$

The substitution of this latest equation in equation (4.7) allows obtaining:

$$\boldsymbol{d}(s) = \boldsymbol{G}(s)\begin{bmatrix}\boldsymbol{d}_A \\ \boldsymbol{d}_B\end{bmatrix} \tag{4.44}$$

where

$$\boldsymbol{G}(s) = \left[\boldsymbol{N}^T(s_A, s) - \boldsymbol{F}_s(s)\boldsymbol{F}^{-1}\boldsymbol{N}^T_{(A,B)} \qquad \boldsymbol{F}_s(s)\boldsymbol{F}^{-1}\right] \tag{4.45}$$

is the matrix which relates the internal displacements of the element to the node displacements, and

$$\boldsymbol{F}_s(s) = \int_{s_A}^{s} \boldsymbol{N}^T(\xi, s)\boldsymbol{C}^T(\xi)\boldsymbol{K}_s^{-1}(\xi)\boldsymbol{C}(\xi)\boldsymbol{N}(\xi, s_B)d\xi \tag{4.46}$$

The expression (4.44) allows obtaining the displacement of any point in the axis of the element from the displacements at the nodes. It is exact only in the case that the deformation of the element is produced by the displacement of the ends. In all other cases (i.e. when deformation due to distributed loads can not be neglected), the expression is an approximation to the field of displacements.

In order to obtain the mass matrix of the element, it is possible to proceed in the same way as for the static case and obtain the forces caused by inertial forces distributed on the basic isostatic configuration of the element (i.e. D'Alembert's principle). Therefore,

$$\boldsymbol{\sigma}^*_{XY}(s) = \int_{s}^{B} \boldsymbol{N}(s, \xi)\boldsymbol{f}_{I_{XY}}(\xi)d\xi \tag{4.47}$$

where $\boldsymbol{f}_{I_{XY}}(\xi)$ is the vector of inertia forces in global coordinates in the section of curvilinear coordinate ξ. Relating the inertia forces to the corresponding nodal accelerations, this vector may be rewritten as follows:

$$\boldsymbol{f}_{I_{XY}}(\xi) = \boldsymbol{C}^T \boldsymbol{M}_s \ddot{\boldsymbol{u}}(s) = \boldsymbol{C}^T \boldsymbol{M}_s \boldsymbol{G}(\xi) \begin{bmatrix} \ddot{\boldsymbol{u}}_A \\ \ddot{\boldsymbol{u}}_B \end{bmatrix} \tag{4.48}$$

The vector $\boldsymbol{d}^*$ of displacements in B corresponding only to the deformation of the element itself, produced by the forces $\boldsymbol{\sigma}^*_{XY}$ of equation (4.47), can be expressed as

$$\boldsymbol{d}^* = \int_A^B \boldsymbol{N}^T(s, s_B) \boldsymbol{C}^T \boldsymbol{K}_s^{-1} \boldsymbol{C} \int_s^B \boldsymbol{N}(s, \xi) \boldsymbol{f}_{I_{XY}}(\xi) d\xi \tag{4.49}$$

In equation (4.24), which relates the forces and node displacements, $\boldsymbol{P}^{*0}$ now is the vector of the inertia forces applied to the nodes, or in other words, the product of the mass matrix by the node accelerations. By substituting equations (4.48) and (4.49) in equation (4.24) the following final expression for the mass matrix may be obtained:

$$\boldsymbol{M} = \begin{bmatrix} \boldsymbol{m}_{11} & \boldsymbol{m}_{12} \\ \boldsymbol{m}_{21} & \boldsymbol{m}_{22} \end{bmatrix} \tag{4.50}$$

where

$$\boldsymbol{m}_{22} = \boldsymbol{F}^{-1} \int_A^B \boldsymbol{N}^T(s, s_B) \boldsymbol{C}^T(s) \boldsymbol{K}_s^{-1}(s) \boldsymbol{C}(s) \left(\int_s^B \boldsymbol{N}(s, \xi) \boldsymbol{C}^T(\xi) \boldsymbol{M}_s(\xi) \boldsymbol{C}(\xi) \boldsymbol{F}_s(s) \boldsymbol{F}^{-1} d\xi \right) ds \tag{4.51}$$

$$\begin{aligned} \boldsymbol{m}_{21} = {} & \boldsymbol{F}^{-1} \int_A^B \boldsymbol{N}^T(s, s_B) \boldsymbol{C}^T(s) \boldsymbol{K}_s^{-1}(s) \boldsymbol{C}(s) \\ & \left(\int_s^B \boldsymbol{N}(s, \xi) \boldsymbol{C}^T(\xi) \boldsymbol{M}_s(\xi) \boldsymbol{C}(\xi) \left(\boldsymbol{N}^T(A, \xi) - \boldsymbol{F}_s(\xi) \boldsymbol{F}^{-1} \boldsymbol{N}^T(A, B) \right) d\xi \right) ds \end{aligned} \tag{4.52}$$

$$\boldsymbol{m}_{12} = \boldsymbol{m}_{21}^T = -\boldsymbol{N}(A, B) \boldsymbol{m}_{22} + \int_A^B \boldsymbol{N}^T(s_A, s) \boldsymbol{C}^T(s) \boldsymbol{M}_s(s) \boldsymbol{C}(s) \boldsymbol{F}_s(s) \boldsymbol{F}^{-1} ds \tag{4.53}$$

$$\boldsymbol{m}_{11} = -\boldsymbol{N}(A,B)\boldsymbol{m}_{21} + \int_A^B \boldsymbol{N}^T(s_A,s)\boldsymbol{C}^T(s)\boldsymbol{M}_s(s)\boldsymbol{C}(s)\left(\boldsymbol{N}^T(s_A,s) - \boldsymbol{F}_s(s)\boldsymbol{F}^{-1}\boldsymbol{N}^T(A,B)\right)ds \tag{4.54}$$

Integration along the axis of the element is carried out using a multiple Simpson's rule with variable number of points. Usually is sufficient, in order to obtain the stiffness matrix of any element with curved 3D axis and variable cross section, considering 11 integration points. On the other hand, the computation of the mass matrix includes three integration levels and needs more accurate rules, together with a set of additional integration points (Molins et al. 1998).

4.4 Integration of the equation of motion. The α-generalized scheme.

Dynamic equilibrium at any instant of time t may be expressed by the following equation:

$$\boldsymbol{M}\ddot{\boldsymbol{u}}(t) + \boldsymbol{C}_D\dot{\boldsymbol{u}}(t) + \boldsymbol{K}\boldsymbol{u}(t) = \boldsymbol{F}(t) \tag{4.55}$$

where $\boldsymbol{M}$ is the mass matrix, $\boldsymbol{C}_D$ is the damping matrix, $\boldsymbol{K}$ is the stiffness matrix, $\boldsymbol{F}(t)$ is the vector of applied loads and $\boldsymbol{u}(t)$ is the vector of displacements. The initial value problem consists on finding a function $\boldsymbol{u}(t)$ which satisfies (4.55) and the initial conditions:

$$\begin{aligned} \boldsymbol{u}(0) &= \boldsymbol{u}_0 \\ \dot{\boldsymbol{u}}(0) &= \boldsymbol{v}_0 \end{aligned} \tag{4.56}$$

Several procedures for the integration of the dynamic equation of motion have been proposed to date. It has been long recognized that a proper time integration scheme should present a series of properties (Hilber and Hughes, 1978). A first desirable property is the unconditionally stability of the solution when is applied to linear problems. This characteristic may be achieved by considering implicit algorithms. Second, the method should be second-order accurate. Third, it should possess algorithmic damping. In

particular, it is desirable to have controllable numerical dissipation over the higher frequency modes (to avoid spurious, non physical oscillations caused by the spatial discretization due to excitation of spatially unresolved modes). In addition, it has been observed that using high-frequency dissipation schemes may improve the convergence of equation solvers in the case of highly non linear problems.

A basic difficulty in designing these kinds of algorithms is to reach equilibrium between addition of high-frequency dissipation without introducing excessive algorithmic damping over the important low frequency modes. For example, the method proposed by Newmark (1959) presents high-frequency dissipation, but is only first-order accurate and is too dissipative in the low-frequency domain. Several dissipative integration schemes have been developed with high-frequency dissipation properties, without excessive dissipation in the low-frequency range and maintaining the second order accuracy, such is the case of those proposed by Wilson (1968), Hilber et al. (1977), Wood et al. (1981), Bazzi and Anderheggen (1982), Hoff and Pahl (1988) and Chung and Hulbert (1993). This last integration scheme, the so called Generalized-α algorithm, has been selected to be implemented in this work, due to its optimal combination of high-frequency dissipation and low-frequency dissipation. Moreover, its second-order accuracy and stability properties have been proved even in the non-linear case (Erlicher et al., 2002)

Let $0 = t_0 < t_1 < \ldots t_i < t_{i+1} \ldots < t_n = t_f$ be a partition of the time domain, where n is the number of time steps with a constant step size Δt. The generalized-α method by Chung and Hulbert (1993) is based on the temporal approximation of velocities and accelerations proposed by Newmark (1959):

$$\ddot{\boldsymbol{u}}_{i+1} = \frac{1}{\beta \Delta t^2}\left(\boldsymbol{u}_{i+1} - \boldsymbol{u}_i\right) - \frac{1}{\beta \Delta t}\dot{\boldsymbol{u}}_i - \left(\frac{1}{2\beta} - 1\right)\ddot{\boldsymbol{u}}_i \tag{4.57}$$

$$\dot{\boldsymbol{u}}_{i+1} = \frac{\gamma}{\beta \Delta t}\left(\boldsymbol{u}_{i+1} - \boldsymbol{u}_i\right) + \left(1 - \frac{\gamma}{\beta}\right)\dot{\boldsymbol{u}}_i + \left(1 - \frac{\gamma}{2\beta}\right)\Delta t \ddot{\boldsymbol{u}}_i \tag{4.58}$$

where $\ddot{\boldsymbol{u}}_i$, $\ddot{\boldsymbol{u}}_{i+1}$, $\dot{\boldsymbol{u}}_i$, $\dot{\boldsymbol{u}}_{i+1}$, $\boldsymbol{u}_i$ and $\boldsymbol{u}_{i+1}$ are the numerical accelerations, velocities and displacement at time t_i and t_{i+1} respectively and β and γ are the original parameters of the Newmark's method.

The generalized-α method applied to equations (4.55) and (4.56) produces the following equilibrium equation

$$\boldsymbol{M}\ddot{\boldsymbol{u}}_{i+1-\alpha_m} + \boldsymbol{C}_D\dot{\boldsymbol{u}}_{i+1-\alpha_f} + \boldsymbol{K}\boldsymbol{u}_{i+1-\alpha_f} = \boldsymbol{F}_{i+1-\alpha_f} \tag{4.59}$$

where the dynamic equilibrium is computed at some instant inside Δt. The time discrete combinations of displacements, velocities, accelerations and times are

$$\begin{aligned}
\ddot{\boldsymbol{u}}_{i+1-\alpha_m} &= (1-\alpha_m)\ddot{\boldsymbol{u}}_{i+1} + \alpha_m\ddot{\boldsymbol{u}}_i \\
\dot{\boldsymbol{u}}_{i+1-\alpha_f} &= (1-\alpha_f)\dot{\boldsymbol{u}}_{i+1} + \alpha_f\dot{\boldsymbol{u}}_i \\
\boldsymbol{u}_{i+1-\alpha_f} &= (1-\alpha_f)\boldsymbol{u}_{i+1} + \alpha_f\boldsymbol{u}_i
\end{aligned} \tag{4.60}$$

Where α_f and α_m are the algorithmic parameters introduced by Chung and Hulbert (1993).

The term $\boldsymbol{F}_{i+1-\alpha_f} = \boldsymbol{F}(\alpha_f, t_i, t_{i+1})$ is usually approximated by means of

$$\boldsymbol{F}_{i+1-\alpha_f} = (1-\alpha_f)\boldsymbol{F}_{i+1} + \alpha_f\boldsymbol{F}_i \tag{4.61}$$

In the non-linear case the equation (4.59) is written as

$$\boldsymbol{M}\ddot{\boldsymbol{u}}_{i+1-\alpha_m} + \boldsymbol{C}\dot{\boldsymbol{u}}_{i+1-\alpha_f} + \boldsymbol{r}_{i+1-\alpha_f} = \boldsymbol{F}_{i+1-\alpha_f} \tag{4.62}$$

where the term $\boldsymbol{r}_{i+1-\alpha_f} = \boldsymbol{r}\left(\alpha_f, \boldsymbol{u}_i, \boldsymbol{u}_{i+1}\right)$ is the vector of non-linear internal forces. Several quadrature rules can be employed to the evaluation of the vector of internal forces. As a matter of simplicity only the generalized trapezoidal rule is considered herein, which may be written as:

$$\boldsymbol{r}_{i+1-\alpha_f} = \left(1-\alpha_f\right)\boldsymbol{r}_{i+1} + \alpha_f \boldsymbol{r}_i \tag{4.63}$$

where the terms $\boldsymbol{r}_{i+1}$ and $\boldsymbol{r}_i$ are obtained from the direct integration of the sectional forces (see section 4.2)

The implementation of the method in the framework of the GMF for the non-linear case is carried out through a Newton-Raphson procedure. By combining equations (4.60), (4.62) and (4.63) the Newton-Raphson method for the iteration k can be expressed as

$$\Delta\boldsymbol{u}_{i+1}^{(k+1)}\left(\boldsymbol{r}_{i+1}^{(k)}, \dot{\boldsymbol{u}}_{i+1}^{(k)}, \ddot{\boldsymbol{u}}_{i+1}^{(k)}\right) = \left(\boldsymbol{K}_{i+1}^{eff\,(k)}\right)^{-1}\boldsymbol{R}_{i+1}^{(k)} \tag{4.64}$$

where $\Delta\boldsymbol{u}_{i+1}^{(k+1)}$ is the vector of displacement increment, $\boldsymbol{R}_{i+1}^{(k)}$ is the vector of residual forces and the matrix $\boldsymbol{K}_{i+1}^{eff\,(k)}$ is the effective stiffness matrix, which takes into account inertial and viscous damping effects and the tangent stiffness matrix of the structure $\boldsymbol{K}_{i+1}^{(k)}$ as follows:

$$\boldsymbol{K}_{i+1}^{eff\,(K)} = \frac{1-\alpha_m}{\left(1-\alpha_f\right)\beta\Delta t^2}\boldsymbol{M} + \gamma\frac{1-\alpha_m}{\left(1-\alpha_f\right)\beta\Delta t}\boldsymbol{C}_D + \boldsymbol{K}_{i+1}^{(k)} \tag{4.65}$$

and the vector of residual forces of the iteration k is calculated as:

$$\boldsymbol{R}_{i+1}^{(k)} = \boldsymbol{F}_{i+1} + \frac{\alpha_f}{1-\alpha_f}\boldsymbol{F}_i - \frac{1-\alpha_m}{1-\alpha_f}\boldsymbol{M}\ddot{\boldsymbol{u}}_{i+1}^{(k)} - \frac{\alpha_m}{1-\alpha_f}\boldsymbol{M}\ddot{\boldsymbol{u}}_i - \boldsymbol{C}_D\dot{\boldsymbol{u}}_{i+1}^{(k)} - \frac{\alpha_f}{1-\alpha_f}\boldsymbol{C}_D\dot{\boldsymbol{u}}_i - \boldsymbol{r}_{i+1}^{(k)} - \frac{\alpha_f}{1-\alpha_f}\boldsymbol{r}_i \tag{4.66}$$

Once the incremental displacement vector is evaluated by means of (4.64) and the total displacements are actualized through

$$\boldsymbol{u}_{i+1}^{(k+1)} = \boldsymbol{u}_{i+1}^{(k)} + \Delta\boldsymbol{u}_{i+1}^{(k+1)} \tag{4.67}$$

then the velocities and accelerations can be actualized by means of

$$\dot{\boldsymbol{u}}_{i+1}^{(k+1)} = \frac{\gamma}{\beta\Delta t}\left(\boldsymbol{u}_{i+1}^{(k+1)} - \boldsymbol{u}_i\right) + \left(1 - \frac{\gamma}{\beta}\right)\dot{\boldsymbol{u}}_i + \left(1 - \frac{\gamma}{2\beta}\right)\Delta t\ddot{\boldsymbol{u}}_i \tag{4.68}$$

$$\ddot{\boldsymbol{u}}_{i+1}^{(k+1)} = \frac{1}{\beta\Delta t^2}\left(\boldsymbol{u}_{i+1}^{(k+1)} - \boldsymbol{u}_i\right) - \frac{1}{\beta\Delta t}\dot{\boldsymbol{u}}_i - \left(\frac{1}{2\beta} - 1\right)\ddot{\boldsymbol{u}}_i \tag{4.69}$$

and the process continue until the convergence criteria is reached. It should be noted that two iteration levels, at the global and at the element level are used, as was explained in section 4.2. In the global level, a convergence criterion in forces has been used, while in the element level, a convergence criterion in sectional forces has been used, as in Molins (1996). Fig. 4.4 shows the flow chart of the implemented time step procedure into the computer program CRIPTA developed by Molins (1996), based on the Generalized Matrix Formulation.

The application of the adopted time integration scheme requires an adequate selection of the parameters for each particular case, in order to obtain desired levels of stability (including unconditional stability), accuracy and optimal dissipation. Table 4.1 reproduces the recommended values for the generalized-α method provided by Erlicher et al. (2002) in order to account for this three aspects. The last row provides the numerical limits for each one of the variables.

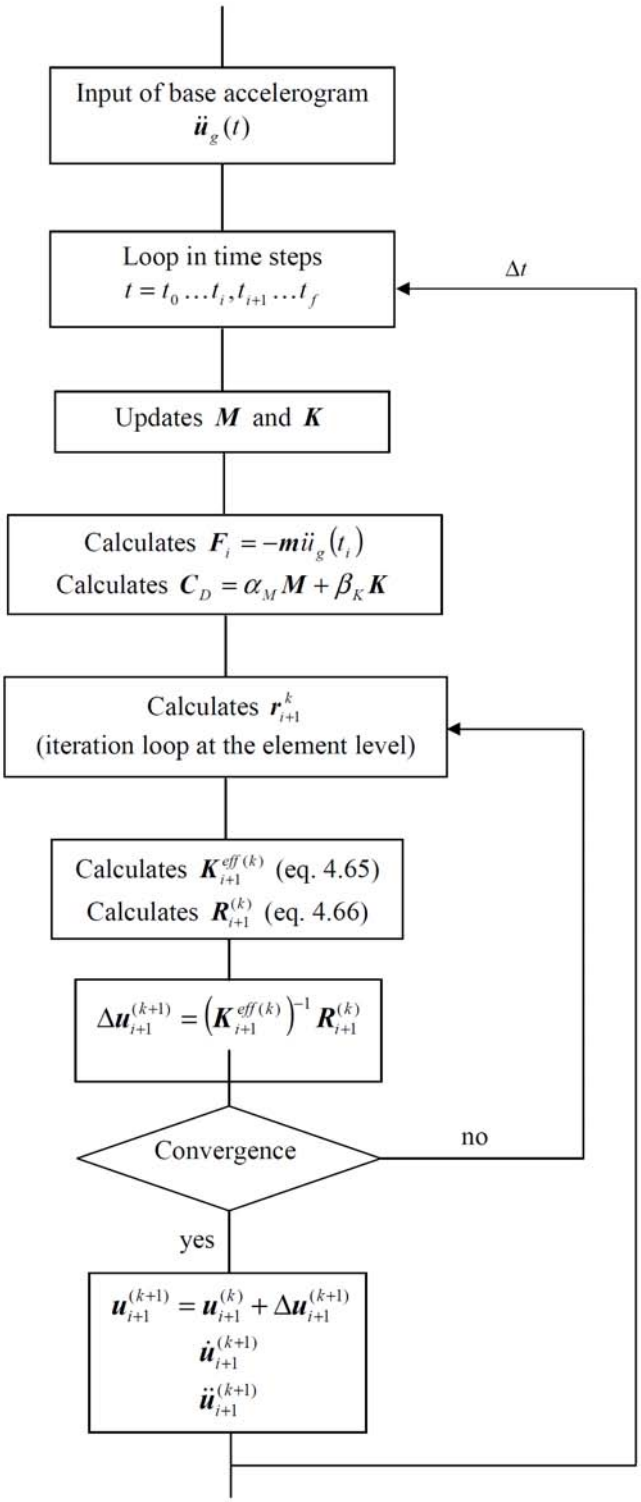

Figure 4.4 – Flow chart of the implemented time integration scheme for the non linear case.

	α_m	α_f	β	γ
Stability	$\frac{1}{2}-(\gamma-\alpha_f)$ $\leq \alpha_m \leq \frac{1}{2}$	$\leq \frac{1}{2}$	$\geq \frac{\gamma}{2}$	$\geq \frac{1}{2}$
Stability and optimal dissipation	$\frac{1}{2}-(\gamma-\alpha_f)$ $\leq \alpha_m \leq \frac{1}{2}$	$\leq \frac{1}{2}$	$\frac{1}{4}\left(\gamma+\frac{1}{2}\right)^2$	$\geq \frac{1}{2}$
Stability and second order accuracy	$\leq \alpha_f$	$\leq \frac{1}{2}$	$\geq \frac{1}{4}+\frac{1}{2}(\alpha_f-\alpha_m)$	$\frac{1}{2}+\alpha_f-\alpha_m$
Stability, optimal dissipation and second order accuracy	$\leq \alpha_f$	$\leq \frac{1}{2}$	$\frac{1}{4}(1+\alpha_f-\alpha_m)^2$	$\frac{1}{2}+\alpha_f-\alpha_m$
Numerical limits	$\left[-1,\frac{1}{2}\right]$	$\left[0,\frac{1}{2}\right]$	$\left[\frac{1}{4},1\right]$	$\left[\frac{1}{2},\frac{3}{2}\right]$

Table 4.1 – Algorithmic parameters of the generalized-α method (Erlicher et al., 2002)

4.5 Constitutive model for reinforcing steel.

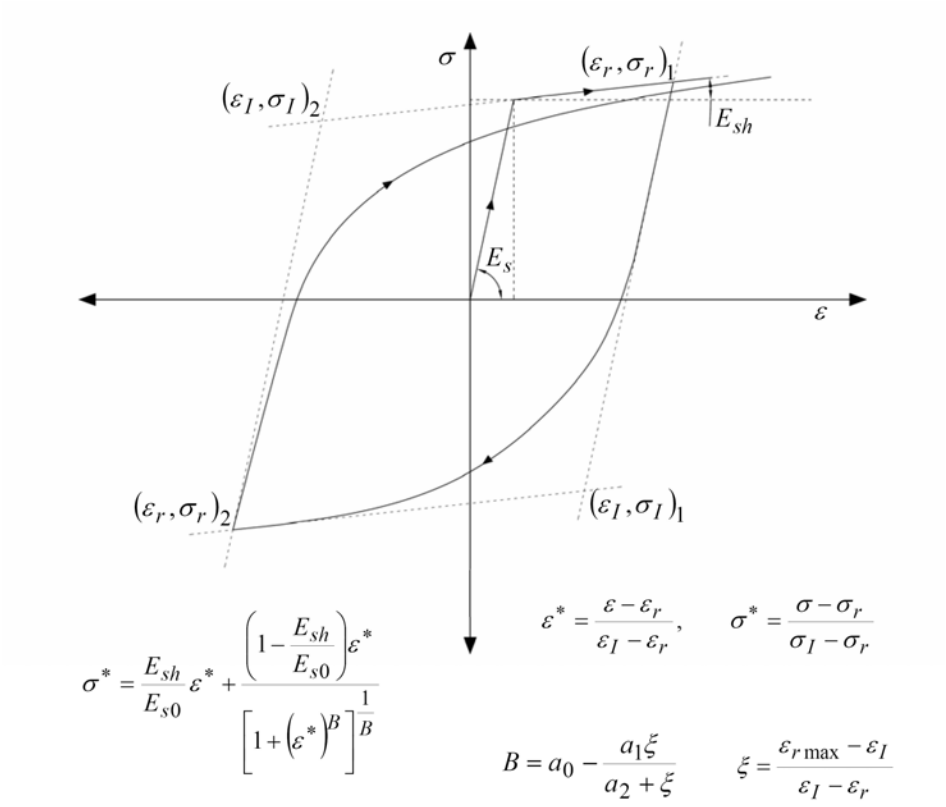

Figure 4.5 – Menegotto-Pinto model for reinforcing steel

In the particular case of reinforced concrete elements, the inclusion of reinforcing bars was implemented. Each one of the reinforcing bars is considered as a point for the sectional integration of each one of the functions. The non linear behavior of the steel reinforcement is simulated through the well known model proposed by Menegotto and Pinto (1973) modified as Filippou et al. (1983) to include strain hardening. The advantage of using this formulation stems from the fact that it is expressed through an explicit algebraic equation for stress as a function of strains, which is in accordance with the form of equation (4.9). At this point, some hypothesis are introduced: (1) the monotonic envelope is considered as

bilinear with strain hardening, (2) perfect bond between reinforcing steel and concrete is assumed, (3) strain-rate effects are not considered, and (4) the model does not take into account buckling of reinforcing bars. The governing equation of the Menegotto-Pinto model characterizes a curved transition from a straight line asymptote with a slope E_{s0} to another asymptote with a slope E_{sh}, the elastic and the hardening modulus of steel respectively (Fig. 4.5). In this equation, ε_I and σ_I are the strain and stress at the intersection of the asymptotes, ε_r and σ_r are the strain and stress at the point where load reversal occurs, and B is a parameter which influences the shape of the transition curve and permits the modelization of the Bauschinger effect. The terms a_0, a_1 and a_2 are parameters which allows adjusting the Bauschinger effect observed on experimental results.

4.6 Final comments on the numerical implementation.

Integration along the axis of the elements is carried out through a multiple Simpson's rule with variable number of uniformly distributed points. As was commented before, eleven integration points are usually sufficient to obtain the stiffness and mass matrices of the element. However in some cases, it is necessary to increase the number of integration points in order to obtain accurate results, depending on the cracking pattern and complexity of the structure.

In the sectional level, the transversal section of the element is defined by a combination of trapezoids determined by the coordinates of their vertices. These trapezoids are normalized as squares through a coordinate transformation which may be expressed using two-dimensional linear functions. The integration of any function over the cross section is obtained by adding the contribution of each one of the trapezoids. The integration within a trapezoid is performed by means of a two-dimensional Simpson's rule with 25 points for each one of the trapezoids. Detailed information regarding these numerical features may be found in Molins (1996).

Chapter 5

Application examples

The capabilities of the proposed model are shown through its application in three different examples of reinforced concrete framed structures and masonry structures. In the first example, the model is applied to the analysis of a rectangular column subjected to a constant axial load and a transversal cyclic load at the center of the span (Atalay and Penzien 1975). The aim of this first example is to test the capabilities of the proposed formulation to reproduce the energy dissipation mechanisms on reinforced concrete member subjected to cyclic loadings and it is focused on the deformational response rather than a comprehensive comparison. In the second example, the proposed model is tested against existing experimental results on a two-storey reinforced concrete frame subjected to seismic loadings (Carydis 1997). A comprehensive comparison is addressed in terms of the dynamic response of the structure. The third example deals with the dynamic response of a three story scaled masonry building subjected to a seismic excitation (Tomazevic and Weiss, 1994), modeled through an equivalent frame scheme. In all cases, the results obtained show a satisfactory agreement with the experimental results.

5.1 Reinforced concrete examples

5.1.1 Reinforced concrete column subjected to transversal cyclic loading

In the present example, the specimen 1S1 from the experiments by Atalay and Penzien (1976) has been modeled. The test consists of a rectangular 3352 mm long simply supported RC column (305 mm x 305 mm reinforced with four 22 mm diameter bars) subjected to a constant axial load of P=267 KN, following by the application of a transversal cyclic load H at the center of the span. Fig. 5.1 shows the transversal load history applied. The behavior is controlled by the bending moments (i.e. span to depth ratio = 11) and the hysteretic behavior is strongly influenced by the application of the axial force.

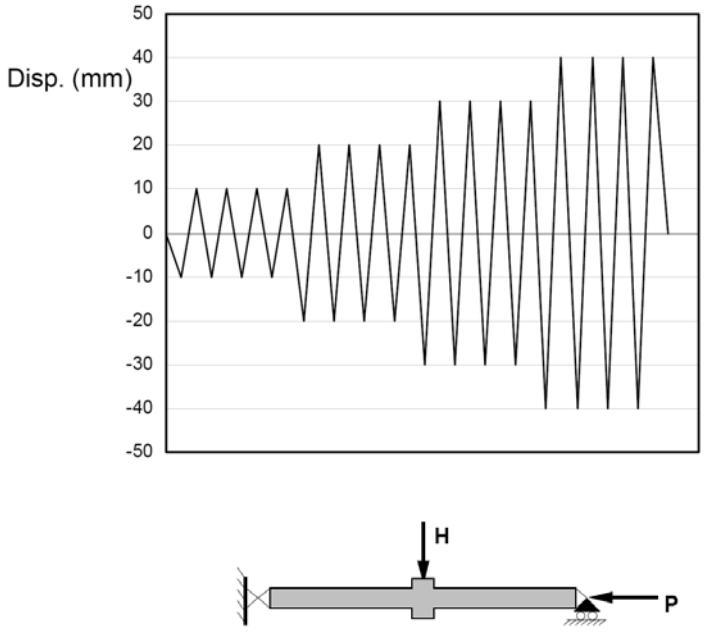

Figure 5.1 – Transversal cyclic load history and test layout by Atalay and Penzien (1975)

Considering the symmetry of the geometry, only one half of the column has been modeled by means of a cantilevered beam element with 27 integration sections along the longitudinal axis. The transversal section has been divided into 10 layers. The material

properties reported in the referred work were: $f'_c = 29.1\ MPa$, $E_s = 200000\ MPa$ and $f_y = 363\ MPa$. The basic properties and model parameters assumed for the concrete were: $E_c = 32000\ MPa$, $f'_{ct} = 2.84\ MPa$ (Eurocode 2, 2004) and $G_f = 250\ {}^{J}/_{m^2}$. Note that the value of the fracture energy assumed is higher than the typical value recommended for concrete material (Oh, 1992; CEB-FIP Model Code, 1990) in the range 80 to 130 J/m^2, depending on the maximum aggregate size and tensile strength. This increased value has been considered after some numerical testing in order to account for the tension stiffening effect.

For the steel reinforcement, the following material properties have been considered: $E_{sh} = 0.0015\,E_s$, $a_0 = 20.0$, $a_1 = 18.5$, and $a_2 = 0.15$ which are typical values adopted for the Menegotto-Pinto model.

The cyclic loading history following the scheme shown on Fig. 5.1 was applied monotonically to the model in a displacement controlled manner. Obtained results for the load-deflection relationship for the experimental test and the proposed model are shown in Fig. 5.2. The model results show a good agreement with the results obtained experimentally, except in the initial stages of the response, where the model shows a linear elastic behavior. The pinching effect produced by the interaction of flexure cracks due to bending moment and axial load is predicted satisfactorily. This effect has a significant influence in the accurately prediction of the energy dissipated by the column.

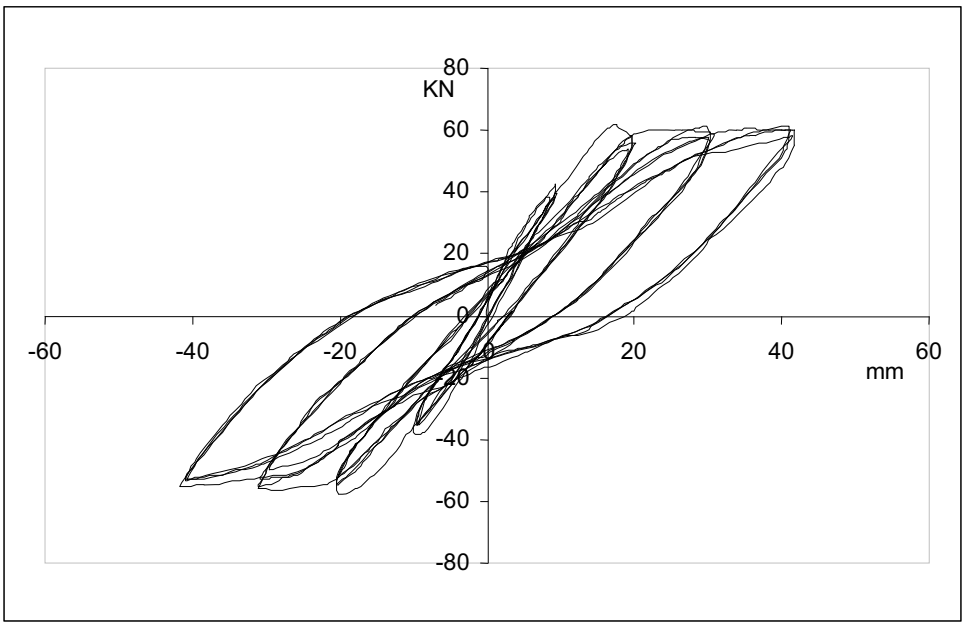

a)

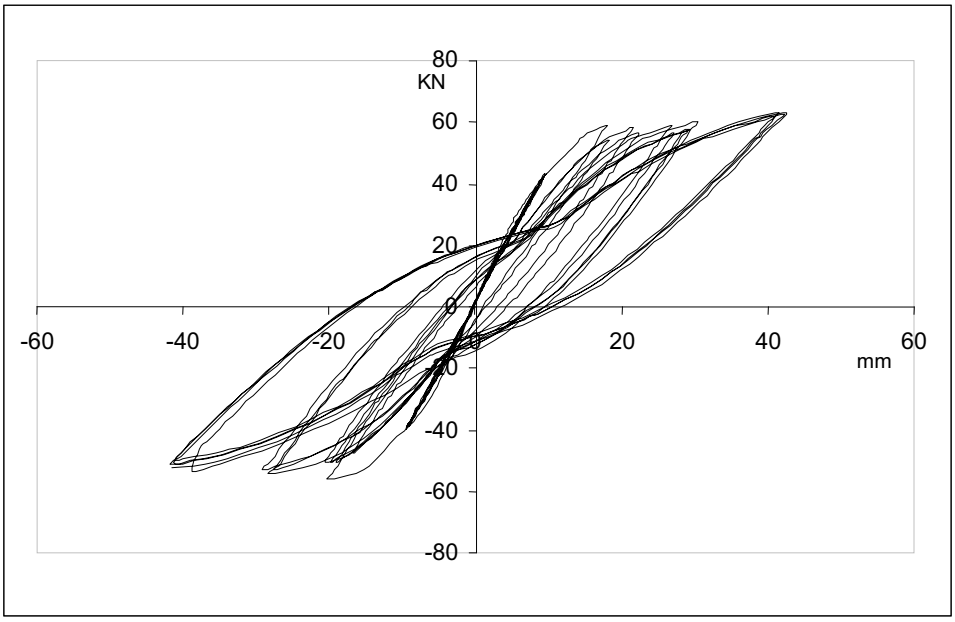

b)

Figure 5.2 – Load-deflection relationship specimen 1S1 (Atalay and Penzien, 1975)
a) Experimental results b) Model results.

5.1.2 Two-storey reinforced concrete frame under seismic loading

This application concerns the numerical simulation of the seismic behavior of a two-storey reinforced concrete frame, experimentally tested on a shaking table at the Laboratory of the National Technical University of Athens (Carydis, 1997). The specimen selected herein is the one named L30 in the test report. This specimen was designed according to Eurocode 2 (2004) and Eurocode 8 (2004) and corresponds to a ductility class low (DCL) structure with a behavioral factor $q = 2.5$ and a design intensity of $a_g = 0.30g$. Fig. 5.3 shows the overall geometry of the structure and the distribution of the reinforcement. The nominal uniaxial compressive strength of the concrete reported was 50 MPa, while the steel reinforcement showed a yield strength limit of 500 MPa.

Additional masses were fixed on the slabs in order to account for (1) a larger "tributary" area of the slab in the prototype as compared to the slab area actually included in the specimen, (2) simulation of the "non structural" masses in the prototype (i.e. partitions and finishes plus live loads) and (3) similitude between prototype and scale model. Table 5.1 shows the mass arrangement in the structure.

	Self mass	Additional Mass	Total
2nd Floor	1270	4000	5270
1st Floor	1410	4520	5930
Total	2680	8520	11200

Table 5.1 – Mass arrangement of the specimen (Kg)

The frame was subjected to three earthquake simulations in sequence, where a single direction of base motion was modeled with an artificial sine-like acceleration record along the plane of the frame. Random vibration tests were performed as complementary testing before each earthquake simulation in order to identify the natural frequencies and damping factors. The frequencies of the input motion were adjusted based on the measured natural frequency of the test structure to achieve a resonant response. The peak table acceleration

during the first test was equal to the design acceleration ($a_g = 0.30g$), while in the subsequent tests the peak table acceleration was two times the design acceleration.

The numerical modeling of the structure can be observed in Fig. 5.4. The tested frame was modeled by 22 GMF elements. Each column was shaped by 3 elements, while the beams were defined by 5 elements. The structure has been considered initially completely fixed at the base of the columns (the foundation slab has not been considered in the analysis).

A typical Rayleigh damping matrix has been adopted for the analysis, where a constant damping of 2% for the first two modes has been aimed. This value has been selected after some numerical tests in order to consider all the energy dissipation mechanisms not included in the proposed model (bond-slip deterioration, for example). The material properties reported for the concrete and steel were: $f'_c = 50.0\ MPa$, $E_c = 31000\ MPa$, $E_S = 201000\ MPa$ and $f_y = 450\ MPa$. The model parameters adopted for the concrete were the following: $f'_{ct} = 4.1\ MPa$ (Eurocode 2, 2004), $G_f = 300\ {}^{J}\!/_{m^2}$. As in the previous example, an increased value of the fracture energy has been considered in order to take into consideration the tension stiffening effects. For the steel reinforcement the following model parameters has been considered: $E_{sh} = 0.0025 E_S$, $a_1 = 18.5$, $a_2 = 0.15$ and $a_0 = 20.0$ which are typical values adopted for the Menegotto-Pinto model.

The time history analysis has been performed considering a time step of $\Delta t = 0.02\ s$ and parameters for the generalized-α method $\alpha_m = -0.1$, $\alpha_f = 0.1$, $\beta = 0.308$ and $\gamma = 0.61$. The selection of these values started by taken into consideration the values recommended by Erlicher et al. (2002) and reproduced in chapter 4, with minor modifications for this particular case, in order to obtain an adequate combination of accuracy, stability and dissipation over higher modes.

No influence of non linear deformation due to shear or torsion was expected, so the shear and torsional sectional relationships have been maintained as linear elastic.

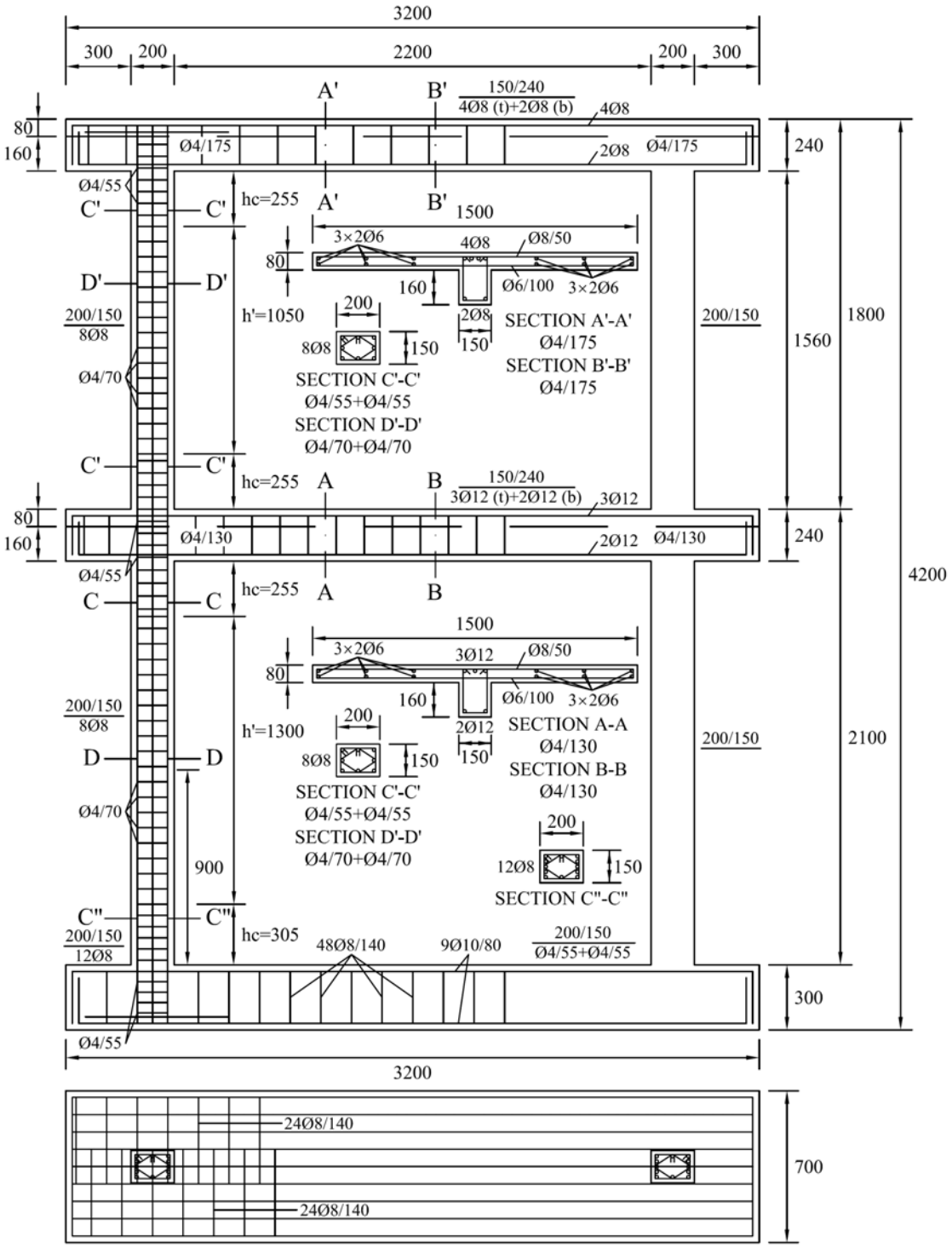

Figure 5.3 – Geometry and reinforcement detailing of the tested frame (Carydis, 1997).

Eigenvalue analysis of the structure was performed in order to identify the natural frequencies of the model, before the test. The analysis showed frequencies for the first two modes of 4.41 Hz and 13.76 Hz. Similar results for the initial natural frequencies have been obtained by Spiliopoulos and Lykidis (2005) with a three dimensional solid finite element model. The obtained initial natural frequencies are higher than those obtained by means of random vibration tests by Carydis (1997): 3.05 and 9.80 Hz. This result is expected to be produced mainly by the difference between the real connection of the base slab with the shaking table and the assumed ideal model support conditions. A new eigenvalue analysis has been performed considering both rotational and translational springs at the base of the columns. The spring constants were adjusted until the first two natural frequencies of 3.05 and 9.80 Hz were achieved. These frequencies have been reached with spring constants of 23,300 KNm/rad and 59,100 KN/m, for the rotational and the translational springs respectively. Table 5.2 summarizes the natural frequencies obtained before each test by means of eigenvalue analysis and those obtained experimentally by Carydis (1997).

As an indicator of the damage experienced by the structure during testing, the natural frequencies decrease as the intensity of the input motion increases. The decrease in the first mode frequency between test 1 and test 3 is 49% for the experimental results and 47% for the model results, while the second natural frequency decreases 43% for the experimental results and 34% for the model one. These differences in the second natural frequencies are mainly produced by the shear deterioration, which has not been considered in the model.

	First Mode Freq. (Hz)		Second Mode Freq. (Hz)	
	Experimental	Model	Experimental	Model
Test 1	3.05	3.05	9.80	9.80
Test 2	2.27	2.74	7.00	9.38
Test 3	1.55	1.61	5.54	6.43

Table 5.2 – Natural frequencies measured by Carydis (1997) and obtained by means of eigenvalue analysis

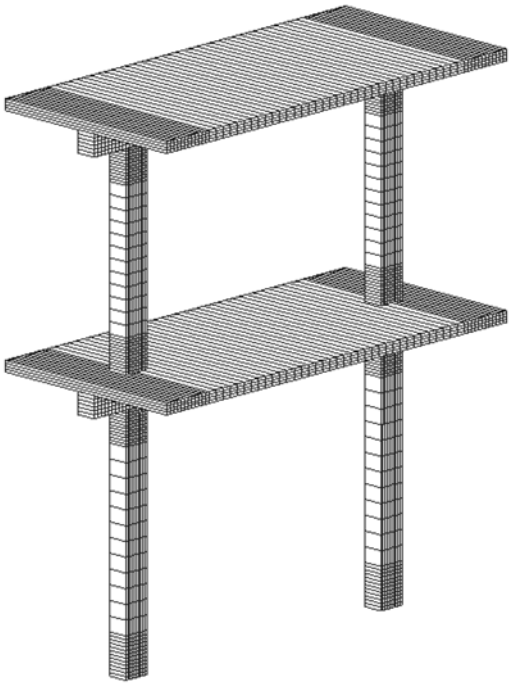

Figure 5.4 – Frame model overview

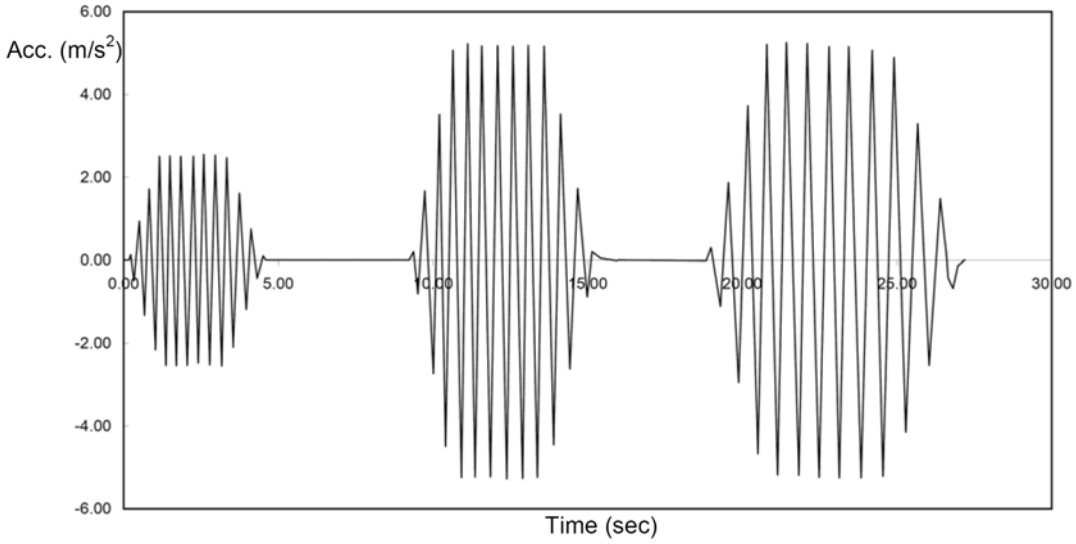

Figure 5.5 – Input base acceleration of shaking table for TEST 1, TEST 2 and TEST 3

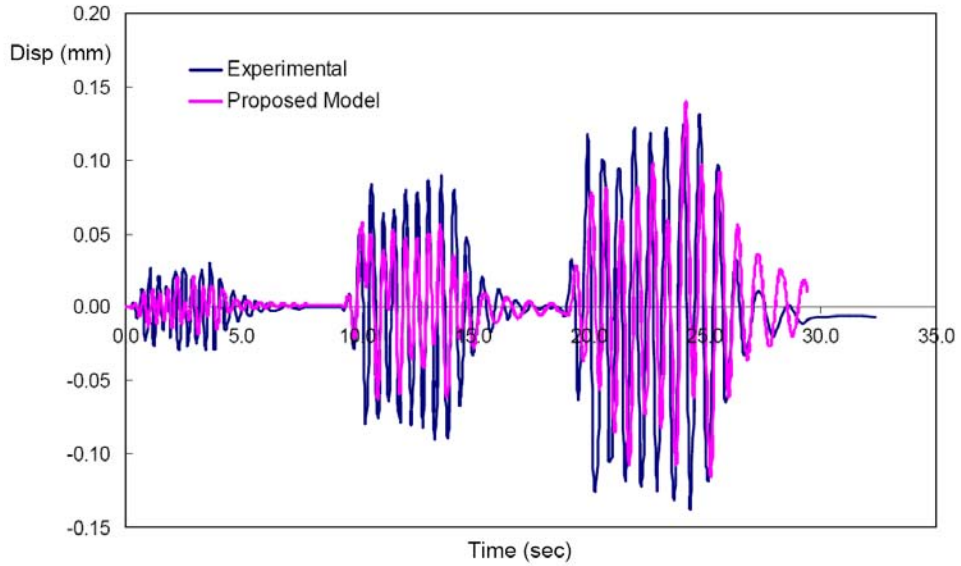

Figure 5.6 – Second floor response under base motion TEST 1, TEST 2 and TEST 3

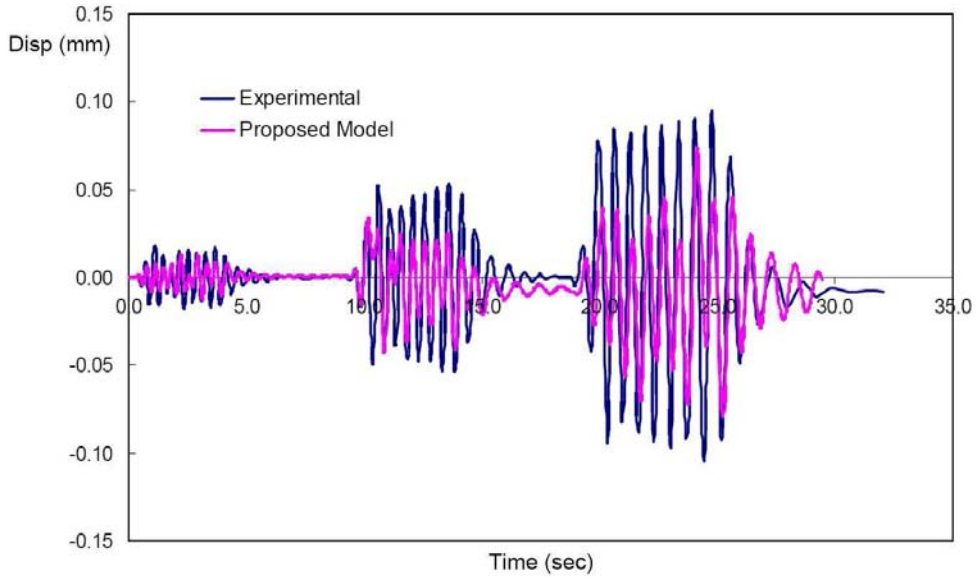

Figure 5.7 – First floor response under base motion TEST 1, TEST 2 and TEST 3

Fig. 5.5 shows the input base acceleration for the tests. The time history displacement responses obtained through the application of the proposed model are shown in Fig. 5.6 and Fig. 5.7 for the second and the first floor respectively and compared with the experimental

ones. The obtained results show a good agreement with the experimental ones. The difference between maximum computed displacements at the second level in the model and in the experiment were around 6%.

Fig. 5.8 shows the crack pattern obtained during the experiment after the third test. Considerable cracks may be observed in the first story columns, second story columns and beam column connections. Spalling of cover concrete and crushing can be observed in the first story columns. The experiment report also describes buckling and fracture of reinforcement bars at the base of the first story columns. Fig. 5.9 and 5.10 show the compressive damage and the tensile damage contour obtained by the model after the third test. It can be observed that the tensile damage concentration (dark red colored areas) coincides with the location of experimental cracking. In the same way, the compressive damage concentrates at the bottom of the columns, where crushing and spalling of concrete was found after the experiment (dark areas in Fig. 5.8). Yielding of several reinforcing bars has been also attained at the base of the first story column.

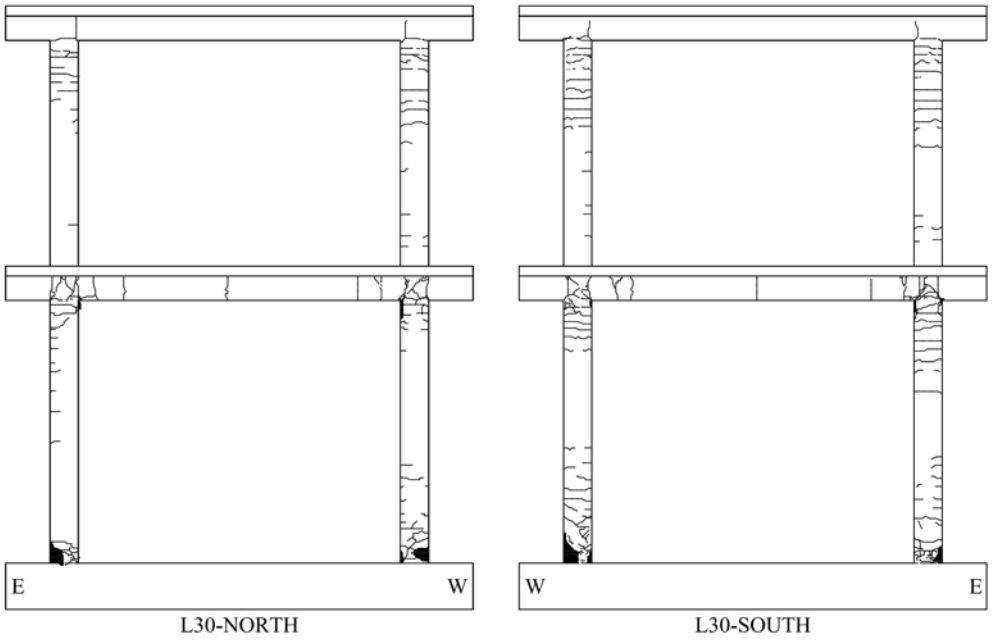

Figure 5.8 – Crack pattern of the tested frame (Carydis, 1997)

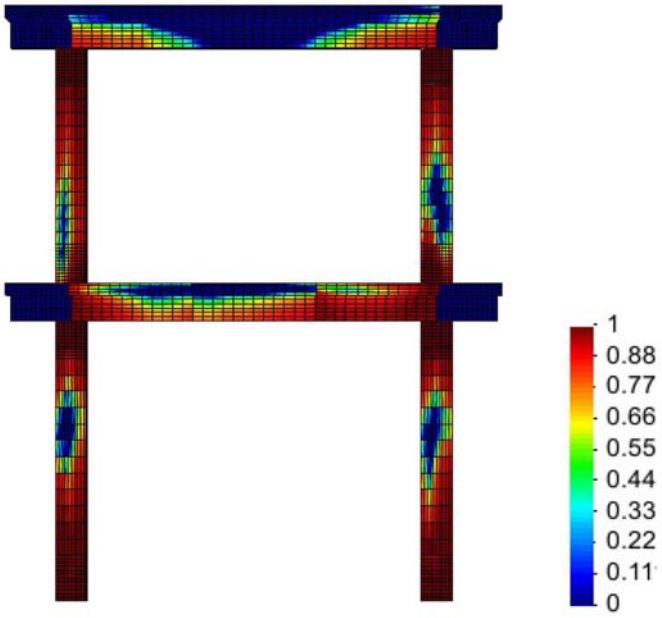

Figure 5.9 – Tensile damage δ^{+} distribution obtained after test 3

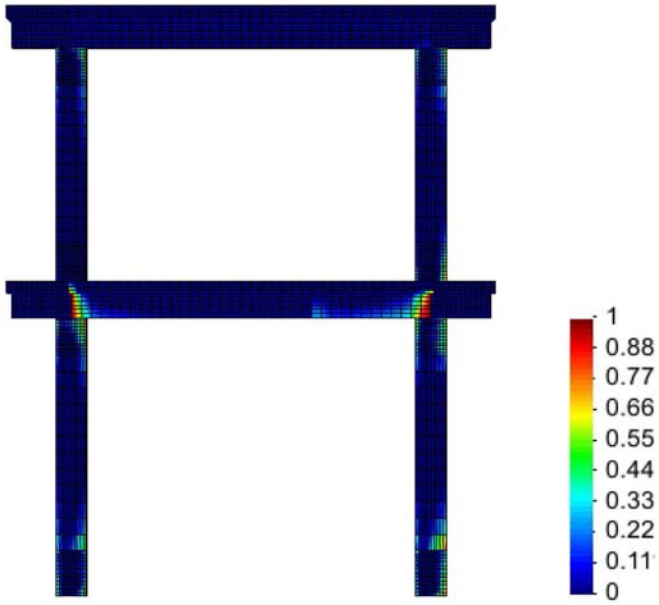

Figure 5.10 – Compressive damage δ^{-} distribution obtained after test 3

5.2 Masonry case study

5.2.1 Three-storey masonry building under seismic loading

The example presented concerns the numerical simulation of a three storey 1:5 scale plain masonry building subjected to a simulated ground motion, experimentally tested at the Institute for Testing and Research in Materials and Structures in Ljubljana, Slovenia by Tomazevic and Weiss (1994).

Fig. 5.11 describes the main characteristics of the experimental model and test. In order to meet the requirements of similitude in mass distribution and vertical stresses in the load bearing walls, concrete blocks were fixed to the floor slabs (300 Kg mass at each floor level) and additional vertical stresses at the load bearing walls were introduced by means of prestressed steel ropes at every corner of the model, each providing a force of 12 KN, fixed to the top slab and anchored into the foundation.

The structure was subjected to a series of ground shaking simulations corresponding to the north-south component of the earthquake acceleration record of the Montenegro earthquake of 1979, with a peak ground acceleration of 0.43 g. The intensity of the shaking was controlled by adjusting the maximum amplitude of the shaking table displacement. The latter was obtained by numerical integration of the earthquake accelerogram scaled according to the laws of similitude.

The test identified as R47 has been modeled herein in order to assess the capability of the proposed model. The shaking table motion, in this case, presents a maximum acceleration of 1.10 g and the duration of the test was 5.5 seconds. The input ground acceleration is shown in Fig. 5.12.

In order to apply the method presented, a structural model was developed consisting of an equivalent system of beam elements to model the entire system. To model the walls, a

series of vertical elements divided longitudinally into 13 integration sections were used. At the sectional level, the number of trapezoidal sub-divisions used varied for each element, a higher number of sub divisions being included where high stress concentration was expected (Fig. 5.13).

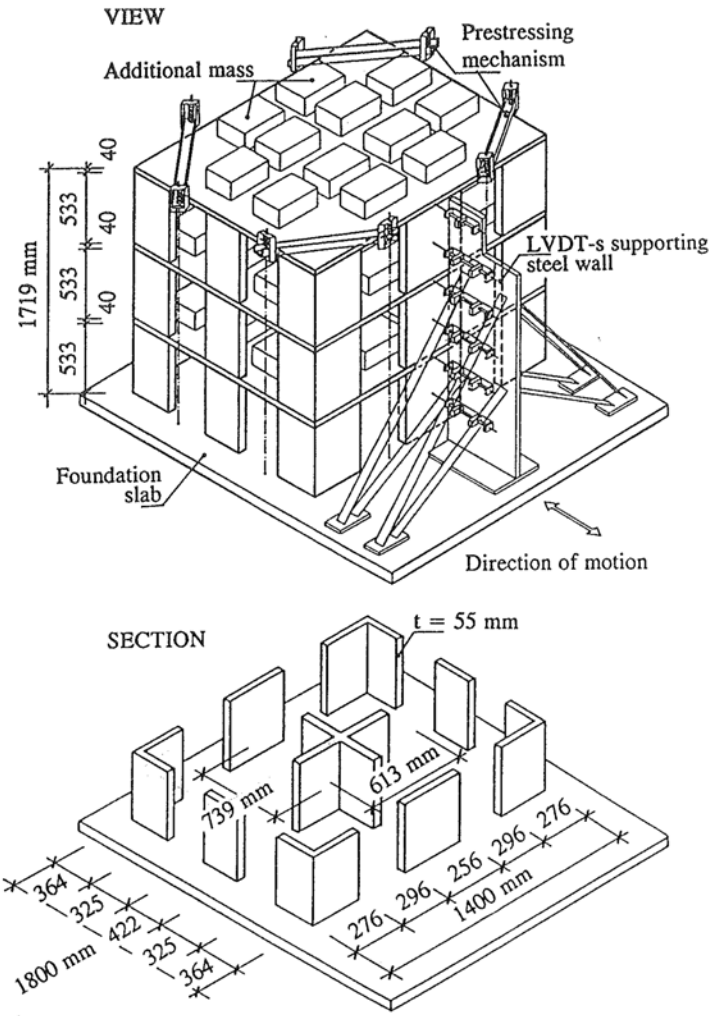

Figure 5.11 – Test set up (Tomazevic and Weiss, 1994)

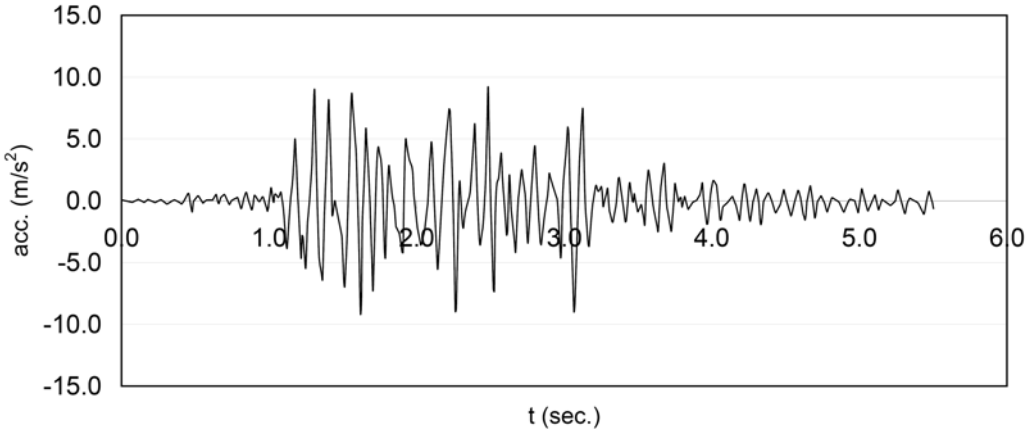

Figure 5.12 – Input ground accelerogram

The mechanical properties of the masonry reported by Tomazevic and Weiss (1994) are compressive strength $f_c = 6.33\ MPa$, tensile strength $f_t = 0.40\ MPa$ and modulus of elasticity $E = 6450\ MPa$. The concrete slab presented a medium compressive strength of $f_c = 25\ MPa$. Details of reinforcement for the slab were not provided in the original paper. The following additional material properties were assumed for the masonry walls: shear modulus $G = 1400\ MPa$ and fracture energy $G_f = 120$ J/m^2. The value of the shear modulus assumed is based on the results obtained by Tomazevic (1999) which show that the shear modulus of masonry obtained in experimental results is lower (from 6 to 25% of the modulus of elasticity) than the recommended value in Eurocode 6 (2005) of 40% of E. The value assumed herein for the fracture energy is in agreement with the values obtained experimentally (Rots, 1997). The concrete slabs were also modeled by means of a series of linear elements and the material was assumed linear elastic with a modulus of elasticity $E = 31500\ MPa$.

The shear behavior is considered as linear elastic and interaction between normal and shear responses is considered through the use of a Mohr-Coulomb criterion as strength envelope. The non linear shear behavior is modeled by considering that the different portions of the section in tension, collaborate in shear depending on the level of tensile damage accumulated (i.e. tensile damage equal 0 means that the portion collaborates in the shear

response, tensile damage equal 1 means that this portion doesn't collaborates in the shear response) with a linear interpolation between the two extreme values.

As reported by Tomazevic and Weiss (1994), the response of the building is governed by the first mode of vibration. It's important that the model could match the governing natural frequencies at the beginning of the simulation. An eigenvalue analysis was performed before the test simulation yielding a first natural frequency of 13.84 Hz, which is very similar to the value obtained experimentally (13.81 Hz), therefore, no additional measures need to be taken to adjust the initial behavior of the model.

The time history analysis has been performed considering a time step of $\Delta t = 0.006\ s$ and parameters for the generalized-α method $\alpha_m = -0.05$, $\alpha_f = 0.1$, $\beta = 0.33$ and $\gamma = 0.65$. The selection of these values has been made by taken into consideration the values recommended by Erlicher et al. (2002) and reproduced in chapter 4, in order to obtain an adequate combination of accuracy, stability and dissipation over higher modes and to obtain a best fit to the experimental response of the structure.

Fig. 5.14 shows the results obtained for the time history analysis in terms of horizontal displacements for each one of the floors. A good overall agreement between the model predictions and the test results was obtained, with the amplitudes and the frequencies, exhibiting acceptable deviations. The difference between the maximum computed displacements on the 3rd floor and those obtained experimentally was 8%, while at the 2nd floor was 3% and at the first floor was a 25%. Fig. 5.15 and 5.16 show the damage distribution at the masonry walls after the test. Even that the crack pattern for the test was not reported in the original work of Tomazevic and Weiss (1994) (i.e. the authors only provided the crack pattern for the test that produced the collapse of the structure) the damage distribution follows the criteria observed at the crack pattern at the ultimate state (Fig. 5.17).

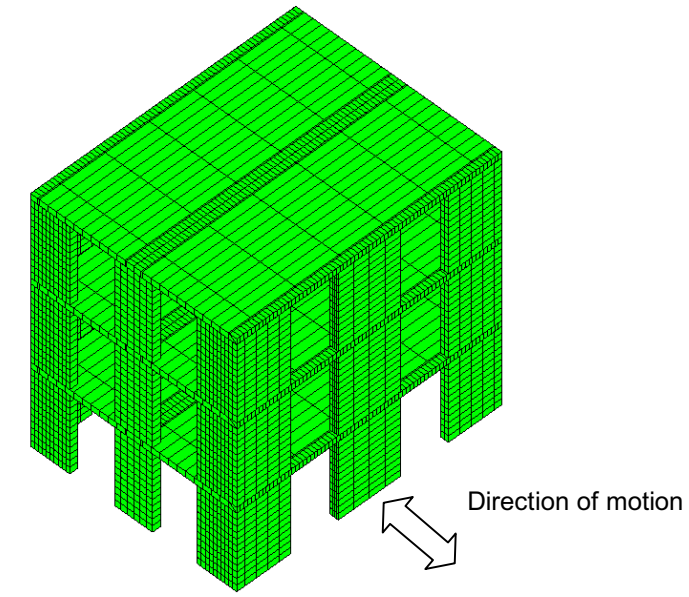

a)

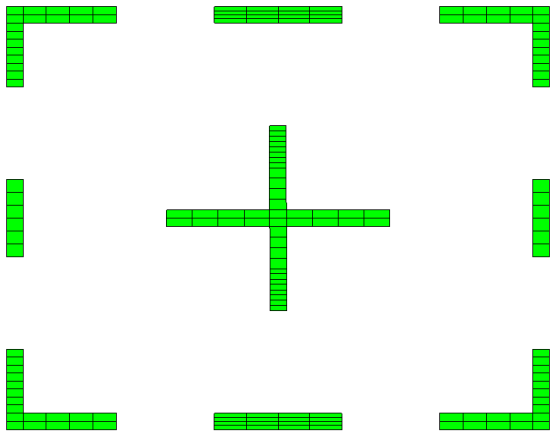

b)

Figure 5.13 – Building model a) overview b) cross section of the walls

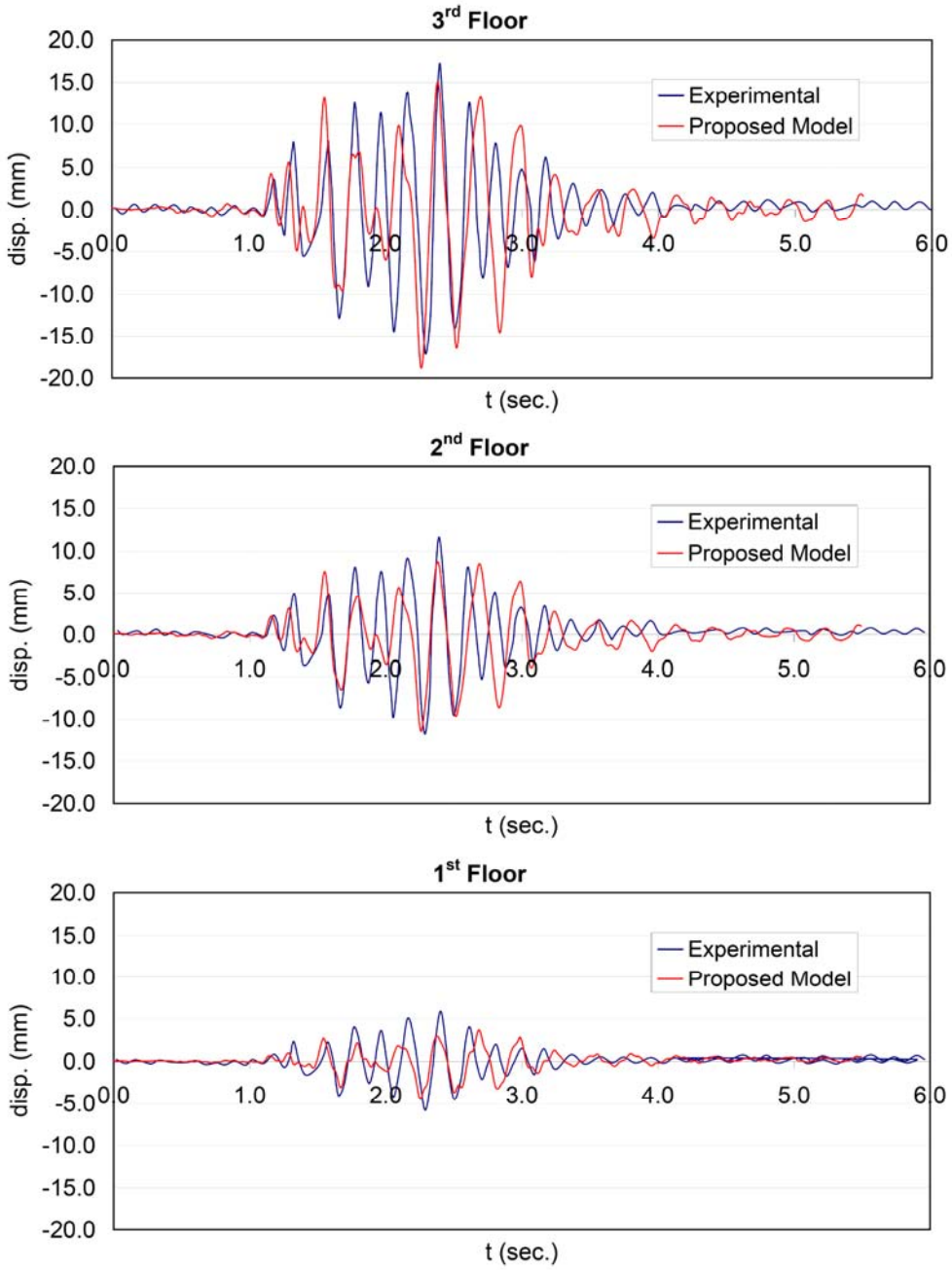

Figure 5.14 – Time history horizontal displacements results

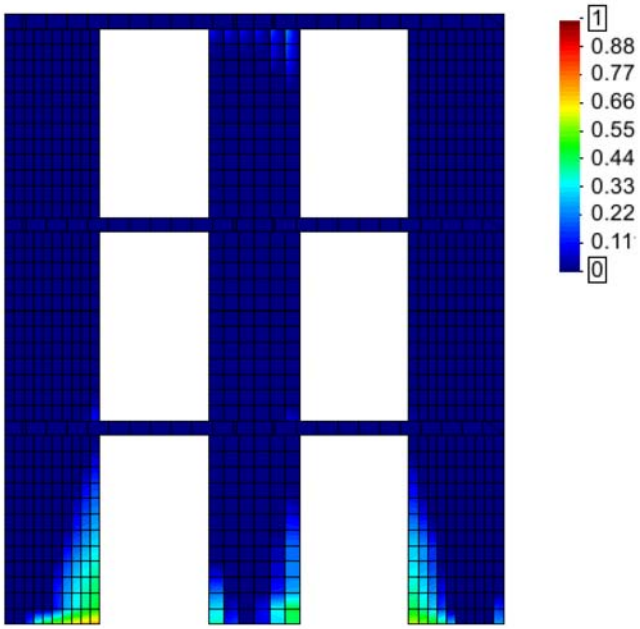

(a)

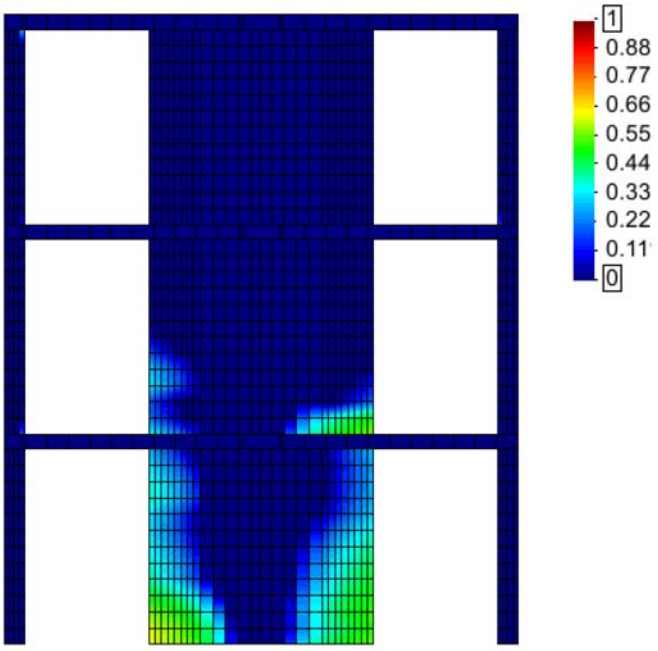

(b)

Figure 5.15 – Compressive damage distribution after the test (a) lateral walls (b) center walls

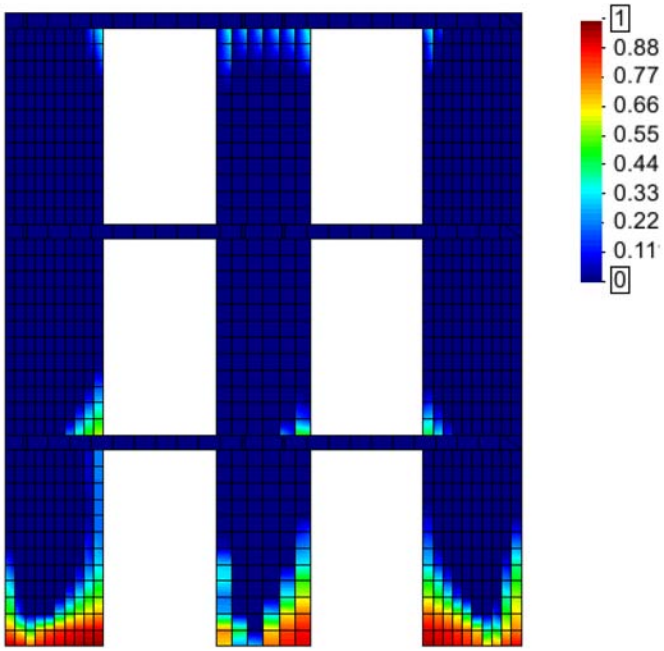

(a)

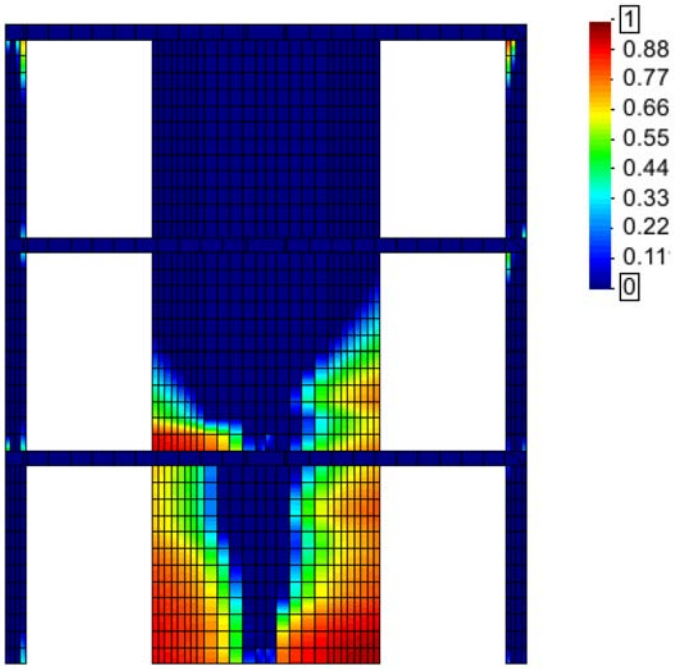

(b)

Figure 5.16 – Tensile damage distribution after the test (a) lateral walls (b) center walls

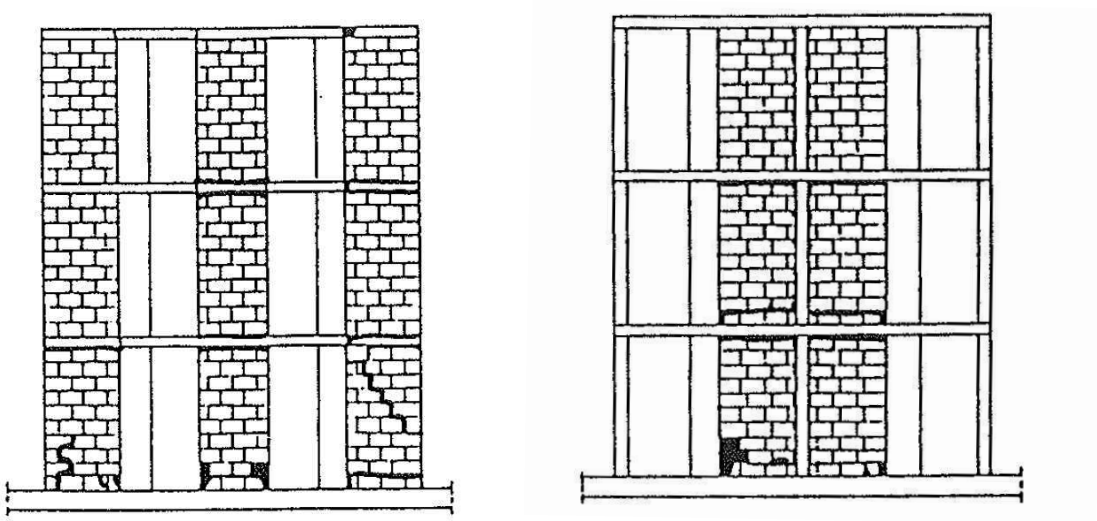

(a) (b)

Figure 5.17 – Crack pattern at the ultimate state (a) lateral walls (b) center walls (Tomazevic and Weiss, 1994)

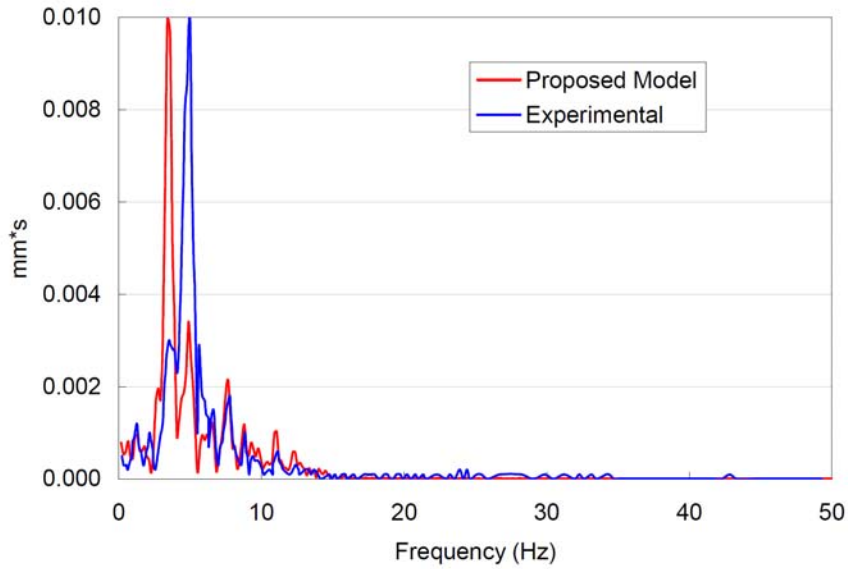

Figure 5.18 – Displacement-response Fourier spectra for the top floor.

Fig 5.18 shows the displacement-response Fourier spectra for the top floor. It can be observed that the higher contribution to the response is produced at a lower value in the computer model than the experimental result (3.45 Hz against 4.99 Hz). This effect seems

to be due to a lower stiffness in the case of the model in the non-linear regime (i.e. mass distribution remains almost invariable), therefore it might be concluded that a higher level of damage was produced in that case.

Interstory drift is an important parameter which is closely related to damage sustained by the building during the seismic excitation. Fig. 5.19 shows the interstory drift profile obtained by means of the time history analysis. The maximum drift angle numerically obtained for the first level was 0.81% corresponding to a maximum base shear coefficient of 23.5 %, given as a percentage of the total gravity load, while the values obtained experimentally were 0.86 % and 19 % for the first floor drift and base shear coefficient respectively.

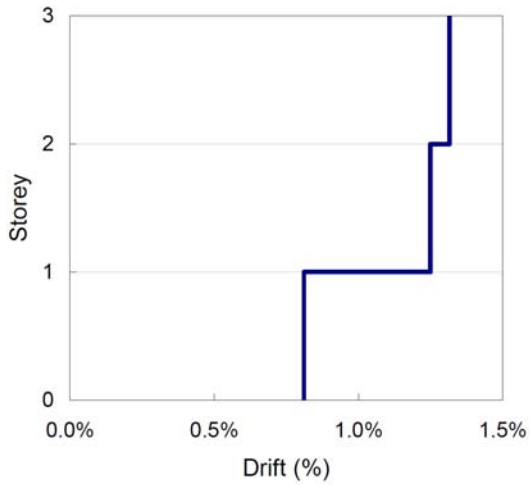

Figure 5.19 – Analytical drift profile obtained through the time history analysis.

Under seismic actions, the structure of a building tends to amplify the acceleration of the base. This becomes of importance when designing equipments or special elements that form part of the construction. Fig. 5.20 shows the acceleration time history for each floor. The maximum amplification factors obtained through the proposed model and experimentally are summarized in Table 5.3.

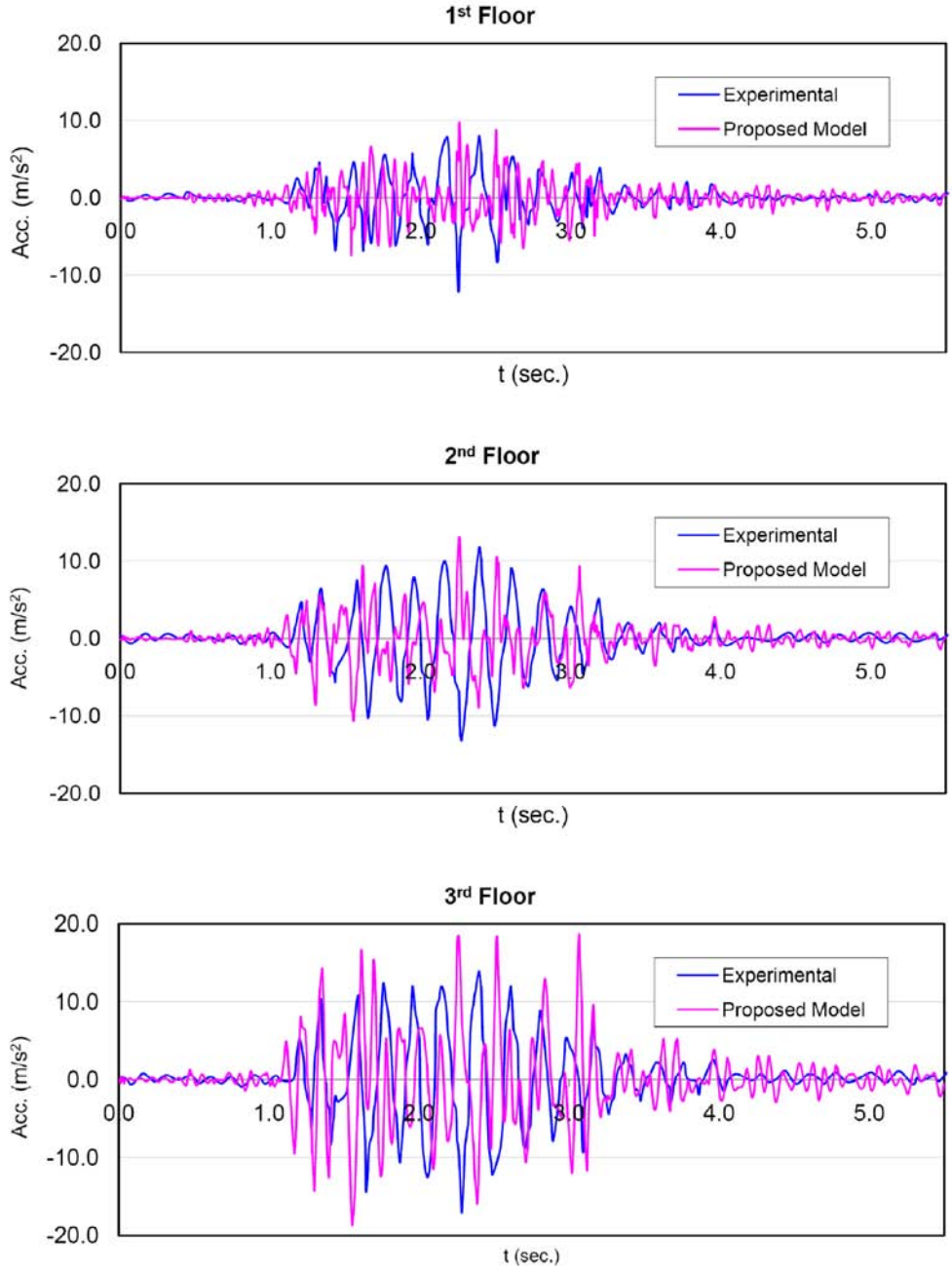

Figure 5.20 – Time history acceleration results

	1st Floor	2nd Floor	3rd Floor
Experimental	1.13	1.22	1.59
Proposed model	0.93	1.21	1.73

Table 5.3 – Acceleration amplification factors

A remarkable feature of the proposed formulation is that the computational cost as well as the time required for the analysis is very low, due to the reduced number of elements necessary for the analysis and the simplicity of the non linear material models. As a matter of example, in this application, the time required for the complete analysis was less than two hours in a standard personal computer (dual core 2 GHz, 4Mb RAM).

Chapter 6

Conclusions

The main purpose of the research reported in this thesis was to extend the Generalized Matrix Formulation to the non linear dynamic analysis of reinforced concrete and masonry framed structures. In general, both the general and specific objectives as indicated in Chapter 1 have been met.

In Chapter 2, an update on the state-of-the-art regarding modeling of reinforced concrete and masonry structures was presented, as well as the most important time step integration procedures available in the literature.

A new uniaxial constitutive model for concrete and masonry was proposed in Chapter 3, which allows the modelization of the complex behavior of masonry and concrete subjected to cyclic loading. The specific conclusions of the proposed cyclic constitutive model are presented in section 6.2.1.

In Chapter 4 the basic formulation for static analysis, the material model for reinforcing steel as well as the adopted time step procedure for the integration of the dynamic equation

of motion were presented. Specific conclusions on the details on the numerical implementation are outlined in section 6.2.2.

In Chapter 5, a series of examples on the application of the proposed formulation to experimental tests available in the literature in both reinforced concrete and masonry structures were presented. Specific conclusions on the obtained results are provided on section 6.2.3.

Finally, recommendations for future works are outlined in section 6.3.

6.1 General conclusions

The general conclusions of the present research are the following:

1) A model for the non linear dynamic analysis of 3D framed reinforced concrete and masonry structures has been proposed. This model is capable to reproduce the main characteristics of the complex behavior of these structures when subjected to dynamic loadings.

2) A uniaxial cyclic constitutive model for concrete and masonry was proposed. The model can reproduce the complex behavior of concrete under any history of uniaxial cyclic loading. Particular emphasis has been paid to the simulation of the strength and stiffness degradation produced by the load cycling. Two independent damage parameters, one for damage in compression and the other for damage in tension, have been introduced to model the deterioration of concrete under increasing loads. A model for the loops due to cyclic compressive loadings has been proposed by considering its dependency with the damage accumulation in the concrete. Models for cyclic tension as well as crack opening and closing have been also proposed.

3) A time step integration procedure has been adopted and implemented on the base of the computer program CRIPTA based on the Generalized Matrix Formulation. The

time integration scheme adopted fulfill the desirable characteristics for a time step procedure and have shown its power and versatility in combination with the Generalized Matrix Formulation.

4) The application of the proposed model in experimental examples available in the literature have shown that the model may adequately predict the response of reinforced concrete and masonry framed structures subjected to dynamic loadings, maintaining the level of accuracy shown by the Generalized Matrix Formulation, with a low computational cost.

6.2 Specific conclusions

6.2.1 Implemented constitutive models

1) The constitutive model proposed for concrete and masonry allows the modelization of the complex behavior of the material subjected to cyclic loading. The main features of the proposed model are the inclusion of two different parameters for damage in tension and compression, as well as the capacity to reproduce incomplete cycles of unloading-reloading and transition between tension and compression (opening and closing of cracks). The model has been validated by comparing the results with a series of tests developed by others authors. In all cases, the proposed model shows satisfactory agreement with the experimental results.

2) The cyclic constitutive model proposed for concrete and masonry may adequately predict the energy dissipated during load cycles, which is an important feature when seismic analysis is performed. This fact has been shown through the explicit calculation of the energy dissipated in a series of cyclic loading tests and compared with the experimental results as well as the results obtained by the application of other constitutive models.

3) The relationship between the model parameters and the damage in compression were specifically derived for normal strength concrete and clay brick masonry. However, with an adequate number of test results, the basic procedure may be applied in order to extend the cyclic constitutive model to different types of masonry (i.e. block masonry, concrete masonry, etc.) and different types of concrete (i.e. high strength concrete).

4) A remarkable feature of the proposed concrete and masonry model lays in the fact that all the input data required can be obtained through the conventional monotonic compression and tension tests.

6.2.2 Adopted formulation

1) The adopted formulation, the so-called Generalized Matrix Formulation has proved to be an efficient framework for the non linear dynamic analysis of reinforced concrete and masonry structures, maintaining the advantages observed in the static analysis of accuracy and reduced computational cost.

2) The time step integration procedure implemented, the generalized-α method, has presented a good performance in combination with the GMF. It has been observed that the use of α parameters, besides the efficient numerical damping over the higher modes introduced, accelerates the convergence of the non linear problem. In the particular cases analyzed, the number of iterations necessary to reach convergence was reduced in the range of 30% in the case of the reinforced concrete frame studied and up to 40% in the case of the masonry building case study.

6.2.3 Application examples

1) In Chapter 5, two numerical applications were presented to illustrate the capability of the proposed model in reproducing the response of reinforced concrete frames

subjected to cyclic and dynamic actions, together with an example concerning the a dynamic analysis of a masonry building. The results obtained show, in all cases, a good agreement with the experimental results.

2) In the first example of a reinforced concrete column subjected to a transversal cyclic loading (Atalay and Penzien, 1975), the main characteristics of the force-displacement results were adequately reproduced. In particular, the pinching effect produced by the interaction between axial force and bending moment (opening and closing of cracks).

3) In the reinforced concrete frame subjected to a seismic loading example (Carydis, 1997), good results have been obtained in terms of amplitudes and periods. The localization and extension of damaged areas, both in tension and compression, matched reasonable with the results obtained experimentally.

4) In the masonry building subjected to a seismic loading (Tomazevic and Weiss, 1994), a good agreement have been obtained in terms of amplitudes and periods with the results obtained experimentally. Good results have been also obtained for the localization and extension of damaged areas, both in tension and compression. Good agreement has been obtained in the evaluation of the maximum drift at the first level, the acceleration amplification factors and base shear coefficients.

6.3 Recommendations for future studies

The research work presented herein has open many possibilities for future studies and improvements on the modelization of framed reinforced concrete structures, both in the computer modeling and the experimental fields, which may be summarized as follows:

- Regarding the adopted formulation, a series of measures may be adopted that could result on improvements on its computational efficiency. One of these measures would be the use Gauss integration points along the element and in the cross

section level instead of Simpson's rule. Another possibility would be the implementation of a procedure for the state determination of the element and the internal forces like the one presented by Neuenhofer and Filippou (1997) in order to avoid the iteration at the element level.

- Further research could be done on the application of the proposed formulation to a good number of structures, aiming to provide a set of recommended range values for the different parameters of the time integration procedure, considering the special characteristics of the structure, such us differences on materials or structural scheme, etc.

- Regarding the modelization of reinforced concrete structures, a further line of research would be the implementation of the shear and torsional non linear effects, by means of couple models like those proposed by Bairán and Marí (2007) or Navarro et al. (2007). Further experimental investigation would be the cyclic behavior of reinforced concrete structures subjected to the general case of axial, bending, shear and torsional couple loadings. Another source of research would be the implementation of other features of the reinforced concrete structures, like the bond slip between reinforcing steel and concrete, which may need modifications on the sectional compatibility of the adopted formulation or the introduction of special elements for joints and D regions.

- Another line of investigation would be the extension of the formulation to the prestressed concrete elements, in particular the consideration of non linear time-dependant effects such as creep, shrinkage and relaxation of presstressing steel.

- Regarding the modelization of masonry structures, an important source of research would be the investigation on couple axial-shear models under cyclic loading.

- Further experimental research would be developed on the behavior of different types of masonry subjected to cyclic loading. Particularly, the behavior of masonry

under cyclic tensile loading and the transition between tension and compression should be further investigated.

References

Abbas S., Scordelis, A.C. (1993) "Nonlinear geometric, material and time-dependent analysis of segmentally erected three-dimensional cable stay bridges", Report UCB/SEMM-93/09. University of California, Berkeley.

Aktan A.E., Karlsson B.I., Sozen M.A. (1973) Stress–strain relationships of reinforcing bars subjected to large strain reversals. In: Civil Engineering Studies, Structural Research Series No, 397. Urbana Champaign: University of Illinois.

AlShebani M.M., Sinha S.N. (1999) Stress-strain characteristics of brick masonry under uniaxial cyclic loading. Journal of Structural Engineering ASCE, 125(6), 600-604.

AlShebani M.M., Sinha S.N. (2000) Stress-strain characteristics of brick masonry under cyclic biaxial compression. Journal of Structural Engineering ASCE, 126(9), 1004-1007.

Armero F., Petöcz E. (1998). Formulation and analysis of conserving algorithms for frictionless dynamic contact/impact problems. Computer Methods in Applied Mechanics and Engineering, 158, 269-300.

AS/NZS 1170.4 (2004) Standard Structural Design. Actions – Part 4 Earthquake Actions. Post Public Comment Draft 8, Standards New Zealand.

ASCE/SEI 7-05 (2005) Minimum Design Loads for Buildings and Other Structures. American Society of Civil Engineers, USA.

Atalay M., Penzien J. (1975) Behavior of critical regions of RC components as influenced by moment, shear and axial force. Earthquake Engineering Research Center, EERC 75-19, University of California, Berkeley.

Backlund J. (1976) Large deflection analysis of elasto-plastic beams and frames. International Journal of Mechanical Science, 18, 269-277.

Bahn B.Y., Hsu C.T. (1998) Stress-Strain Behavior of Concrete under Cyclic Loading. ACI Materials Journal, 95(2), 178-193.

Bairán J.M., Mari A.R. (2007) Multiaxial-coupled analysis of RC cross-sections subjected to combined forces. Engineering Structures 29(8), 1722–1738.

Balan T.A., Filippou F.C., Popov E.P. (1998) Hysteretic model of ordinary and high-strength reinforcing steel. Journal Structural Engineering, ASCE, 124, 288–297.

Banon H., Biggs J., Irvine M. (1981) Seismic Damage in Reinforced Concrete Frames. Journal Structural Engineering ASCE, 107(ST9), 1713-1729.

Barbat A.H., Canet, J. M. (1994). Estructuras Sometidas a Acciones Sísmicas. Centro Internacional de Métodos Numéricos en Ingeniería, Barcelona.

Baron F. (1961) Matrix analysis of structures curved in space. Journal of Structural Division ASCE, 87, 17-38.

Bathe K.J., Wilson E.L. (1973) Stability and accuracy analysis of direct integration methods. Earthquake Engineering and Structural Dynamics, 1, 283-291.

Bažant Z.P., Oh B.H. (1983) Crack band theory for fracture of concrete. Materials & Structures RILEM, 16(93), 155-177.

Bazzi G., Anderheggen E. (1982) The ρ-family of algorithms for time-step integration with improved numerical dissipation. Earthquake Engineering & Structural Dynamics, 10, 537-550.

Bertero V.V., Aktan A., Charney F., Sauce R. (1984) Earthquake Simulator Tests and Associated Experimental, Analytical and Correlation Studies of One-Fifth Scale Model. Earthquake Effects on Reinforced Concrete Structures ACI, SP-84-13: 375-424.

Berto L., Saetta A., Scotta R., Vitaliani R. (2000) An orthotropic damage model for masonry structures. International Journal of Numerical Methods in Engineering, 55, 127-157.

Brancaleoni F., Ciampi V., Di Antonio R. (1983) Rate-Type Models for Non Linear Hysteretic Structural Behavior. EUROMECH Colloquium, Palermo.

Buckle I.G., Jackson A.T. (1981) A filamented beam element for the nonlinear analysis of reinforced concrete shells with edge beams. Department of Civil Engineering, University of Auckland, New Zealand.

Buyukozturk O., Tseng T.M. (1984) Concrete in biaxial cyclic compression. Journal Structural Engineering, 110(3), 461-76.

Calvi G. M., Gregory R. K., Magenes G. (1996) Testing of masonry structures for seismic assessment. Earthquake Spectra, 12 (1), 145-162.

Carol I., Murcia J. (1989) Non linear time-dependent analysis of planar frames using an exact formulation – I Theory. Computers and Structures, 33(1), 79-87.

Carrascón S., Marí A.R., Carol I. (1987) Análisis instantáneo y diferido de puentes curvos de hormigón armado y pretensado. Publication ES-015, Department of Construction Engineering, Technical University of Catalonia, Barcelona.

Carydis P.G. (1997) European Comission - Human Capital and Mobility Programme, Prenormative Research in Support of Eurocode 8, Shaking Table Tests of Reinforced Concrete Frames. Report No 8, LNEC, Lisbon.

Chan E.C. (1981) Nonlinear geometric, material and time dependent analysis of reinforced concrete shells with edge beams. Report UCB-SESM 82/8. University of California, Berkeley.

Chang G.A., Mander J.B. (1994) Seismic Energy Based Fatigue Damage Analysis of Bridge Columns: Part I – Evaluation of Seismic Capacity, Technical Report NCEER-94-0006, State University of New York at Buffalo, Buffalo, New York.

Charney F., Bertero V.V. (1982) An Evaluation of the Design and Analytical Seismic Response of a Seven Story Reinforced Concrete Frame-Wall Structure. EERC report 82/08, Earthquake Engineering Research Center, University of California, Berkeley.

Chen S.W.J., Hidalgo P.A., Mayes R.L., Clough R.W., McNiven H.D. (1978) Cyclic loading tests of masonry single piers, Volume 2 - Height to width ratio of 1.

EERC Rep. No. 78/28, Environmental Engineering Research Council, University of California, Berkeley.

Chung J., Hulbert G.M. (1993) A time integration algorithm for structural dynamics with improved numerical dissipation: The generalized-α method. ASME Journal Applied Mechanics, 60, 371-375.

Chung J., Hulbert G.M. (1994). A family of single-step Houbolt time integration algorithms for structural dynamics. Computer Methods in Applied Mechanics and Engineering, 118(1-2), 1-11.

Ciampi, V, Carlesimo, L. (1986) A non linear beam element for seismic analysis of structures. Proc., 8th European Conference on Earthquake Engineering, Laboratorio Nacional de Engenharia Civil, Lisbon, Portugal.

Clough R., Benuska L. (1967). Nonlinear Earthquake Behavior of Tall Buildings. Journal of Mechanical Engineering ASCE, 93(EM3), 129-146.

Clough R., Jhonston S. (1966) Effect of Stiffness Degradation on Earthquake Ductility Requirements. Transactions of Japan Earthquake Engineering Symposium, Tokyo, 195-198.

Clough R., Penzien J. (1992) Dynamics of structures. McGraw-Hill, New York.

Committee Euro-International du Beton (1993) CEB-FIP Model Code 1990, London, Thomas Telford.

Committee Euro-International du Beton (1996) RC Frames under Earthquake loading-State of the Art Report, London, Thomas Telford.

Comite Euro-International du Beton (1996) RC Elements under cyclic loading-State of the Art Report. Thomas Telford, London.

Cornelissen H.A.W., Hordijk D.A., Reinhardt H.W. (1985) Experiments and theory for the application of fracture mechanics to normal and lightweight concrete. Proceedings International Conference on Fracture Mechanics of Concrete, F. H. Wittman Ed., Elsevier, Amsterdam, The Netherlands.

Crisfield M.A., Shi J. (1994) A co-rotational element/time-integration strategy for non-linear dynamics. International Journal for Numerical Methods in Engineering, 37, 1897-1913.

Crisfield M.A., Galvanetto U., Jelinié G. (1997) Dynamics of 3-D co-rotational beams. Computational Mechanics, 20, 507-519.

Cruz P.J.S., Marí A.R., Roca P. (1998) Non linear time-dependent análisis of segmentally constructed structures. Journal of Structural Engineering, ASCE, 124, 3, 278-287.

Dahlquist, G. (1963) A special stability problem for linear multi-step methods. BIT, 3, 27-43.

D'Ambrisi A., Filippou F.C. (1997) Correlation Studies on a RC Frame Shaking-Table Specimen. Earthquake Engineering and Structural Dynamics, 26 (10), 1021-1040.

Dhanasekar M., Page A.W., Kleeman P.W. (1985) The failure of brick masonry under biaxial stresses. Proceedings of the ICE, Part 2, 79, 295-313.

Dodd L.L., Restrepo-Posada J.I. (1995) Model for predicting cyclic behavior of reinforcing steel. Journal Structural Engineering ASCE, 121, 433–445.

Erlicher S., Bonaventura L., Bursi O.S. (2002) The analysis of the Generalized-a method for non-linear dynamic problems. Computational Mechanics, 28, 83-104.

European Committee for Standardization CEN EN-1992-1-1. (2004) Eurocode 2: Design of concrete structures, Part 1-1 General rules and rules for buildings.

European Committee for Standardization CEN EN-1996-1-1. (2005) Eurocode 6: Design of masonry structures, Part 1-1 General rules for reinforced and unreinforced masonry structures.

European Committee for Standardization CEN EN-1998-1. (2004) Eurocode 8: Design of structures for earthquake resistance, Part 1: General rules, seismic actions and rules for buildings.

Ewing B.D., Kowalsky M.J. (2004) Compressive behaviour of Unconfined and Confined Clay Brick Masonry. Journal of Structural Engineering ASCE, 130(4), 650-661.

Faria R., Oliver J., Cervera M. (1998) A strain-based plastic viscous-damage model for massive concrete structures. International Journal Solids Structures, 35(14), 1533-58.

Filippou F.C., Issa A. (1988) Nonlinear Analysis of Reinforced Concrete Frames Under Cyclic Loads Reversals. EERC Report 88/12, Earthquake Engineering Research Center, University of California, Berkeley.

Filippou F.C., Popov E., Bertero V.V. (1983) Effects of Bond Deterioration on Hysteretic Behavior of Reinforced Concrete Joints. Report No. UCB/EERC 83-19. EERC, University of California, Berkeley.

Galvanetto U., Crisfield M.A. (1996) An energy-conserving co-rotational procedure for the dynamics of planar beam structures. International Journal for Numerical Methods in Engineering, 39, 2265-2282.

Ganz H.R., Thürlimann B. (1983) Strength of brick walls under normal force and shear. Proc. 8th Int. Symposium on Load Bearing Brickwork, London, 27-29.

Ghali, A., Elbadry, M.M. (1985) "User's manual and computer program CPF: Cracked plane frames in prestressed concrete". Department of civil Engineering, The University of Calgary, Research Report CE 85-2, Calgary.

Giberson M. (1967) The Response of Nonlinear Multy-Story Structures Subjected to Earthquake Excitations. Earthquake Engineering Research Laboratory, Pasadena.

Gopalaratman V.S., Shah S.P. (1985) Softening Response of plain concrete in direct tension. ACI Journal, 82(3), 310-323.

Goudreau G.L., Taylor R.L. (1972) Evaluation of numerical methods in elastodynamics. Cumputers Methods in Applied Mechanics and Engineering, 2, 69-97.

Grelat A. (1978) Comportament non linéaire et stabilité des ossatures en betón armé. Annales de l'Inst Tech du Batiment et des Travaux Publics, 111(1), 19-36.

Gutiérrez E., López Cela J.J. (1998) Improving explicit time integration by modal truncation techniques. Earthquake Engineering and Structural Dynamics, 27, 1541-1557.

Hilber H.M., Hughes T.J.R., Taylor R.L. (1977) Improved numerical dissipation for time integration algorithms in structural dynamics. Earthquake Engineering & Structural Dynamics, 5, 283-292.

Hilber H.M., Hughes T.J.R. (1978) Collocation, dissipation and 'overshoot' for time integration schemes in structural dynamics. Earthquake Engineering & Structural Dynamics, 6, 99-117.

Hoeler M.S., Stanton J.F. (2006) Simple Phenomenological Model for Reinforcing Steel under Arbitrary Load. Journal Structural Engineering ASCE, 132(7), 1061-1069.

Hoff C., Pahl P.J. (1988 a) Development of an implicit method with numerical dissipation from a generalized single-step algorithm for structural dynamics. Computational Methods Applied Mechanical Engineering, 67, 367-385.

Hoff C., Pahl P.J. (1988 b) Practical performance of the θ_1-method and comparison with other dissipative algorithms in structural dynamics. Computer Methods in Applied Mechanics and Engineering, 67, 87-110.

Hognestad E., Hanson N.W., McHenry D. (1955) Concrete stress Distribution in Ultimate Strength Design, Journal ACI, 27(4), 455-479.

Hordijk D.A. (1991) Local approach to fatigue of concrete. Delft University of Technology, The Netherlands.

Hsu T.T.C., Zhu R.R.H. (2002) Softened Membrane Model for Reinforced Concrete Elements in Shear. ACI Structural Journal, 99(4), 460-469.

Hughes T.J.R., Caughey T.K., Liu W.K. (1978) Finite element methods for nonlinear elastodynamics which conserve energy. Journal of Applied Mechanics, Transactions of the ASME, 45, 366-370.

Kaba S., Mahin S.A. (1984) Refined Modeling of Reinforced Concrete Columns for Seismic Analysis. EERC Report 84/03, Earthquake Engineering Research Center, University of California, Berkeley.

Kang Y.J., Scordelis A.C. (1980) Nonlinear Analysis of Prestressed Concrete Frames. Journal Structural Division ASCE, 106, 445-62.

Karsan I.D., Jirsa J.O. (1969) Behavior of Concrete under Compressive Loadings. Journal of the Structural Division, ASCE. 95(ST12), 2543-2563.

Katona M.G., Zienkiewicz O.C. (1985) A unified set of single step algorithms. Part 3: The beta-m method, a generalization of the Newmark scheme. International Journal for Numerical Methods in Engineering, 21, 1345-1359.

Ketchum, M.A. (1986) "Redistribution of stresses in segmentally erected prestressed concrete bridges", Report UCB-SESM 86/07. University of California, Berkeley.

Kuhl D., Crisfield M.A. (1999) Energy-conserving and decaying algorithms in non-linear structural dynamics. International Journal for Numerical Methods in Engineering, 45, 569-599.

Kuhl D., Ramm E. (1996) Constraint Energy-Momentum algorithm and its application to nonlinear dynamics of shells. Computer Methods in Applied Mechanics and Engineering, 136, 293-315.

Kwan, A. K. H. (1991) Analysis of coupled wall/frame structures by frame method with shear deformation allowed. Proceeding of the ICE, Structures and Buildings, 91, 273–297.

Leger P., Dussault S. (1992) Non linear seismic response analysis using vector superposition methods. Earthquake Engineering and Structural Dynamics, 21, 163-176.

Légeron F., Paultre P., Mazars J. (2005) Damage Mechanics of Nonlinear Seismic Behavior of Concrete Structures. Journal Structural Engineering ASCE, 131(6), 946-55.

Lin C.S., Scordelis A. (1975) Non linear analysis of RC shells of general forms. Journal Structural Engineering ASCE, 101(ST3), 523-38.

Lofti H.R., Shing P.B. (1994) Interface model applied to fracture of masonry structures. Journal of Structural Engineering, ASCE, 120 (1), 63-80.

Lourenço PB. (1996) Computational strategies for masonry structures, Ph.D. Thesis, Delft University of Technology, Delft, The Netherlands.

Lourenço P.B., Rots J.G. (1997) Multisurface interface model for analysis of masonry structures. Journal of engineering mechanics ASCE, 123(7), 660-668.

Luciano R, Sacco E. (1997) Homogenisation technique and damage model for old masonry material. International Journal of Solids and Structures 1997;34(24):3191–208.

Ma S-Y.M., Bertero V.V., Popov E.P. (1976) Experimental and Analytical Studies of the Hysteretic Behavior of Reinforced Concrete Rectangular and T-Beams. Report EERC-76-2. EERC, University of California, Berkeley.

Macchi G. (1985) Behavior of masonry under cyclic actions and seismic design. Proc. 6th International Brick Masonry Conference, LI-XXIV.

Magenes G. (1992) Comportamento sismico di murature di mattoni: resistenza e meccanismi di maschi murari. PhD Thesis, Structural Mechanics Department, University of Pavia.

Magenes G., Calvi G.M. (1997) In-plane seismic response of brick masonry walls. Earthquake Engineering and Structural Dynamics, 26, 1091-1112

Mahasuverachai M., Powell G.H. (1982) Inelastic Analysis of Piping and Tubular Structures. EERC Report 82/27, Earthquake Engineering Research Center, University of California, Berkeley.

Mander J.B., Priestley M.J.N., Park R. (1988) Theoretical stress-strain model for confined concrete. Journal of Structural Engineering ASCE, 114(8), 1804-1826.

Mann W., Müller H. (1982) Failure of Shear-Stressed Masonry – An Enlarged Theory, Tests and Application to Shear Walls. Proc. of the British Ceramic Society, 223-235

Mansour M., Hsu T.T.C. (2005) Behavior of Reinforced Concrete Elements under Cyclic Shear II: Theoretical Model. Journal of Structural Engineering ASCE, 131(1), 54-65.

Marí A.R. (1984) Nonlinear geometric, material and time dependent analysis of three dimensional reinforced and prestressed concrete frames. Report UCB-SESM 84/12. University of California, Berkeley.

Marí A.R. (1985) A general Method for the analysis of curved beams and space frames. Department of Construction Engineering, Technical University of Catalonia, Barcelona.

Marí A.R. (1991) Estudio Comparativo entre diversos métodos de análisis no lineal de estructuras reticulares de hormigón armado y pretensado: Estado actual y líneas de futura actuación. Modelos de Análisis de estructuras de Hormigón, GEHO, Comisión II, Madrid.

Marí A.R. (2000) Numerical simulation of segmental construction of three dimensional concrete frames. Engineering Structures, 22, 6, 585-596.

Martinez-Rueda E., Elnashai A.S. (1997) Confined concrete model under cyclic load. Materials and Structures, 30, 139-47.

Mazars J., Pijaudier-Cabot G. (1989) Continuum damage theory. Application to concrete. Journal Engineering Mechanics ASCE, 115(2), 345-365.

Mazars J., Ragueneau F., Casaux G., Colombo A, Kotronis P. (2004) Numerical modeling for earthquake engineering: the case of lightly RC structural walls. International Journal of Numerical and Analytical Methods in Geomechanics, 28, 857-874.

Menegotto M., Pinto P.E. (1973) Method of analysis of cyclically loaded RC plane frames including changes in geometry and non-elastic behavior of elements under normal force and bending. Preliminary Report IABSE, 13, 15–22.

Milani G., Lourenço P.B., Tralli A. (2006) Homogenised limit analysis of masonry walls, Part I: Failure surfaces. Computers and Structures, 84, 166–180.

Molins, C. (1996). Un model per a l'anàlisi del comportament resistent de construccions de maçoneria. Ph.D. Thesis, Universitat Politècnica de Catalunya, Barcelona.

Molins C., Roca P., Barbat A.H. (1998) Flexibility-based linear dyamic analysis of complex structures with curved-3D members. Earthquake Engineering & Structural Dynamics, 27, 731-747.

Molins C., Roca P. (1998) Capacity of Masonry Arches and Spatial Frames. Journal Structural Engineering ASCE, 124(6), 653-663.

Monti G., Nuti C. (1992) Nonlinear cyclic behavior of reinforcing bars including buckling. Journal Structural Engineering, ASCE, 118, 3268–3284.

Mohraz B., Elghadamasi F.E., Chang C.J. (1991) An incremental mode superposition for non linear dynamic análisis. Earthquake Engineering and Structural Dynamics, 20, 471-481.

Murcia J., Herkenhoffm L. (1994) Time dependent analysis of continuous bridges composed by precast concrete elements. Hormigón y Acero. Vol. 192, 55-71.

Naraine K., Sinha S.N. (1989) Behaviour of brick masonry under cyclic compressive loading. Journal of Construction Engineering Management ASCE, 115(2), 1432-1445.

Naraine K., Sinha S.N. (1991 a) Cyclic behaviour of Brick Masonry under biaxial compression. Journal of Structural Engineering ASCE, 117(2), 1336-1355.

Naraine K., Sinha S.N. (1991 b) Model for Cyclic Compressive Behaviour of Brick Masonry. ACI Structural Journal, 88(5), 603-609.

Navarro J., Miguel P., Fernandez M.A., Filippou F.C. (2007) A 3D numerical model for reinforced and prestressed concrete elements subjected to combined axial, bending, shear and torsión loading. Engineering Structures. 29, 3404-3419.

Neuenhofer, A., Filippou, F.C. (1997) Evaluation of nonlinear frame finite element models. Journal of Structural Engineering ASCE, 123 (7), 958-966.

Newmark N.M. (1959) A method of computation for structural dynamics. Journal Engineering Mechanics Div, Proc ASCE, 8, 67-94.

Okamoto S., Shiomi S., Yamabe K. (1976) Earthquake Resistance of Prestressed Concrete Structures. Procedings Annual Convention AIJ, 1251-1252.

Okamura H., Maekawa K. (1991) Non linear analysis and constitutive models of reinforced concrete. Giho-do Press, University of Tokyo, Japan.

Oh B. H. (1992) Fracture energy of concrete and equivalent crack length. Fracture mechanics of concrete structures. Proc. of the 1st international conference (FraMCoS1), Colorado, USA. pp 419-423.

Oliveira D. V. (2002) Experimental and numerical analysis of blocky masonry structures under cyclic loadings. PhD Thesis, Escola de Engenharia, Universidade de Minho, Portugal.

Oliveira D, Lourenço P, Roca P. (2006) Cyclic behavior of stone and brick masonry under biaxial compressive loading. Materials and Structures, 39 (2), 247-257.

Oliver J. (1989). A Consistent Characteristic Length for Smeared Cracking Models. International Journal Numerical Methods in Engineering, 28, 461-474.

Otani S. (1974) Inelastic Analysis of R/C Frame Structures. Journal Structural Engineering ASCE, 100(ST7), 1433-1449.

Page A.W. (1981) The biaxial compressive strength of brick masonry. Proceedings of the ICE, Part 2, 71, 893-906.

Page A.W. (1983) The strenght of brick masonry under biaxial tension compresion. International Journal of masonry construction, 3(1), 26-31.

Palermo D., Vecchio J. (2003) Compression Field Modeling of Reinforced Concrete Subjected to Reversed Loading: Formulation. ACI Structural Journal, 100(5), 616-625.

Park R., Kent D.C., Sampson R.A. (1972) Reinforced concrete members with cyclic loading. Journal Structural Division ASCE, 98(7), 1341–1360.

Pegon P., Anthoine A. (1997). Numerical strategies for solving continuum damage problems with softening: Application to the homogenization of masonry. Computers and structures, 64(1-4), 623-642.

Petrangeli M., Ciampi V. (1997) Equilibrium based numerical solutions for the nonlinear beam problem. International Journal Numerical Methods in Engineering, 40(3), 423-438.

Petrangeli M., Pinto P.E., Ciampi V. (1999) Fiber element for cyclic bending and shear of RC structures I: Theory. Journal of Engineering Mechanics, ASCE. 125(9), 994–1009.

Popovics S. (1973) A review of Stress-Strain Relationships for Concrete. Journal of the ACI, 67(3), 243-248.

Priestley M.J.N., Elder D.M. (1983). Stress-Strain Curves for Unconfined Concrete Masonry, ACI Journal, 80(3), 192-201.

Ramberg W.A., Osgood W.R. (1943) Description of stress-strain curves by three parameters. National Advisory Committee for Aeronautics, Technical Note No. 902.

Ramtani S., Berthaud Y., Mazars J. (1992) Orthotropic Behavior of concrete with directional aspects: modeling and experiments. Nuclear Engineering and Design, 133, 97-111.

Reinhardt H.W. (1984) Fracture Mechanics of an Elastic Softening Material like Concrete. Heron, 29.

Reinhardt H.W., Cornelissen H.A.W., Hordijk D.A. (1986) Tensile test and failure analysis of concrete. Journal Structural Engineering ASCE, 112(11), 2462-2477.

Roca P., Molins C., Marí, R. (2005) Strength capacity of masonry wall structures by the equivalent frame method. Journal Structural Engineering ASCE, 131(10), 1601-1610.

Rots, J.G. (1997) Structural masonry. Centre for Civil Engineering Research and Codes. Balkema, Rotterdam.

Rots J.G., Nauta P., Kusters G.M., Blaauwendraad J. (1985) Smeared crack approach and fracture localization in concrete. Heron, 30.

Saetta A., Scotta R., Vitaliani R. (1999) Coupled environmental-mechanical damage model of RC structures. Journal Engineering Mechanics ASCE, 125(8), 930-940.

Saetta A., Scotta R., Vitaliani R. (2000) Analysis of masonry vaulted structures by using 3-D damage model. Proceedings European Congress on Computational Methods in applied sciences and Engineering, ECOMAS, Barcelona.

Sakai J., Kawashima K. (2006) Unloading and Reloading Stress–Strain Model for Confined Concrete. Journal Structural Engineering ASCE, 132(1), 112-22.

Samarasinghe W., Hendry A.W. (1980) Strength of brickwork under biaxial stress. Proc. 7th Int. Symposium on Loadbearing Brickwork, London, British Ceramic Society, Stoke-on-trent.

Saritas A., Filippou F.C. (2006) A beam finite element for shear critical RC beams. ACI Special Publication SP-237, 295–310.

Sima J.F., Roca P., Molins C. (2008) Cyclic Constitutive model for concrete. Engineering Structures, 30(3), 695-706.

Simo J.C., Tarnow N., Doblaré M. (1995) Non-linear dynamics of three-dimensional rods: exact energy and momentum conserving algorithms. International Journal for Numerical Methods in Engineering, 38, 1431-1473.

Simo J.C., Tarnow N., Wong K.K. (1992) Exact energy-momentum conserving algorithms anda sympletic schemes for nonlinear dynamics. Computer Methods in Applied Mechanics and Engineering, 100, 63-116.

Simo J.C., Wong K.K. (1991) Unconditionally stable algorithms for rigid body dynamics that exactly preserve energy and momentum. International Journal for Numerical Methods in Engineering, 31, 19-52.

Sinha, B.P. (1978) A simplified ultimate load analysis of laterally loaded model orthotropic brickwork panels of low tensile strength. The Structural Engineer, 56B, 4, 81-84.

Sinha B.P., Gerstle K.H., Tulin L.G. (1964) Stress-Strain Relations for Concrete under Cyclic Loading. Journal of the ACI, 61(2), 195-211.

Spacone, E. (1994) Flexibility-based finite element models for the non linear static and dynamic analysis of concrete frame structures. PhD Thesis, University of California, Berkeley.

Spacone E., Filipou F.C., Taucer F.F. (1996) Fiber Beam-Column Model for Nonlinear Analysis of RC Frames. Earthquake Engineering & Structural Dynamics, 25(7), 711-742.

Spiliopoulos K.V., Lykidis G.C. (2005). An efficient three-dimensional solid finite element dynamic analysis of reinforced concrete structures. Earthquake Engineering & Structural Dynamics, 35, 137-157.

Spooner D.C., Dougill J.W. (1975) A quantitative assessment of damage sustained in concrete during compressive loading. Magazine of Concrete Research, 27(92), 151-160.

Syrmankezis C.A., Asteris P.G (2001) Masonry failure criterion under biaxial stress state. Journal of Materials in Civil Engineering, 58-64

Stanton J.F., McNiven, H.D. (1979) The development of a mathematical model to predict the flexural response of reinforced concrete beams to cyclic loads, using system identification." Earthquake Engineering Research Center (EERC), Rep. UBC/EERC 79-02, Univ. of California, Berkeley.

Takeda T., Sozen M., Nielsen N. (1970) Reinforced Concrete Response to Simulated Earthquakes. Journal Structural Engineering ASCE, 96(ST12), 2557-2573.

Takizawa H. (1976) Notes on Some Basic Problems in Inelastic Analysis of Planar RC Structures. Transactions of AIJ, Part I: Feb 51-62;Part II: March 65-67.

Tanigawa Y., Uchida Y. (1979) Hysteretic Characteristics of Concrete in the Domain of High Compressive Strain. Proceedings Annual Convention AIJ, 449-450.

Taucer, F. F., Spacone, E., Filippou, F. C. (1991) A fiber beam columns element for seismic response analysis of reinforced concrete structures. Rep. 91/17, EERC, Earthquake Engineering Research Center, University of California, Berkeley.

Tomazevic, M. (1999) Eathquake resistant design of masonry buildings / Miha Tomazevic. Series on innovation in structures and construction – Vol I. Eds. Elnashai & Dowling. Imperial College Press, London.

Tomazevic, M, Weiss, P. (1994) Seismic behavior of plain and reinforced masonry buildings. Journal of Structural Engineering ASCE, 120(2), 323-338.

Tsai W.T. (1988) Uniaxial Compression Stress-Strain Relations of Concrete. Journal of Structural Engineering ASCE, 114(9), 2133-2136.

Ulm F.J., Clement J.L., Guggenberger J. (1994) Recent Advances in 3D nonlinear FE-analysis of R/C and P/C beam structures. Proc ASCE Structures Congress XII, Atlanta (USA), 1427-1432.

Van der Pluijm R. (1997) Non linear behaviour of masonry under tension. Heron, 42(1), 24-54.

Vecchio F.J., Collins M.P. (1986). The Modified Compression Field Theory for Reinforced Concrete Elements Subjected to Shear. ACI Journal, 83(2), 219-231.

Wilson E.L. (1968) A computer program for the dynamic stress analysis of underground structures. SESM Report Nº 68-1, Div of Struct Engrg and Struct Mech, University of California, Berkeley.

Wood W.L. (1984) A unified set of single step algorithms. Part 2: Theory. International Journal for Numerical Methods in Engineering, 20, 2303-2309.

Wood W.L., Bossak M., Zienkiewicz O.C. (1981) An alpha modification of Newmark's method. International Journal Numerical Methods Engineering, 15, 1562-1566.

Yankelevsky D.Z., Reinhardt H.W., (1987) Model for cyclic compressive behavior of concrete. Journal of Structural Engineering ASCE, 113(2), 228-240.

Zeris C.A., Mahin S.A. (1988) Analysis of Reinforced Concrete Beam-Columns Under Uniaxial Excitation. Journal Structural Engineering ASCE, 114(ST4), 804-820.

Zienkiewicz O.C., Wood W.L., Hines N.H. (1984) A unified set of single step algorithms. Part 1: General Formulations and Applications. International Journal for Numerical Methods in Engineering, 20, 1529-1552.